Non-leptonic B-decays in and beyond QCD Factorisation

A thesis presented for the degree of

Doctor of Philosophy

by

Angelique N Talbot

Institute for Particle Physics Phenomenology

University of Durham

September 2005

Abstract

This thesis examines the non-leptonic B-decays within QCD factorisation and beyond, to challenge the assumptions and limitations of the method. We analyse the treatment of the distribution amplitudes of light mesons and present a new model described by simple physical parameters. The leading twist distribution amplitudes of light mesons describe the leading non-perturbative hadronic contributions to exclusive QCD reactions at large energy transfer, for instance electromagnetic form factors. Importantly, they also enter into the two-body B decay amplitudes described by QCD factorisation. They cannot be calculated from first principles and are described by models based on a fixed-order conformal expansion, which is not always sufficient in phenomenological applications. We derive new models that are valid to all orders in the conformal expansion and characterised by a small number of parameters related to experimental observables.

Motivated by the marginal agreement between the QCD factorisation results with the experimental data, in particular for $B \to \pi\pi$, we scrutinise the incalculable non-factorisable corrections to charmless non-leptonic decays. We use the available results on $B \to \pi\pi$ to extract information about the size and nature of the required non-factorisable corrections that are needed to reconcile the predictions and data. We find that the best-fit scenarios do not give reasonable agreement to 2σ until at least a 40% non-factorisable contribution is added. Finally we consider the exclusive $B \to V\gamma$ decays, where we analyse the recently updated experimental data within QCD factorisation and present constraints on generic supersymmetric models using the mass insertion approximation.

Acknowledgements

First and foremost I would like to thank my supervisor, Patricia Ball for giving me the opportunity to work with her. I am grateful for the continued help and guidance throughout my time here, and if I have gained even a little of her efficiency and dedication then I am all the more thankful.

My thanks also go to the others I have had the pleasure to work with, especially to Martin Gorbahn for always trying to answer even my most stupid of questions, and to Gareth Jones, to whom I pass the torch to continue our project as I move on to higher climbs. A special mention must also go to the most excellent IPPP Céilidh Band for two fun years and three successful performances, particularly to Gudi Moortgat-Pick for her endless enthusiasm even when 800 miles away.

To Tom Birthwright, Paul Brooks, Mark Morley-Fletcher, Richard Whisker and James Haestier, the best office mates anyone could ever ask for. I am thankful for the relaxed atmosphere and willingness to share advice and adventures, despite the noise and the odd cricket ball.

Above all others, I have eternal gratitude for the unlimited support and encouragement from my Mum & Dad and my boyfriend Michael. People you can always talk to about anything is a wonderful blessing, even if far away. I have learnt so much from their calm and balanced outlook, that I hope I close this chapter of my life a better person. I know at least, there is nothing that a hug and a glass of Amarone cannot solve.

This work was supported by a PPARC studentship which is gratefully acknowledged.

Declaration

I declare that no material presented in this thesis has previously been submitted for a degree at this or any other university.

The research described in this thesis has been carried out in collaboration with Dr. Patricia Ball and has been published as follows:

- *Models for Light-Cone Meson Distribution Amplitudes*,
  Patricia Ball and Angelique N Talbot
  JHEP **0506** (2005) 063 [arXiv:hep-ph/0502115]

Contents

Introduction

The quest for comprehension of the physical world around us has dominated philosophy and science since the beginning of history. The ancient peoples looked up to the stars and the Gods for answers. The philosophers called upon the elements of nature – the Ancient Greeks, such as Leucippus, Democritus or Epicurus were the first to analyse and categorise the nature of all things. The belief that matter was composed of the four fundamental elements: earth, air, fire and water survived for over two thousand years. It was they who introduced the first "elementary particles", the indivisible *atomos*. As mysticism and natural philosophy morphed into scientific principle, the foundations of modern particle physics were established; beginning with the physical theories of Newtonian mechanics and gravity to the work of Thompson and Rutherford which allowed physics to leave the 19th century knowing the "indivisible atoms" were not in fact, indivisible at all.

The birth of the 20th century and the pioneering study of quantum mechanics was followed in the 1950s and 60s by the discovery of a bewildering variety and number of particles, once physicists had discovered that protons and neutrons were themselves composite particles. Yet, as with Mendeleev's periodic table of 1869, these particles could again be categorised and classified revealing a simple underlying structure in terms of a few elementary particles. The ideal to capture the beauty and complexity of nature in a simple mathematical form culminated in the formulation of the Standard Model of particle physics. This is based upon quantum field theory and gauge principles – combining the electromagnetic, weak and strong interactions into one unified theory. To date the Standard Model is the most successful mathematical theory of particle physics ever created. Particle accelerators have probed scales down to 10^{-16}cm, and this theory is consistent with virtually all physics down to this scale – indeed the Standard Model has passed indirect tests which probe even shorter distances.

The Standard Model has 25 elementary particles, so perhaps one may ask "how deep the rabbit hole goes"? The search for another layer of structure beneath the quarks and leptons has however so far been fruitless. More importantly, the Higgs boson which is required to generate mass for all of the Standard Model particles, has still not been discovered in collider experiments. There are a number of other unresolved issues with the Standard Model, that have led to recent conclusions that it cannot be complete, and is more likely to be an "effective theory" of some more encompassing theory at higher energy. These issues include some fundamental questions – such as the large number of arbitrary parameters that appear in the Standard Model Lagrangian. Why are there copies of quarks and leptons in three generations? Why are the masses split in the way they are? Why is the weak scale so different from the expected Planck scale? These questions cannot be answered with our current understanding. On top of all these questions, the problem of including General Relativity with the Standard Model still remains – combining gravity and quantum mechanics produces a non-renormalisable quantum field theory – this again suggests the presence of another theory, and hence some new physics at some higher energy.

Many ideas have been put forward to solve these problems, the most popular being supersymmetry, string theory or extra dimensions. Yet to date there is no theory that is truly simpler or less arbitrary than the Standard Model. More importantly, there is little experimental evidence for the existence of the holy grail of "new physics" and to guide the directions of the model builders. There are perhaps a handful of discrepancies between the theoretical predictions and experimental results, none of which have been significant enough to claim as new physics.

Within this thesis I work predominantly within the Standard Model, taking some brief forays into generic supersymmetric models. To summarise the motivation in a line, I say the following: 'before any claims of new physics can be made, we must be absolutely sure that our theory predictions are as accurate as we can make them'. The general aim being to better understand some elements of the Standard Model – specifically relating to the weak decays of B-mesons.

Beauty decays are a rich and powerful playground for studying flavour physics and CP violation – we can test predictions and constrain Standard Model parameters. From experimental observables (decay rates, parameters etc.) we can perform indirect searches for new physics via any measured deviation from the Standard Model expectation. Due to the rapid decay of the top quark, the b quark is the heaviest quark to bind into mesons which can be observed. Theoretical techniques based upon an expansion in the heavy b quark mass can provide vast simplifications of calculations and model-independent predictions of observables.

The theoretical framework within which any B-physics analysis is based is that of effective field theory, where the operator product expansion and renormalisation group evolution are invaluable techniques which we exploit. These encompass the concepts of factorisation which allow the calculation of decay amplitudes to be separated into perturbatively calculable short-distance Wilson coefficients, and long-distance matrix elements. We need some non-perturbative method such as QCD sum rules or Lattice QCD to calculate these matrix elements fully. For the exclusive two-body decays of the B-meson we can make use of the powerful technique of QCD factorisation which makes use of the hierarchy between the heavy b quark mass m_b, and the intrinsic scale of QCD, Λ_{QCD}. This gives a factorisation formula for the evaluation of hadronic matrix elements, and is a further separation of long-distance contributions from a set of perturbative short-distance contributions. The long-distance part must still be calculated via some non-perturbative technique, but is of much less complexity than the original matrix element.

QCD factorisation was developed by Beneke, Buchalla, Neubert and Sachrajda (BBNS) [1–3] for exclusive decays of the B into two mesons. The method is however not without its uncertainties, nor gaps where calculations cannot be completed without some model-dependent assumptions. It is these uncertainties, in the decays of the B-meson into non leptonic final states, that we discuss in this work.

The main new result of this work involves examining the uncertainty from one of the important non-perturbative inputs in the factorisation formulae, namely the light-cone distribution amplitudes of the light mesons. We develop and introduce a set of new models for the distribution amplitude which improve upon the truncated conformal expansion that is widely used in the literature. We quantitatively take into account contributions from higher order moments in the conformal expansion by a resummation to all orders. We show how these models can be expressed in terms of a few simple physical parameters that are directly related to experimental observables.

We then present an analysis of the second major source of uncertainty to QCD factorisation, namely corrections of order $(\Lambda_{\rm QCD}/m_b)$ to the leading calculation performed in the heavy quark limit $(m_b \to \infty)$, that cannot be calculated in a model-independent manner. Evidence suggests that QCD factorisation may considerably underestimate these corrections in some decay channels, specifically $B \to \pi\pi$. We construct various scenarios of additional non-factorisable contributions and use the wealth of experimental data currently available from the B factories and accelerator experiments to quantify how good the agreement is with the experimental measurements.

Finally, we present an analysis using recently released (August 2005) results on the $B \to (\rho, \omega)\,\gamma$ decays, based on the extension of QCD factorisation to radiative decays $B \to V\gamma$ by Bosch and Buchalla [4]. We also consider the possibility of new physics in the $b \to d\gamma$ and $b \to s\gamma$ decays, and use the new experimental results to constrain contributions from generic minimal supersymmetric models using the mass insertion approximation.

The structure of the thesis can be outlined as follows:

We begin with a whistlestop tour of the basic concepts of the Standard Model and the theoretical techniques required for an analysis in effective field theory; renormalisation group perturbation theory and a discussion of the $\Delta B = 1$ effective Hamiltonian. We conclude this introductory chapter with a brief introduction to two important non-perturbative techniques: QCD sum rules and Lattice QCD. We make use of many results from these methods and so it is important to understand their basis and limitations.

Chapter 2 provides an in-depth discussion on the formulation of QCD factorisation. We begin by placing it in context with a discussion of naive factorisation, and then follow with details of the structure of the factorisation formula and its input. We introduce the "non-factorisable corrections" and the problems with calculation of power-suppressed diagrams in a model-independent manner. We also include the isospin decomposition of $B \to \pi\pi$ amplitudes which is used extensively in our Chapter 4 analysis, and finally conclude with the limitations of the QCD factorisation framework.

Chapter 3 presents the main result of this work: the development of a new resummed model of the light-cone distribution amplitude for light mesons. We present a detailed discussion of the treatment of the DA, beginning with the application of conformal symmetry techniques, and the expression of the DA as a partial wave expansion in conformal spin. In order to place our new models in context we give a brief review of the literature and previous constructions with specific reference to the pion wavefunction, before going on to present full details of our new models. These sections are primarily based on the work presented in [5]. We discuss the full implications of the new models, and give numerical results to show how variation of the size of contribution from the higher-order moments can affect the branching ratios and CP asymmetry predictions, using the example of $B \to \pi\pi$.

We then go on in Chapter 4, to present our analysis on the non-factorisable corrections to the charmless B-decays. We investigate how the extensive experimental information available can be used to extract information about the size and nature of non-factorisable corrections that are needed to provide agreement between the prediction and measurement of $B \to \pi\pi$ branching fractions and CP asymmetries. We split the $B \to \pi\pi$ isospin amplitudes into factorisable and non-factorisable parts – the former being calculated via QCD factorisation and the later fitted to the experimental data. We show that there is evidence for sizable non-factorisable corrections in the $B \to \pi\pi$ system, and discuss the application of these results to $B \to \pi K$. We also discuss the possibility and likelihood of a charming penguin contribution to the charmless decays.

Our final analysis is presented in Chapter 5, and discusses the exclusive radiative decays $B \to (\rho, \omega)\gamma$ and $B \to K^*\gamma$. We examine the predictions from QCD factorisation in the context of the recent experimental results for this system. These decays are rare decays occurring with branching fractions of 10^{-5} or less, as they occur only at the loop level within the Standard Model. They are as such, very sensitive to the possibility of new physics. After introducing the basic principles and motivation for one of the most popular extensions of the Standard Model – the Minimal Supersymmetric Standard Model (MSSM) – we discuss how the mass insertion approximation can be utilised to constrain the parameter space for new physics in the $b \to (d, s)$ transitions. We give graphical constraints on insertions δ^d_{13} and δ^d_{23}.

Finally, we present our conclusions and outlook for the future in Chapter 6.

We consign various technical details to the Appendices: We give the explicit formulae for the $\Delta B = 1$ Wilson coefficients; the analytic evolution of the LCDA; a set of useful expressions from QCD factorisation, specifically the decay amplitudes for $B \to \pi\pi$ and the annihilation contributions to the $B \to V\gamma$ decays. We also present a full summary of numerical input parameters that have been used in our analyses.

Chapter 1

Basic concepts of B-physics

It's a job that's never started that takes longest to finish

J.R.R. Tolkien

The Standard Model is the cornerstone of particle physics and this chapter introduces its most pertinent features. We begin with a brief summary of the structure of the Standard Model and then introduce the concepts of effective theories that underpin calculations of B-decays. Via a discussion on the renormalisation group we give the full effective Hamiltonian for $\Delta B = 1$ decays. Finally, we discuss two important methods of calculating non-perturbative information – QCD sum rules and Lattice QCD.

1.1 The Standard Model

The Standard Model is the most successful and comprehensive theory of particle interactions to be developed in modern times. The model conjoins the theories of strong and electroweak forces into a unified framework based upon gauge symmetries. The dynamics can be described by a single fundamental Lagrangian, constructed of contributions from the three sectors: Quantum Chromodynamics (QCD), electroweak interactions and the Higgs sector. The gauge structure of the Standard Model is summarised as

$$SU(3)_C \otimes SU(2)_L \otimes U(1)_Y$$

QCD is the theory of the strong interaction that describes the gauge interactions between quarks and gluons, and was first introduced in the 1970's [6–10]. This force acts upon "colour charge" and is based upon the gauge group $SU(3)_C$. The eight generators of this group represent eight force carriers (the gluons) which communicate the force between coloured objects. The quarks carry colour charge and most importantly so do the gluons due to the *Yang-Mills* or non-Abelian nature of the QCD gauge theory; this allows the gluons to interact with each other and is an essential ingredient in the *asymptotic freedom* of QCD. This property allows the perturbative treatment of the strong interactions at short distances – where the coupling constant α_s becomes small. At long distances, i.e small energies, the coupling becomes large and there is a total confinement of the quarks into colourless hadrons. Figure 1.1 shows the running of the strong coupling with the energy scale.

The next sector of the Standard Model is that of the electroweak interactions, described by the Glashow-Salam-Weinberg model [12–14] and which is based on the gauge group $SU(2)_L \otimes U(1)_Y$. This theory is a unified treatment of the weak and electromagnetic interactions, where the full group is spontaneously broken to QED $U(1)_Q$. This is the Abelian theory of pure electromagnetic interactions, which has the photon as its propagator. The weak interaction controls all particle decays which do not proceed via the dominant strong

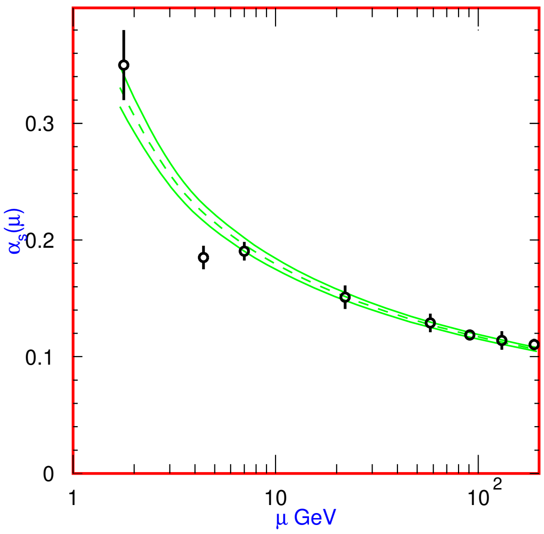

Figure 1.1: Running of $\alpha_s(\mu)$ with energy scale μ and summary of experimental measurements. Data points are (in increasing μ) from τ widths, Υ decays, deep inelastic scattering, JADE data, TRISTAN data and e^+e^- event shapes [11].

or electromagnetic interactions. The weak decays of the B-meson involve a change of flavour of the b quark, and are controlled by a *charged current interaction*. We discuss the dynamics of flavour in detail in the next section. The spontaneous symmetry breaking of the electroweak theory occurs via the non-zero vacuum expectation value of the Higgs field – a scalar isospin doublet

$$\phi = \begin{pmatrix} \phi^+ \\ \phi^0 \end{pmatrix} \tag{1.1}$$

The Higgs field has four degrees of freedom, three of which provide masses to the electroweak gauge bosons W^+, W^-, Z^0. The remaining degree of freedom is theorised to manifest itself as a massive scalar boson, but to date there has been no experimental detection to verify this claim. Data from electroweak precision tests suggest the Higgs mass m_H, should be light, and a lower bound from LEP exists of ~ 114GeV [15].

It would seem that the Higgs is the last missing piece in the particle puzzle. However even if the Higgs is found, there are still a number of issues that need to be addressed: for example, there is yet to be a consistent method of incorporating gravity into the model, nor is there an inclusion of masses for the neutrinos and their recently discovered oscillations. We also must address the *hierarchy problem* that exists if the Higgs is discovered as light, instead of having a mass $\sim 10^{16}$GeV as would be expected from calculation of quantum corrections to m_H.

Many different scenarios have been developed to explain these issues and many more which are not elaborated upon here. However, before one can study extensions and revisions of the Standard Model, we must understand properly the Standard Model itself! This thesis is concerned with the theory behind decays of the B-meson, and so we now introduce and discuss in detail the most relevant sector of the Standard Model – the dynamics of flavour.

1.1.1 The flavour sector

The fermions appear in the Standard Model in three generations, each generation identical in all its quantum numbers differing only by the masses of the particles. Concerning the electroweak interactions, the quarks and leptons are spilt into left-handed doublets and a right-handed singlet under the gauge group $SU(2)_L$. These contain the leptons:

$$\begin{pmatrix} \nu_e \\ e^- \end{pmatrix}_L \quad \begin{pmatrix} \nu_\mu \\ \mu^- \end{pmatrix}_L \quad \begin{pmatrix} \nu_\tau \\ \tau^- \end{pmatrix}_L$$

$$e_R \qquad\quad \mu_R \qquad\quad \tau_R$$

and the quarks:

$$\begin{pmatrix} u \\ d' \end{pmatrix}_L \quad \begin{pmatrix} c \\ s' \end{pmatrix}_L \quad \begin{pmatrix} t \\ b' \end{pmatrix}_L$$

$$\begin{array}{ccc} u_R & c_R & t_R \\ d_R & s_R & b_R \end{array}$$

The existence and nature of the right-handed neutrino is still under question and is currently subject to a great amount of theoretical and experimental probing [16, 17]. This does not affect our subset of non-leptonic B-decays so we retain the "standard", massless neutrino version of the Standard Model.

The electroweak interactions are described by the following Lagrangian, which is made up of a *charged current* and a *neutral current*.

$$\begin{aligned} \mathcal{L}_{\rm int}^{\rm EW} &= \mathcal{L}_{CC} + \mathcal{L}_{NC} \\ &= -\frac{g}{\sqrt{2}} \left[J_\mu^+ W^{+\mu} + J_\mu^- W^{-\mu} \right] - e\, J_\mu^{\rm em} A^\mu - \frac{g}{\cos\theta_W} \left[J_\mu^0 Z^\mu \right] \end{aligned}$$

The neutral current part of the Lagrangian is made up of the neutral electromagnetic and weak currents $J_\mu^{\rm em}$ and J_μ^0 which are given in terms of the (electric) charge and isospin of the fermions. We have:

$$\begin{aligned} J_\mu^{\rm em} &= Q_f\, \bar{f} \gamma_\mu f \\ J_\mu^0 &= \bar{f} \gamma_\mu \left[\left(I_z^f - 2 Q_f \sin^2\theta_W \right) - I_z^f \gamma_5 \right] f \end{aligned}$$

summing over all flavours. The charged current in the quark sector is given by

$$J_\mu^+ = \left(\bar{u},\, \bar{c},\, \bar{t}\right)_L \gamma_\mu \, V_{\rm CKM} \begin{pmatrix} d \\ s \\ b \end{pmatrix}_L$$

where the L subscript again represents the left-handed projector $\frac{1}{2}(1-\gamma_5)$ which reflects the vector – axial-vector $(V-A)$ structure of the weak interaction. $V_{\rm CKM}$ is the Cabbibo-Kobayashi-Maskawa (CKM) matrix [18, 19] and is a 3×3 unitary mixing matrix which rotates the mass eigenstates $(d,\, s,\, b)$ into their weak eigenstates $(d',\, s',\, b')$, and allows for transitions between the quark generations. The leptonic sector is described by an analogous mixing matrix which (in the absence of neutrino masses) is given by the unit matrix.

Symbolically the CKM matrix is written as

$$V_{\rm CKM} = \begin{pmatrix} V_{ud} & V_{us} & V_{ub} \\ V_{cd} & V_{cs} & V_{cb} \\ V_{td} & V_{ts} & V_{tb} \end{pmatrix} \tag{1.2}$$

Unitarity ensures that there are no flavour changing neutral currents at tree level. The elements V_{ij} are in general complex numbers which are restricted only by the unitarity condition – they are free parameters of the Standard Model and can only be determined by experiment. In general, an $n \times n$ unitary matrix is described by n^2 parameters. If this were to correspond to n quark doublets say, then the phases of each of the $2n$ quark states can be redefined whilst leaving the Lagrangian invariant. Hence, V should contain $n^2 - (2n-1)$ real parameters. As an orthogonal $n \times n$ matrix can have only $\frac{1}{2}n(n-1)$ real parameters, then we will be left with $n^2-(2n-1)-\frac{1}{2}n(n-1) =$

$\frac{1}{2}(n-1)(n-2)$ independent residual phases in the quark mixing matrix. Thus, we see that $V_{\rm CKM}$ must be parameterised by three independent angles and one complex phase; it is this phase which leads to a non-zero imaginary part of V and which is essential to describing CP violation in the Standard Model.

The standard parameterisation of $V_{\rm CKM}$ is written in terms of three angles θ_{ij} $(i,j = 1,2,3)$ and a CP violating phase δ [11]. The most useful parameterisation we use in this work is the *Wolfenstein parametrisation* [20], where each element is expanded as a power series in the small parameter $\lambda = |V_{us}| \approx 0.22$. This reads to $\mathcal{O}(\lambda^3)$ as

$$V_{\rm CKM} = \begin{pmatrix} 1-\frac{\lambda^2}{2} & \lambda & A\lambda^3(\rho - i\eta) \\ -\lambda & 1-\frac{\lambda^2}{2} & A\lambda^2 \\ A\lambda^3(1-\rho-i\eta) & -A\lambda^2 & 1 \end{pmatrix} \tag{1.3}$$

We can extend this to higher orders in λ, and corrections up to order $\mathcal{O}(\lambda^5)$ alters only the element V_{td}, transforming $\rho \to \bar{\rho} = \rho\,(1-\lambda^2/2)$ and $\eta \to \bar{\eta} = \eta\,(1-\lambda^2/2)$. The latest experimental determination of these parameters is included in a full summary of input parameters which is given in Appendix D.

1.1.2 Unitarity triangle

The unitarity of the CKM matrix gives six independent relations, each of which can be geometrically represented as triangles in an Argand diagram. The relation that is normally employed to represent unitarity in the B-system is

$$V_{ud}V_{ub}^* + V_{cd}V_{cb}^* + V_{td}V_{tb}^* = 0 \tag{1.4}$$

A phase convention is chosen where $V_{cd}V_{cb}^*$ is real and we rescale the triangle by $|V_{cd}V_{cb}^*| = A\lambda^3$. Graphing this in the complex plane (ρ, η) leads to a the *unitarity triangle* with co-ordinates of the vertices at (0,0) and (1,0) and the apex at $(\bar{\rho}, \bar{\eta})$ as shown in Figure 1.2.

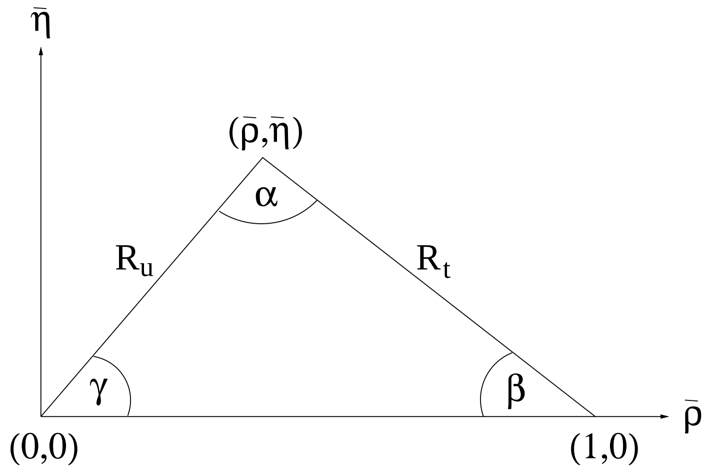

Figure 1.2: The unitarity triangle.

The sides are expressed as

$$\begin{aligned} R_u &\equiv \frac{|V_{ud}V_{ub}^*|}{|V_{cd}V_{cb}^*|} = \sqrt{\bar{\rho}^2 + \bar{\eta}^2} \\ R_t &\equiv \frac{|V_{td}V_{tb}^*|}{|V_{cd}V_{cb}^*|} = \sqrt{(1-\bar{\rho})^2 + \bar{\eta}^2} \end{aligned} \tag{1.5}$$

We introduce the shorthand $\lambda_p^{(d)} = V_{pb}V_{pd}^*$ which is used extensively in phenomenological applications. The unitarity relation (1.4) is invariant under phase transformations, which means that the sides and angles of the triangle remain unchanged with a change of phase – hence they are physical observables. These, and the elements of V_{CKM} have been subject to as many experimental determinations as possible in an attempt to over-constrain the parameters of the triangle and to test the Standard Model. The constraints can come from a wide variety of different decays and parameters: for example

$B^0 \to J/\psi K_S$ for $\sin 2\beta$; $B \to \rho\pi$, $B \to \pi\pi$ for α... These constraints are neatly summarised graphically in Figure 1.3[1].

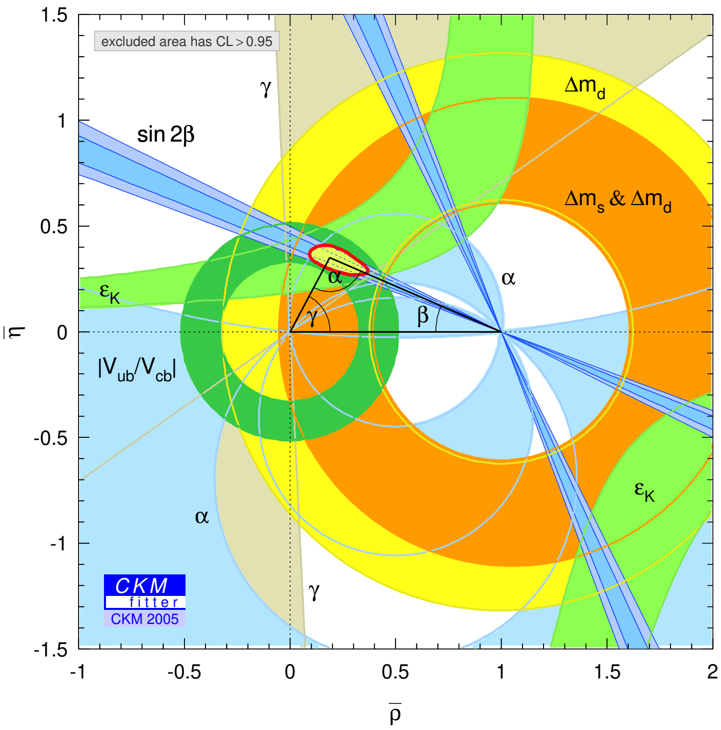

Figure 1.3: Constraints on the unitarity triangle from global CKM fit as performed by CKM Fitter Group [21].

1.2 B decays and effective field theory

There are three types of decays of the B-meson, categorised by the final state decay products. Firstly there are the leptonic decays, such as $B^+ \to \ell^+\nu_\ell$ and semi-leptonic decays such as $B^0 \to D^-\ell^+\nu_\ell$. The decays $B \to \ell^+\nu_\ell + X$, with X as anything, accounts for around 10% of the total B decay rate. Finally, and most important in the context of this work, are the fully hadronic (non-leptonic) decays. The complication of calculating weak decays in QCD is illustrated in Figure 1.4. This demonstrates the non-trivial interplay between

[1]Updated results and plots available at: http://ckmfitter.in2p3.fr.

the strong and electroweak forces which determine the dynamics of the decay.

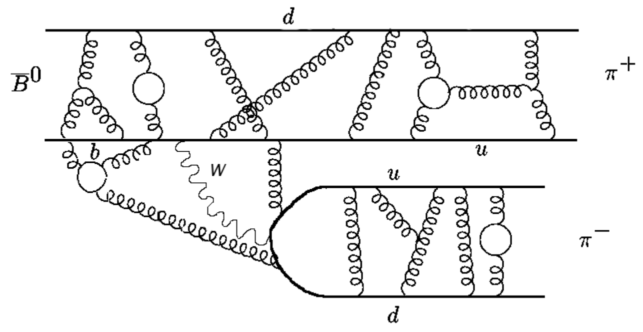

Figure 1.4: Illustration of QCD effects in $B \to \pi\pi$ decay.

The decay is characterised by several very different energy scales, from the mass of the W-boson and the heavy quarks to the intrinsic QCD scale and the masses of the light quarks. We have the ordering

$$m_t, M_W \gg m_{b,c} \gg \Lambda_{QCD} \gg m_{u,d,s}$$

QCD effects at short distances (i.e. that at higher energies) can be calculated perturbatively thanks to the asymptotic freedom of the theory. However, there are unavoidable long-distance dynamics from the confining of light-quarks into bound states – the hadrons. These are characterised by a typical hadronic scale of $\mu \sim 1\text{GeV}$, $\alpha_s(\mu)$ is no longer small at this scale so we cannot use perturbation theory. This means that there are non-perturbative QCD interactions which enter into the calculation of the decay.

To systematically disentangle the long and short distance contributions we make use of the *operator product expansion* (OPE) [22–24]. The basic idea is that any decay amplitude can be expanded schematically in terms of $1/M_W$, since M_W is much heavier than all of the other relevant momentum scales. The products of the quark current operators that interact (via the $W-$ exchange) are expanded into a series of local operators Q_i multiplied by a *Wilson coefficient* C_i. These coefficients represent the strength that a given operator enters into the amplitude. Schematically we have

$$A = C_i \left(M_W/\mu, \alpha_s \right) \cdot \langle Q_i \rangle + \mathcal{O}\left(p^2/M_W^2 \right) \tag{1.6}$$

In this way we can define an *effective weak Hamiltonian* to describe weak interactions at low energies. In this effective theory the W boson and the top quark are removed as explicit degrees of freedom – i.e. they are "integrated out". We describe this as an effective field theory with n_f "active" quarks, i.e. at the scale of m_b, we have 5 active flavours. As a practical example of this we can consider the basic (tree-level) $W-$ exchange process of $b \to du\bar{u}$, for which the OPE gives the amplitude:

$$\begin{aligned} A(b \to du\bar{u}) &= -\frac{G_F}{\sqrt{2}} V_{ud}^* V_{ub} \frac{M_W^2}{k^2 - M_W^2} \langle Q \rangle \\ &= \frac{G_F}{\sqrt{2}} V_{ud}^* V_{ub}\, C \cdot \langle Q \rangle + \mathcal{O}\left(\frac{k^2}{M_W^2} \right) \end{aligned}$$

with $C = 1$ and the local operator $Q = \left(\bar{d}u\right)_{V-A} \left(\bar{u}b\right)_{V-A}$ This is represented diagrammatically in Figure 1.5.

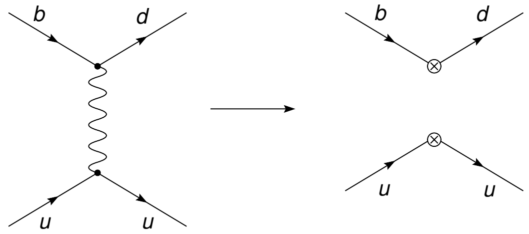

Figure 1.5: Tree-level diagram for $b \to du\bar{u}$.

The full weak (effective) Hamiltonian, including QCD and electroweak corrections has the following structure

$$\mathcal{H}_{eff} = \frac{G_F}{\sqrt{2}} \sum_i V^i_{\mathrm{CKM}}\, C_i(\mu)\, Q_i \tag{1.7}$$

where the factor V^i_{CKM} denotes the CKM structure of the particular operator. The decay rate for a two-body non-leptonic decay $B \to M_1 M_2$, is then simply

$$\Gamma = \frac{S}{16\pi m_B} |\langle M_1 M_2 | \mathcal{H}_{\mathrm{eff}} | B \rangle|^2 \tag{1.8}$$

with $S = 1/2$ if M_1 and M_2 are identical or $S = 1$ otherwise. The Q_i denote the relevant local operators which govern the particular decay in question; they can be considered as effective point-like vertices. The Wilson coefficients are then seen as "coupling constants" of these effective vertices, summarising the contributions from physics at scales higher than μ. Operators of higher dimensions corresponding to the terms of $\mathcal{O}\left(p^2/M_W^2\right)$ can be neglected.

In short, the OPE gives essentially a factorisation of short and long distance physics. The Wilson coefficients contain all the information about the short distance dynamics of the theory, i.e. that at energy scales greater or equal to μ. They depend intrinsically on the properties of the particles that have been integrated out of the effective theory, but not on the properties of the external particles. The factorisation implies that the coefficients are entirely independent of the external states, i.e, the C_i are the same for all amplitudes.

The long-distance physics, that at energy scales lower than μ, is parameterised purely by the process-dependent matrix elements of the local operators. The renormalisation scale μ can be thought of as a "factorisation scale" at which the full contribution splits into the high and low energy parts.

The matrix elements of the local operators are not easily calculated and as we have discussed, must contain a degree of non-perturbative information. Methods of determining these matrix elements using a systematic formalism are introduced in the next chapter. The Wilson coefficients however, can be fully calculated perturbatively by *matching* the full theory (with the W propagators) onto the effective theory; this ensures that the effective theory reproduces the corresponding amplitudes in the full theory. The steps to compute the C_i are summarised as:

- Compute full amplitude $\mathcal{A}_{full}$ with arbitrary external states
- Compute the matrix elements $\langle Q_i \rangle$ with same external states
- Extract the C_i using expression (1.6)

Both ultraviolet and infrared divergences occur in calculation of the amplitude $\mathcal{A}_{full}$; we discuss the removal of the UV-divergences in the next section. In the matching procedure, the IR-divergences are regulated by setting the momenta of the external quarks to $p^2 \neq 0$. From the point of view of the effective theory, all of the dependence on p^2 (representing the long-distance structure of the full amplitude) is contained in the matrix elements $\langle Q_i \rangle$. Hence, the Wilson coefficients are free from this dependence – and so independent of the external states. For convenience, in the matching the external states are chosen to be all on-shell quarks (or all off-shell), but in general any arbitrary momentum configuration will work.

This procedure will give the initial conditions for the Wilson coefficients at the matching scale, in our case $\mu = M_W$. We can then use the equations of *Renormalisation Group Evolution* (RGE) [25] to find the value at any desired scale.

1.2.1 Renormalisation group evolution

Put simply, renormalisation removes infinities from a theory. Feynman diagrams with internal loops often give ultraviolet divergences, as the virtual particle running through the loop is integrated over all possible momenta (from zero to infinity). Renormalisation allows the isolation and removal of all of these infinities from any physical quantity [26]. We relate the bare (unphysical) parameters with a set of renormalised (physical) parameters – such as masses or coupling constants – and rewrite all of the observables we need in terms of the new physical quantities. We can then "hide" all of the divergences in redefinitions of the parameters in the theory Lagrangian.

The procedure of renormalisation introduces a dependence on a dimensionful parameter known as the *renormalisation scale*, μ. We can subsequently obtain the scale dependence of the renormalised parameters from the μ-independence of the bare ones. If we choose a set of parameters at a certain scale q (which gives $g(q), m(q)$ etc.), then the set of all transformations that relate parameter sets with different values of q is known as the *renormalisation group*.

An an example, we can consider the coupling constant of QCD: $\alpha_s(\mu) = g^2/(4\pi)$. The *renormalisation group equation* (RGE) for the running coupling is given by

$$\mu \frac{dg(\mu)}{d\mu} = \beta(g) \tag{1.9}$$

where the *beta function*, $\beta(g)$, is related to the renormalisation constant for the coupling. In QCD this is given by

$$\beta(g) = -g \left\{ \left(\frac{g}{4\pi}\right)^2 \beta_0 + \left(\frac{g}{4\pi}\right)^4 \beta_1 + \dots \right\} \tag{1.10}$$

with

$$
\begin{aligned}
\beta_0 &= \frac{11}{3}N_c - \frac{2}{3}n_f \\
\beta_1 &= \frac{34}{3}N_c^2 - \frac{10}{3}N_c n_f - 2C_F n_f
\end{aligned}
$$

N_c is the number of colours, n_f the number of active flavours and $C_F = \frac{N_c^2-1}{2N_c}$. The leading order solution for the coupling $\alpha_s(\mu)$ is then found via

$$
\alpha_s(\mu) = \frac{\alpha_s(\mu_0)}{1 + \frac{\beta_0}{2\pi}\alpha_s(\mu_0)\ln\left(\frac{\mu}{\mu_0}\right)} \tag{1.11}
$$

This equation can be re-expressed in terms of a mass scale Λ, which is the momentum scale at which the coupling becomes strong as q^2 is increased. We have:

$$
\alpha_s(\mu) = \frac{2\pi}{\beta_0 \ln\left(\frac{\mu}{\Lambda}\right)} \tag{1.12}
$$

From (1.11) we can see that the renormalisation group equations allow for the resummation of large logarithms, which could otherwise be problematic. The large logarithms can spoil the validity of the perturbative expansion, even if the value of α_s is still small. The form of the correction terms to higher orders can be summarised in the following diagram [27], denoting for example, the "large log" at scale $\Lambda = M_W$: $L \equiv \ln \mu/M_W$.

$$
\begin{array}{cccccc}
 & & \text{LL} & \text{NLL} & & \\
\alpha_s^1 & \rightarrow & \alpha_s L & \alpha_s & & \\
\alpha_s^2 & \rightarrow & \alpha_s^2 L^2 & \alpha_s^2 L & \alpha_s^2 & \\
\alpha_s^3 & \rightarrow & \alpha_s^3 L^3 & \alpha_s^3 L^2 & \alpha_s^3 L & \alpha_s^3 \\
 & & \Downarrow & \Downarrow & & \\
 & & \mathcal{O}(1) & \mathcal{O}(\alpha_s) & &
\end{array}
$$

The rows of this table correspond to the expansion in powers of α_s from ordinary perturbation theory. This is no longer true in the presence of the large logarithms, but is resolved by resumming the terms $(\alpha_s L)^n$ to all orders in n. This re-organisation is obtained by solving the RGE equation. Expanding the leading order terms in (1.11) we have

$$\alpha_s(\mu) = \alpha_s(\mu_0) \sum_{m=0}^{\infty} \left(\frac{\beta_0}{4\pi} \alpha_s(\mu_0) \ln \frac{\mu_0^2}{\mu^2} \right)^m \tag{1.13}$$

This sums logs of the form $\ln \mu_0^2/\mu^2$ which can become large if $\mu_0 \gg \mu$. We then speak of "leading logarithmic order" (LL) and "next-to-leading logarithmic order" (NLL), although we carelessly use these synonymously with the terms LO and NLO.

1.2.2 RGE for Wilson coefficients

As discussed, the Wilson coefficients can be interpreted as effective couplings for the operators Q_i of the effective Hamiltonian. These operators still have to be renormalised (or more specifically the operator matrix elements $\langle Q_i \rangle^{(0)}$). This is done using renormalisation constants for each of the four external quark fields $Z_q^{1/2}$ and a matrix Z_{ij} which allows operators with equivalent quantum numbers to mix under renormalisation: we have $\langle Q_i \rangle^{(0)} = Z_q^{-2} Z_{ij} \langle Q_j \rangle$. Since the operators are always accompanied by their corresponding Wilson coefficients the operator renormalisation is in general entirely equivalent to the renormalisation of their "coupling constants" C_i. We can therefore write the RGE for the Wilson coefficients as

$$\mu \frac{d}{d\mu} C_i(\mu) = \gamma_{ji}(\mu) C_j(\mu) \tag{1.14}$$

where $\gamma_{ij} = \hat{\gamma}$ is the *anomalous dimension matrix* for the operators, defined via

$$\gamma_{ij}(\mu) = Z^{-1}_{ik} \frac{dZ_{kj}}{d\,\ln\mu} \tag{1.15}$$

The anomalous dimension matrix (ADM) is itself given in terms of a perturbative expansion in α_s

$$\gamma_{ij} = \left(\frac{\alpha_s}{4\pi}\right)\gamma^{(0)}_{ij} + \left(\frac{\alpha_s}{4\pi}\right)^2\gamma^{(1)}_{ij} + \mathcal{O}(\alpha_s^3) \tag{1.16}$$

We can then give the solution for the Wilson coefficients in terms of an evolution matrix $U_{ij}(\mu,\mu_0)$

$$C_i(\mu) = U_{ij}(\mu,\mu_0)C_j(\mu_0)$$

The evolution matrix is given generally by

$$\hat{U}(\mu,\mu_0) = \int_{g(\mu_0)}^{g(\mu)} dg \frac{\hat{\gamma}^T(g)}{\beta(g)} \tag{1.17}$$

At leading order, this reduces simply to

$$\begin{aligned} \hat{U}^{(0)}(\mu,\mu_0) &= \left(\frac{\alpha_s(\mu_0)}{\alpha_s(\mu)}\right)^{\frac{\hat{\gamma}^{(0)T}}{2\beta_0}} \\ &= V\left[\left(\frac{\alpha_s(\mu_0)}{\alpha_s(\mu)}\right)^{\frac{\boldsymbol{\gamma}^{(0)}}{2\beta_0}}\right]_D V^{-1} \end{aligned} \tag{1.18}$$

where V is the matrix that diagonalises $\hat{\gamma}^{(0)T}$ and $\boldsymbol{\gamma}^{(0)}$ is the vector (with elements $\gamma_i^{(0)}$) containing all of the eigenvalues of the leading order ADM $\hat{\gamma}^{(0)}$.

$$\gamma_D^{(0)} = V^{-1}\gamma^{(0)T}V$$

It is also possible to calculate the exponentiated matrix directly without diagonalisation. At the next-to-leading order, we find that the evolution matrix becomes a little more involved, and includes dependence on the NLO ADM $\hat{\gamma}^{(1)}$. The solution is

$$\hat{U}(\mu,\mu_0) = \left[1 + \frac{\alpha_s(\mu)}{4\pi}\hat{J}\right] \hat{U}^{(0)}(\mu,\mu_0) \left[1 - \frac{\alpha_s(\mu_0)}{4\pi}\hat{J}\right] \tag{1.19}$$

with

$$\begin{aligned}
\hat{J} &= V\hat{S}V^{-1} \\
S_{ij} &= \delta_{ij}\gamma_i^{(0)}\frac{\beta_1}{2\beta_0^2} - \frac{G_{ij}}{2\beta_0 + \gamma_i^{(0)} - \gamma_j^{(0)}} \\
\hat{G} &= V^{-1}\hat{\gamma}^{(1)T}V
\end{aligned}$$

In the weak decays of B-mesons the matching is performed at the scale M_W, so that both the top-quark and the W-boson are integrated out (removed as explicit degrees of freedom). This gives matching conditions and hence values for the Wilson coefficients at this scale. We can then use the procedures just outlined to evolve these down to the appropriate scale, e.g m_b. We write

$$C_i(\mu) = \hat{U}(\mu, M_W)C_i(M_W) \tag{1.20}$$

with an expansion of the coefficients given to the same accuracy as the evolution, i.e. to NLO

$$C_i(M_W) = C_i^{(0)}(M_W) + \frac{\alpha_s(M_W)}{4\pi}C_i^{(1)}(M_W) \tag{1.21}$$

The scale can be any required, e.g $\mu = m_b$ for B-decay amplitudes or $\mu \sim$

1GeV for discussions on the wavefunctions of light mesons. Care must be taken to include the effects of the flavour thresholds at lower energies, which can be done simply, by applying the evolution equations in two stages with the correct number of active quark flavours in each stage.

1.2.3 The $\Delta B = 1$ effective Hamiltonian

We consider a basis for computing non-leptonic B decays with change in beauty of $\Delta B = 1$. The expressions below are for those decays with unchanging strangeness and charm, $\Delta S = \Delta C = 0$, but can easily be adapted to decays with $\Delta S = 1$ by replacing $d \to s$.

We begin with the tree-level process without QCD corrections, which is described by one dimension 6 operator. When we include QCD corrections, another current-current operator is generated: these are labelled as Q_1 and Q_2, although sometimes in the literature their definitions are interchanged. The tree-level diagram and the $\mathcal{O}(\alpha_s)$ corrections to it are shown in Figure 1.6.

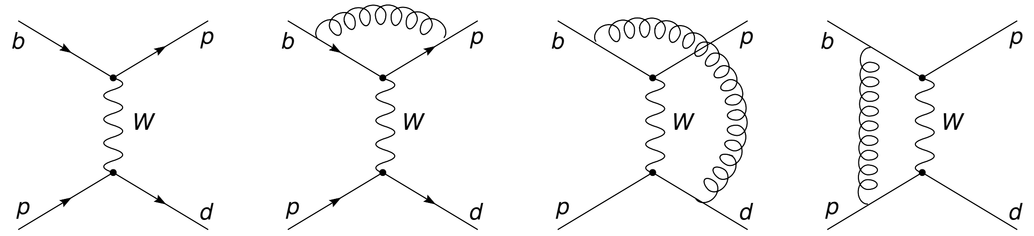

Figure 1.6: Tree-level exchange and $\mathcal{O}(\alpha_s)$ corrections; $p = u, c$.

QCD corrections also produce four new gluonic *penguin operators* Q_3 to Q_6. If we include terms from the electroweak sector up to $\mathcal{O}(\alpha)$ we obtain an additional set of *electroweak penguin operators* Q_7 to Q_{10}. These are considered as a next-to-leading order effect due to their proportionality to the electroweak gauge coupling α. There are, in principle, QED corrections to the matrix elements of the QCD operators $Q_1 \ldots Q_6$, but these are suppressed and usually neglected. We also have additional terms which contribute in some $\Delta B = 1$ processes, namely the magnetic penguin operator $Q_{7\gamma}$ (which is important for the radiative decays) and the chromomagnetic penguin Q_{8g}. Examples of all these diagrams are shown below in Figures 1.7 and 1.8.

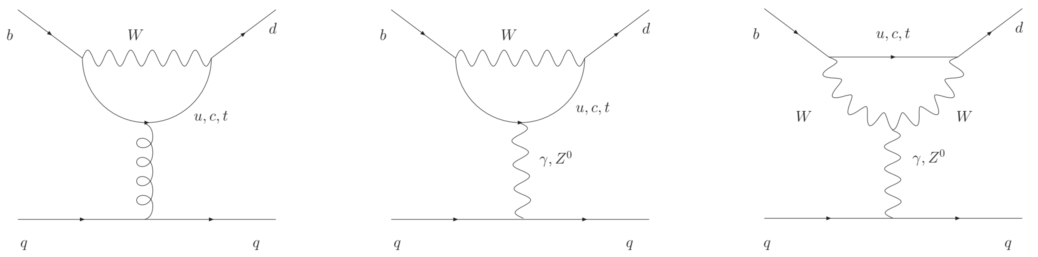

Figure 1.7: Gluonic and electroweak penguin diagrams.

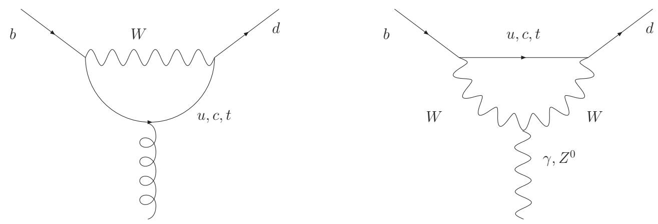

Figure 1.8: Magnetic photon and chromomagnetic penguin diagrams.

This leads us to a $\Delta B = 1$ effective Hamiltonian of

$$\mathcal{H}_{\text{eff}} = \frac{G_F}{\sqrt{2}} \sum_{p=u,c} \lambda_p \left[C_1 Q_1^p + C_2 Q_2^p + \sum_{i=3,\ldots,10} C_i Q_i + C_{7\gamma} Q_{7\gamma} + C_{8g} Q_{8g} \right] + \text{h.c.} \tag{1.22}$$

with the full operator basis given as

$$
\begin{aligned}
Q_1^p &= \left(\bar{d}_i p_j\right)_{V-A} (\bar{p}_j b_i)_{V-A} \\
Q_2^p &= \left(\bar{d} p\right)_{V-A} (\bar{p} b)_{V-A} \\
Q_3 &= \left(\bar{d} b\right)_{V-A} \sum_q (\bar{q} q)_{V-A} \\
Q_4 &= \left(\bar{d}_i b_j\right)_{V-A} \sum_q (\bar{q}_j q_i)_{V-A} \\
Q_5 &= \left(\bar{d} b\right)_{V-A} \sum_q (\bar{q} q)_{V+A} \\
Q_6 &= \left(\bar{d}_i b_j\right)_{V-A} \sum_q (\bar{q}_j q_i)_{V+A} \\
Q_7 &= (\bar{s} b)_{V-A} \sum_q \tfrac{3}{2} e_q \, (\bar{q} q)_{V+A} \\
Q_8 &= (\bar{s}_i b_j)_{V-A} \sum_q \tfrac{3}{2} e_q \, (\bar{q}_j q_i)_{V+A} \\
Q_9 &= (\bar{s} b)_{V-A} \sum_q \tfrac{3}{2} e_q \, (\bar{q} q)_{V-A} \\
Q_{10} &= (\bar{s}_i b_j)_{V-A} \sum_q \tfrac{3}{2} e_q \, (\bar{q}_j q_i)_{V-A} \\
Q_{7\gamma} &= \frac{e}{8\pi^2} m_b \, \bar{s} \, \sigma^{\mu\nu} (1+\gamma_5) F_{\mu\nu} \, b \\
Q_{8g} &= \frac{g}{8\pi^2} m_b \, \bar{s}_i \, \sigma^{\mu\nu} (1+\gamma_5) T^a_{ij} \, b_j \, G^a_{\mu\nu}
\end{aligned}
$$

We use the usual notation that $(\bar{q}_1 q_2)_{V\pm A} = \bar{q}_1 \gamma_\mu (1 \pm \gamma_5) q_2$; i, j are colour indicies, $F_{\mu\nu}$ and $G_{\mu\nu}$ are the photonic and gluonic field strength tensors respectively. There is also implied summation over all flavours q. The matching conditions for the Wilson coefficients and the anomalous dimension matrices required for scale evolution are given in detail in Appendix A.

1.3 QCD sum rules

In later chapters we make use of a number of results from the technique to study hadronic structure known as *QCD sum rules* [28]. Without any detailed technical discussion, we take a moment here to briefly describe the purpose and form of the sum rule approach. They were originally used to calculate simple characteristics of hadrons, such as masses, but are also applicable to more complicated parameters such as form factors or hadronic wave functions. The sum rule approach is used to calculate non-perturbative effects in QCD.

The hadrons are represented by interpolating quark currents, which are formed into correlation functions. These are treated in an operator product expansion to separate the short and long distance contributions from the quark-gluon interactions. The short distance parts are again calculable in normal perturbative QCD. The long-distance contributions are parameterised by universal vacuum condensates or by *light-cone distribution amplitudes*. (See later chapters). The results of this calculation are then matched via rigorous *dispersion relations* to a sum over the hadronic states. This gives us a sum rule which allows us to calculate the observable characteristics of hadronic ground states. Together with experimental data this can be used to determine quark masses and universal non-perturbative parameters.

There are some limitations in the accuracy of the sum rules which come from the approximation of the correlation functions. Additionally there is uncertainty from the dispersion integrals, which have complicated and often unknown structure. The method is however very successful and all uncertainties can be traced and estimated well.

The classical sum rule approach is based on two-point correlators, but this is not the only approach. Combining sum rule techniques with a light-cone expansion gives the very successful technique of *light-cone sum rules* [29,30]. This procedure expands the products of currents near the light-cone and involves a partial resummation of local operators.

1.4 Lattice QCD

Ideally we would like to be able to estimate all of the fundamental parameters of QCD from first principles. To do this, we need complete quantitative control over both the perturbative and non-perturbative aspects of QCD. The numerical simulations of *Lattice QCD* in principle are able to do this – answering almost any question about QCD and confinement, from Yang-Mills theories to the running coupling constant to the topology of the QCD vacuum. In our work, the relevant parameters that can be determined via lattice techniques include decay constants [31, 32], form factors [33, 34] and hadronic matrix elements [32]. As with the results we frequently rely upon from QCD sum rules, it is important to understand the importance and limitations of lattice results that we use; a full review can be found in [35].

QCD can be expressed in Feynman path integrals, which need to be calculated in the continuous space-time in which we exist. This is very difficult but we can make an approximation by discretising the continuous four-dimensional space-time onto a 4-D lattice as represented in Figure 1.9. The Lagrangian consisting of fields and derivatives of fields is also discretised by replacing the continuum fields with fields at the lattice sites, and replacing the derivatives with finite differences of these fields. The path integrals over different field configurations become multi-dimensional integrals over the values of the fields at the lattice sites and on the links. These can be evaluated numerically, for example using Monte Carlo simulation; this is the basic tenet behind lattice QCD. The problem of solving a non-perturbative relativistic quantum field theory in transferred into a “simple” matter of numerical integration.

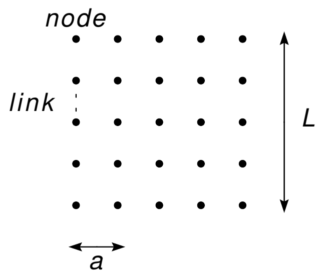

Figure 1.9: Nodes are separated by a lattice spacing of a. Quark fields live on the lattice sites (nodes) and gluons on the links connecting these sites.

Large amounts of computing power are required for simulations, and the computation time depends on a number of factors – the overall volume of the spacetime L^4 where L is often taken as $L \sim 1-2$fm, and the finiteness of the grid, $a \sim 0.05 - 0.1$fm. Ideally the grid spacing should be small enough that results are within a few percent of the continuum results. Errors associated with the discretisation are an important source of systematic errors in a lattice calculation that need to be controlled.

The purely gluonic part of QCD can be simply discretised onto the lattice but complications arise for the quarks due to their fermionic nature. There are however a number of different methods of including quarks on the lattice such as *Wilson quarks* or *staggered quarks*, each with its own improvements and disadvantages. Implementing an algorithm for quarks gives an additional problem as fermionic variables in path integrals require the calculation of a fermionic determinant – requiring hundreds of matrix inversions for every vacuum configuration considered. This calculation amounts to determining the non-local interaction between the gluons, i.e the computation of dynamical quark loops. There is no technical obstruction to performing this calculation and a number of methods exist for the discretisation of fermions, however the computation time and difficulty of the calculation increases by several orders of magnitude!

This has led to many simulations being performed in the *quenched approximation*, where vacuum configurations that include only gluons are considered. This neglects the additional term which gives rise to the sea quarks (and hence the ability to produce $q\bar{q}$ pairs from the vacuum). The quenched approximation performs satisfactorily for processes dominated by valence quarks, but for the converse dynamical quarks are required to produce correct answers. Unquenching can have other side effects such as allowing processes which require decays into $q\bar{q}$ pairs e.g. $g \to q\bar{q} \to g$ which will enable the strong coupling to run at the correct rate. This also means that decays such as $\rho \to \pi\pi$ are now visible on the lattice, but it will be difficult to determine m_ρ. The cost of including the dynamical quarks increases as we move to lighter and lighter quarks, and it is the lightest three u, d, s that have the most significant effect on most quantities.

Heavy quarks, such as the b quark could in principle be treated the same as the lighter quarks, however in order to gain sufficient accuracy an extremely fine lattice would be needed. Instead, exploiting the non-relativistic nature of the b quark bound states proves much more efficient. This can be done using several techniques including *static quarks* – using the heavy-quark limit of $m_b = \infty$ and *NRQCD* – a non-relativistic formulation of QCD.

Chapter 2

QCD factorisation

Still round the corner there may wait,

A new road or a secret gate.

"The Lord of the Rings", J.R.R. Tolkien

The concept of factorisation in its various forms is key to many of the applications of perturbative QCD, including deep inelastic scattering or jet production in hadron colliders. Perturbative QCD only describes quarks and gluons, so in observed, hadronic physics there will always be some relevant non-perturbative dynamics that must be isolated and dealt with in a systematic fashion. In the following sections, we describe the ideas of "naive factorisation" for the hadronic decays of heavy mesons, and then introduce the "improved QCD factorisation" formalism – a systematic method for treating exclusive two-body B decays. There have been a number of other approaches to try to describe non-leptonic B decays, although none have been nearly as successful as QCD factorisation. These methods include the perturbative QCD (pQCD) methods (which treats the form factors as perturbatively calculable quantities) or the soft-collinear effective theory (SCET), which is based upon factorisation of two energy scales: $m_b^2 \gg \Lambda_{\text{QCD}} m_b \gg \Lambda_{\text{QCD}}$. QCD factorisation is currently the accepted and most widely used methodology for treating B decays, and we work exclusively in this framework in this thesis. Finally, we conclude this chapter with a discussion of the limitations of the QCD factorisation method and ask how well predictions match up with the experimental data.

2.1 Naive factorisation

A complete understanding of the theoretical framework for non-leptonic B decays is a continuing challenge which is yet to be resolved. For two-body decays of $B \to M_1 M_2$, the major difficulty involves the evaluation of the hadronic matrix elements $\langle M_1 M_2 | Q_i | B \rangle$.

We introduced the concept of factorisation in relation to the OPE where we separate the long and short-distance contributions to decay amplitudes. Similarly, the hadronic matrix elements for B decays can also be factorised by disentangling the long and short-distance contributions. This seems intuitive for leptonic and semi-leptonic decays, where we can factorise the amplitude into a leptonic current and the matrix element of a quark current. Gluons do not interact with the leptonic current and so the factorisation is exact. For non-leptonic decays, the full matrix element is separated into a product of matrix elements of two quark currents; so we must also have "non-factorisable" contributions from gluons which can connect these two currents.

The first general method proposed is that of *naive factorisation* [36, 37].

Here the full matrix element is assumed to factorise into a product of matrix elements of simple, colour singlet, bilinear currents. The first is the transition matrix element between the B-meson and one of the final state mesons, and the second is the matrix element of the other final state meson being "created" from the vacuum. For example

$$\langle\pi^+\pi^-|(\bar{u}b)_{V-A}(\bar{d}u)_{V-A}|\bar{B}^0\rangle \longrightarrow \langle\pi^-|(\bar{d}u)_{V-A}|0\rangle\langle\pi^+|(\bar{u}b)_{V-A}|\bar{B}^0\rangle \tag{2.1}$$

These matrix elements can then be expressed in terms of a *form factor* $F^{B\to M_1}$ and *decay constant* f_{M_2}. The Hamiltonian is re-expressed in terms of effective coefficients C_i^{eff}. These are constructed from the Wilson coefficients and all of the scheme and scale dependent contributions from the hadronic matrix elements. This ensures the effective coefficients are free from these dependencies. The complete matrix element is then made up of the factorised matrix elements and the coefficients a_i, which are combinations of the effective Wilson coefficients

$$a_i = \left(C_i^{\text{eff}} + \frac{C_{i\pm1}^{\text{eff}}}{N_c}\right) + P_i \tag{2.2}$$

where P_i involves the QCD and electroweak penguins (but not taking into account final state flavour) and are zero for $i = 3,\, 5$.

A qualitative justification for this approach comes from the concept of *colour transparency* [38, 39] which implies the decoupling of soft (low-energy) gluons from colour-singlet pairs of quarks, e.g. the final state pion in example (2.1). This occurs as the heavy-quark decays are highly energetic, so the hadronisation of the $q\bar{q}$ pair occurs far away from the remaining quarks.

The main source of uncertainty in this approach is the neglect of the "non-factorisable" contributions, exacerbated by the assumption that all final state interactions are absent. Corrections arise from the exchange of gluons between the two quark currents, which allows a dynamical mechanism (namely re-scattering in the final state) to create a strong phase between different amplitudes. The second major issue is that the cancellation of renormalisation scale dependence in the amplitude is destroyed, as the scale independence of the form factor and decay constants in the factorised matrix element is in conflict with the scale dependence of the original matrix element. Unphysical dependencies are also caused by the Wilson coefficients at NLL level which develop scheme dependence in addition to the scale dependence, and for which there is no cancellation from the (scheme independent) factorised matrix elements.

2.2 QCD factorisation

QCD factorisation was introduced by Beneke, Buchalla, Neubert and Sachrajda (BBNS) [1, 2, 40], and is based upon the important simplifications that occur in the limit where the b quark mass is large as compared with the strong interaction scale, $m_b \gg \Lambda_{QCD}$. The factorisation that occurs in this approach is the separation of the long-distance dynamics (the matrix elements) and the short-distance interactions which depend only on the large scale m_b. The short-distance contributions are calculated perturbatively to order α_s, and the long-distance information is encoded in various process independent non-perturbative parameters, or is obtained directly from experiment. However, it is structurally much simpler than the original matrix elements.

In the limit $m_b \gg \Lambda_{QCD}$, the underlying physics involves the decoupling of fast-moving light mesons, produced from point-like interactions from the weak effective Hamiltonian, from the soft QCD interactions. This is a result of the concept of colour transparency as discussed above, the systematic implementation of which is provided by QCD factorisation. It also provides a soft factorisation which allows the matrix elements to be given at leading order in the Λ_{QCD}/m_b expansion. The full matrix elements can then be represented in the form

$$\langle M_1 M_2|Q_i|B\rangle = \langle M_1|j_1|B\rangle\langle M_2|j_2|0\rangle \left[1 + \sum_n r_n \alpha_s^n + \mathcal{O}\left(\Lambda_{QCD}/m_b\right)\right] \quad (2.3)$$

where r_n denote the radiative corrections in α_s, and j_i are bilinear quark currents. If the order α_s corrections are neglected, we see that at leading order in Λ_{QCD}/m_b we recover the naive factorisation results.

In the QCD factorisation approach, the non-factorisable power-suppressed corrections are in general neglected, with two non-trivial exceptions: the hard-scattering spectator interactions and annihilation contributions which are *chirally enhanced* and cannot be ignored. In the context of this thesis, it is important to note that these cannot be calculated within the actual framework of QCD factorisation; they are included in the BBNS approach via model-dependent assumptions. This will be discussed in detail in the following sections.

2.2.1 Structure of the QCD factorisation formula

The QCD factorisation framework is represented by a "master formula" for the matrix element $\langle M_1 M_2|Q_i|B\rangle$, where the final state mesons can be “heavy-light”(e.g. $B \to D\pi$) or “light-light” (such as $B \to \pi\pi$). For exclusive non-leptonic decays to two light mesons, we have the following expression for $\langle M_1 M_2 | Q_i | B \rangle$, to leading order in the Λ_{QCD}/m_b expansion:

$$\begin{aligned}\langle M_1 M_2 | Q_i | B \rangle &= F_j^{B\to M_1}(m_2^2) \int_0^1 du\, T_{ij}^I(u)\, \Phi_{M_2}(u) + [M_1 \leftrightarrow M_2] \\ &\quad + \int_0^1 d\xi\, du\, dv\, T_i^{II}(\xi, u, v)\, \Phi_B(\xi)\, \Phi_{M_1}(v)\, \Phi_{M_2}(u)\end{aligned} \tag{2.4}$$

Φ_M denote the *light cone distribution amplitudes* (LCDA) for the valence quark states. Both the LCDA Φ_M and the $B \to M$ form factor, are much simpler than the original non-leptonic matrix element, and can be calculated by some non-perturbative technique such as QCD sum rules, on the lattice, or taken directly from experiment.

The perturbative information is contained in the hard-scattering kernels $T_{ij}^I(u)$, $T_{ik}^I(v)$ and $T_i^{II}(\xi, u, v)$, which are calculable functions dependent on the light-cone momentum fractions of the constituent quarks in the light final state mesons (u, v) and the B meson (ξ). All of the hard-scattering kernels and the LCDA have a factorisation scale dependence. The expression is split into two categories of contributions – “type I” and “type-II”. The type-I contributions consist of the leading terms which give the tree level contributions, and hard vertex and penguin corrections at $\mathcal{O}(\alpha_s)$. The type II contributions originate from hard interactions between the spectator quark and the emitted meson, which enter at $\mathcal{O}(\alpha_s)$. If the spectator quark in the interaction can only form into one of the final state mesons (such as in $B^0 \to \pi^+ K^-$), then the second form factor term is absent.

We can see that from the tree level terms in T^I we reproduce the naive factorisation results, and the convolution integral in (2.4) will reduce to a meson decay constant. We also get a large simplification in the case where one of the mesons is heavy ($B \to H_1 M_2$), as the spectator interactions will be power-suppressed in the heavy quark limit and the type II kernel T^{II} is absent.

2.2.2 Non-perturbative parameters

We will now elaborate further on the non-perturbative input into the factorisation master formula, and introduce the concept of light-cone distribution amplitudes which will be discussed in detail in Chapter 3.

Light-cone distribution amplitudes for light mesons

The distribution amplitude $\Phi_M(u, q^2)$ is in essence a probability amplitude for a meson to be found in a particular state, i.e for finding a valence quark with a *light-cone* longitudinal momentum fraction u in the meson at a momentum q^2, independent of the process. The light-cone frame for some vector $p_\mu = (p_0,\, p_1,\, p_2,\, p_3)$, is a choice of co-ordinates which naturally distinguishes between the transverse and longitudinal degrees of freedom. Two of the spatial dimensions (transverse) remain unchanged and the other (longitudinal) spatial dimension is combined with the temporal co-ordinate via

$$p_\pm = \frac{p_0 \pm p_3}{\sqrt{2}} \tag{2.5}$$

so that $p_\mu = (p_+,\, p_-,\, \vec{p}_\perp)$, and $p^2 = 0$ for a light-like vector. The distribution amplitude is defined in terms of the expectation value of non-local operators, near the light-cone. For example, considering the pion distribution amplitude ϕ_π, we express the LCDA in terms of a matrix element of a gauge-invariant non-local operator defined between the vacuum and the pion [41]

$$\langle 0|\bar{d}(z)\gamma^{\mu}\gamma_5[z,0]u(0)|\pi(P)\rangle \tag{2.6}$$

$[x, y]$ is a path-ordered gauge factor along the straight line connecting the points x, y in order to preserve gauge invariance and is known as a *Wilson line*

$$[x,y] = Pexp\left[ig\int_0^1 dt\,(x-y)_{\mu}A^{\mu}(tx+(1-t)y)\right] \tag{2.7}$$

These matrix elements give a set of integral equations of two and three particle light-cone distribution amplitudes. These distribution amplitudes can be classified in terms of *twist*. The twist of an operator is defined as its "dimension minus spin", i.e.

$$t = d - s \tag{2.8}$$

This is related to power counting of $1/Q$, where Q denotes momentum transfer, and controls the relative size of contributions from the operator product expansion. In general, an operator of dimension d in the OPE has a coefficient function with dimension $(\text{mass})^{6-d}$ [42], corresponding to a suppression factor in the Fourier transform of the OPE of

$$\left(\frac{1}{Q}\right)^{d-2} \tag{2.9}$$

If the operator has spin s, the operator matrix element gains s contributions from the momentum P^{μ}, so the total contribution is of the order of

$$\left(\frac{2P\cdot q}{Q^2}\right)^{s}\left(\frac{1}{Q}\right)^{d-s-2} \tag{2.10}$$

with $q^2 = -Q^2$. The leading twist is then $t = 2$, allowing us to identify a distribution amplitude of twist-2 and also of higher twists. The higher-twist distribution amplitudes contain contributions from lower twists as well. For example the twist-3 DA has contributions from both twist-3 and twist-2 operators. In the QCD factorisation formalism, and in Chapter 3, where we study models of LCDAs, we consider the simplest case of the leading-twist distribution amplitudes. From the matrix element in (2.6) the twist-2 DA is defined as

$$\langle 0|\bar{d}(z)\gamma^\mu\gamma_5[z,0]u(0)\pi(P)\rangle|_{z^2=0} = if_\pi P^\mu \int_0^1 du\, e^{iu(z\cdot P)}\phi_\pi(u,q^2) \qquad (2.11)$$

A detailed discussion of light-cone distribution amplitudes is continued in Chapter 3.

Light-cone distribution amplitude for B-meson

Unlike the distribution amplitudes for the light mesons, there is very limited knowledge of the parameters determining the B-meson wavefunction. In the context of QCD factorisation, it is the inverse moment of the distribution amplitude that is most relevant (see below). For scales much larger than m_b, ϕ_B should tend to a symmetric form, as with a light meson distribution amplitude. However, at or below m_b, the distribution is expected to be very asymmetric in momentum fraction ξ, with $\xi \sim \mathcal{O}(\Lambda_{QCD}/m_b)$.

The B-meson light-cone distribution amplitude only appears in the type-II (hard spectator interaction) term in the main QCD factorisation formula. The amplitudes for these interactions, at order α_s, depend only on the product of the momenta of the light meson which absorbs the spectator quark,

p', and that of the spectator quark itself, l. Converting to light-cone coordinates we can arrange the momenta so that the hard-spectator amplitude is dependent only on l_+. The wavefunction can then be integrated over the other momenta $l_\perp$ and l_-. Following the method of [2], the hard-spectator integrals are re-expressed in terms of the longitudinal momentum fraction ξ, and the B-meson LCDA can be decomposed (at leading order in $1/m_b$) into two scalar wavefunctions. These wavefunctions describe the distribution of the longitudinal momentum fraction $\xi = l_+/p_+$ of the spectator quark inside the meson and are defined via:

$$\langle 0|\bar{q}_\alpha(0) b_\beta(z)|\bar{B}(p)\rangle = \frac{i f_B}{4}[(\not{p}+m_b)\gamma_5]_{\beta\gamma} \int_0^1 d\xi\, e^{-i\xi p_+ z_-}\, [\Phi_{B1}(\xi) + \not{n}_-\, \Phi_{B2}(\xi)]_{\gamma\alpha} \tag{2.12}$$

where n is an arbitrary light-like vector, which is chosen in the direction of one of the final state momenta, $n_- = (1,0,0,-1)$. The wavefunctions are normalised

$$\int_0^1 d\xi\, \Phi_{B1}(\xi) = 1 \qquad \int_0^1 d\xi \Phi_{B2}(\xi) = 0 \tag{2.13}$$

In the calculations involving the B-meson distribution amplitude, we need only the first inverse moment of the wavefunction $\Phi_{B1}(\xi)$, parameterised as

$$\int_0^1 d\xi\, \frac{\Phi_{B1}(\xi)}{\xi} = \frac{m_B}{\lambda_B} \tag{2.14}$$

There is little information as to the actual value of the parameter λ_B. There is a known upper bound which implies $3\lambda_B \leq 4\bar{\Lambda}$ [43], where $\bar{\Lambda} = m_B - m_b$, corresponding to $\lambda_B \lessapprox 600$MeV. Numerical estimates have been suggested from a number of different models [43–45] which we can combine to give an estimate of around $\lambda_B = 350 \pm 150$MeV.

Form factor

Hadronic form factors describe the inner structure of the hadron, and are functions of scalar variables arising from the decomposition of some matrix element. In the coupling of a particle to a photon, we have an *electromagnetic form factor*, which is a momentum dependent function reflecting the charge and magnetic moment distribution, and hence the internal structure. In this case we are interested in the *transition form factor*, which describes the overlap of the B meson and the decay product (i.e. some pseudoscalar meson) during the actual decay. Decays of $B \to \pi$ are fully described by three form factors F_+, F_0 and F_T, which are defined by [46]

$$\langle \pi(p)|\bar{u}\gamma_\mu b|\bar{B}(p_B)\rangle = F_+(q^2)\left\{(p_B+p)_\mu - \frac{m_B^2 - m_\pi^2}{q^2}q_\mu\right\} + \frac{m_B^2 - m_\pi^2}{q^2}F_0(q^2)q_\mu \tag{2.15}$$

$$\langle \pi(p)|\bar{d}\sigma_{\mu\nu}q^\nu(1+\gamma_5)b|\bar{B}(p_B)\rangle = i\left\{(p_B+p)_\mu q^2 - q_\mu(m_B^2 - m_\pi^2)\right\}\frac{F_T(q^2)}{m_B+m_\pi} \tag{2.16}$$

where $q = p_B - p$, $q^2 = m_B^2 - 2m_B E_\pi$. In QCD factorisation the vector current arises most often. We should also note that at the scale $q^2 = 0$ the two form factors coincide, $F_+(0) = F_0(0)$. The asymptotic scaling behaviour of the form factors at $q^2 = 0$ is given as [47]

$$F_+(0) = F_0(0) \sim \frac{\Lambda_{QCD}}{m_b}^{3/2} \tag{2.17}$$

The form factors can be calculated using various non-perturbative techniques, such as QCD sum rules (as we discussed in Section 1.3), and on the lattice [33,34]. The method of light-cone sum rules [46] allows the calculation of the form factor within a controlled approximation, relying on the factorisation of an unphysical correlation function whose imaginary part is related to the form factor in question. This correlation function is that of a weak current and a current with the same quantum numbers as the B-meson, evaluated between the vacuum and the π; it is related to the form factor via

$$\begin{aligned}\Pi_\mu(q, p_B) &= i\int d^4x\, e^{iq.x}\langle\pi(p)|TV_\mu(x)j_B^\dagger(0)|0\rangle \qquad (2.18)\\ &= \Pi_+(q^2, p_B^2)(p+p_B)_\mu + \Pi(q^2, p_B^2)q_\mu \qquad (2.19)\end{aligned}$$

where $j_B = im_b\bar{d}\gamma_5 b$. When $p_B^2 \ll m_b^2$, these correlation functions can be expanded on the light-cone

$$\Pi_\pm^{LC}(q^2, p_B^2) = \sum_n \int_0^1 du\, T_\pm^{(n)}(u, q^2, p_B^2, \mu)\phi^{(n)}(u, \mu) \qquad (2.20)$$

This sum runs over contributions from the pion distribution amplitude in increasing twist, where $n = 2$ is the leading-twist contribution. The functions $T_\pm$ are hard-scattering amplitudes, determined by a perturbative series in α_s, known to $\mathcal{O}(\alpha_s)$ at twist-2 and twist-3. The form factor can then be extracted via a light-cone sum rule which depends on the *spectral density* ρ_+^{LC} of the correlation Π_+^{LC}

$$e^{-m_B^2/M^2} m_B^2 f_B F_+^{B\to\pi}(q^2) = \int_{m_b^2}^{s_0} ds\, e^{-s/M^2}\, \rho_+^{LC}(s, q^2) \qquad (2.21)$$

where M^2 and s_0 are specific parameters from the sum rule, related to a Borel transformation [46].

2.2.3 Contributions to hard-scattering kernels

It is useful to discuss qualitatively the diagrams that contribute to the hard-scattering kernels $T^I_{ij}(u)$ and $T^{II}_i(\xi, u, v)$ at the leading order and with exchange of one gluon. We use the decay of $B^0_d \to \pi^+\pi^-$ as an illustrative example. The factorisation formula of equation (2.4) has been proved to one-loop for decays into two light mesons and to two loops for decays into heavy-light final states. There is also proof to all orders for $B \to D\pi$ [48].

The leading order diagram represents the quark level process $b \to u\bar{u}d$, and there is only one contributing diagram with no hard gluon interactions, as shown in Figure 2.1. Since the spectator quark is soft and does not undergo

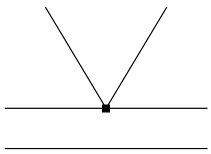

Figure 2.1: Leading order contribution to the hard-scattering kernel T^I.

a hard interaction, it is absorbed by the recoiling meson, and is described by the $B \to \pi$ form factor. In the heavy-quark limit, we can represent the scaling of the decay amplitudes as [40]

$$\mathcal{A}(\bar{B}^0 \to \pi^+\pi^-) \sim G_F m_b^2 F^{B\to\pi}(0) f_\pi \tag{2.22}$$

Radiative corrections to this diagram are suppressed by a power of α_s or Λ_{QCD}/m_b, or are already accounted for by the definition of $F^{B\to\pi}$ or f_π; gluon exchange diagrams that do not fall into the above category are those that are "non-factorisable" with respect to the naive factorisation formalism. The hard-scattering kernel T^I contains contributions from diagrams of this type, including vertex corrections, penguin contractions and contributions from the chromomagnetic dipole operator. These are illustrated in Figures 2.2 and 2.3.

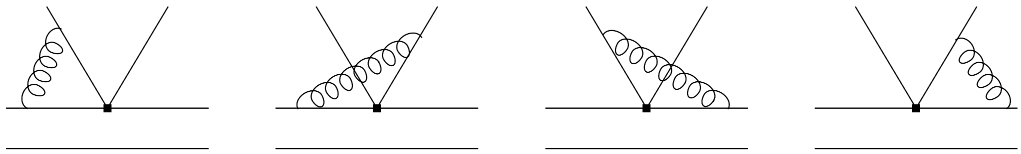

Figure 2.2: The "non-factorisable" vertex corrections.

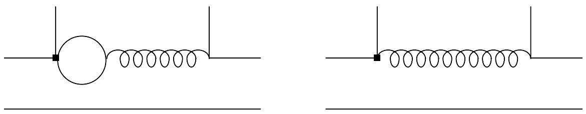

Figure 2.3: Contributions from penguin dipole operator (left) and chromomagnetic dipole operator (right).

The type-II hard-scattering kernel T^{II} contains the hard spectator interactions, of the type shown in Figure 2.4. These would violate factorisation if there was soft-gluon exchange at leading order, however they are suppressed because of the endpoint suppression of the light-cone distribution amplitude for the recoiling π.

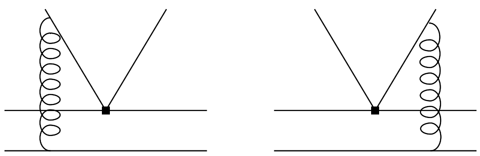

Figure 2.4: Hard-spectator contributions to kernel T^{II}.

2.3 Basic formulae for charmless B-decays

It is not necessary to reproduce all of the numerous expressions of which the QCD factorisation framework is composed, as they are discussed at length in the literature. On the other hand, an exposition of the most important of these formulae which make up the backbone to the QCD factorisation method is illuminating, and will be outlined here. We highlight the places where *model-dependent* contributions arise, and discuss the methods used by BBNS to parameterise them (Section 2.3.2). Our in-depth analysis of non-factorisable contributions to non-leptonic decays is found in Chapter 4. The full decay amplitude expressions as expressed in [2] for $B \to \pi\pi$ are given for completeness in Appendix B.

2.3.1 Factorisable contributions

We have introduced the non-perturbative input for the factorisation formula (2.4); what remains is to discuss the perturbative part. We will concentrate on the factorisable part – that which is fully calculable in the factorisation framework. This is done by translating the effective weak Hamiltonian into a transition operator so that the matrix element is expressed, for example, as

$$\langle \pi\pi | \mathcal{H}_{eff} | \bar{B} \rangle = \frac{G_F}{\sqrt{2}} \sum_{p=u,c} \lambda_p \langle \pi\pi | T_p | \bar{B} \rangle \tag{2.23}$$

The transition operator T_p is constructed from operators labelled by the flavour composition of the final state, corresponding to the operators of the weak Hamiltonian. These are multiplied by a QCD factorisation coefficient, $a_i^p(\pi\pi)$, which contains all of the information from evaluation of diagrams corresponding to that topology.

For example, the coefficients $a_1(\pi\pi)$ and $a_2(\pi\pi)$ are related to the current-current operators and $a_3(\pi\pi) \ldots a_6(\pi\pi)$ are related to the QCD penguin operators. The coefficients $a_7(\pi\pi) \ldots a_{10}(\pi\pi)$ are partially induced by the electroweak penguin operators $Q_7 \ldots Q_{10}$ and are of order $\mathcal{O}(\alpha)$. These coefficients do not include any annihilation topologies – they are model-dependent, power suppressed corrections and as such are evaluated separately, as discussed in the next section.

The general form of the factorisation coefficients at the next-to-leading order in α_s is

$$
\begin{aligned}
a_i^p(M_1M_2) &= \left(C_i + \frac{C_{i\pm1}}{N_c}\right) N_i(M_2) \\
&+ \frac{C_{i\pm1}}{N_c}\frac{C_F}{4\pi}\left[\alpha_s(m_b)V_i(M_2) + \frac{\alpha_s(\mu_h)4\pi^2}{N_c}H_i(M_1M_2)\right] + P_i^p(M_2)
\end{aligned}
\tag{2.24}
$$

where the upper signs apply for i odd and lower for i even, and the superscript p again runs over $p = u, c$ (except for $i = 1, 2$ where there is no flavour dependence and p is omitted). The Wilson coefficients $C_i \equiv C_i(\mu)$ are taken at next-to-leading order in α_s. The quantities that enter these coefficients are split up as follows:

Leading order – the coefficient $N_i(M_2)$ describes the normalisation of the relevant LCDA, and is unity in all cases except $i = 6, 8$.

Vertex contributions – $V_i(M_2)$, originate from processes as in Figure 2.2. These are calculated via convolution integrals of the LCDA for the meson M_2 with a scalar hard-scattering function (this function takes different forms depending on i). The pion LCDA ϕ_π is used for $B \to \pi\pi$ decays, while both ϕ_π and ϕ_K are used in $B \to \pi K$ decays. For all i except $i = 6, 8$, the leading twist distribution amplitude is used; the $i = 6, 8$ terms use the twist-3 distribution amplitude, which is $\Phi^3(x) = 1$ for pseudoscalar mesons.

Penguin contributions – $P_i(M_2)$, as in Figure 2.3. These are present at order α_s only for $i = 4, 6$. Again, these are convolutions of a light-cone distribution amplitude with a hard-scattering function, where the function is dependent on the internal quark mass in the penguin diagrams. This enters as z_p, where $z_u = 0$ and $z_c = m_c^2/m_b^2$.

Hard spectator terms – $H_i(M_1 M_2)$, as in Figure 2.4. These terms originate from the hard gluon exchange between the final state meson (M_2) and the spectator quark, and make up the kernel T^{II}. They are calculated at a lower scale than the other contributions which are evaluated at $\mu = m_b$. For these terms we associate a lower "hard" scale $\mu_h \sim (\Lambda_{QCD} m_b)^{1/2}$, where we use $\Lambda_{QCD} \sim \Lambda_h = 0.5$GeV. We also evaluate the relevant Wilson coefficients in (2.24) at the same scale. The contributions are again convolution integrals of the distribution amplitudes of the light, final state mesons and that of the B-meson. The light LCDA enter both at leading twist, and in the *chirally enhanced* twist-3 contributions. Only the twist-2 contribution is dominated by the hard gluon exchange and so is calculable, the twist-3 terms having logarithmic endpoint singularities.

The coefficients $a_6(M_1 M_2)$ and $a_8(M_1 M_2)$ are power suppressed by a ratio r_χ^M which is proportional to the QCD quark condensate – these are therefore referred to as chirally enhanced corrections. The suppression ratio is

$$r_\chi^\pi(\mu) = \frac{2m_\pi^2}{\overline{m}_b(\mu)(\overline{m}_u(\mu) + \overline{m}_d(\mu))} \tag{2.25}$$

for $B \to \pi\pi$ decays. Although this factor is formally suppressed by Λ_{QCD}/m_b, it always appears in conjunction with the coefficients a_6, a_8, and can cause a large enhancement of power-suppressed corrections, as we consider next.

2.3.2 Power-suppressed corrections

The first main source of non-factorisable corrections to QCD factorisation is through the chirally-enhanced power corrections that are identified with the endpoint divergences arising in the hard spectator terms. These terms are calculated via

$$H_i(M_1M_2) = \frac{f_B f_\pi}{m_B^2 F_0^\pi(0)} \int_0^1 \frac{d\xi}{\xi}\Phi_B(\xi) \int_0^1 dx \int_0^1 dy \left[\frac{\Phi_{M_2}(x)\Phi_{M_1}(y)}{\bar{x}\bar{y}} + r_\chi^{M_1} \frac{\Phi_{M_2}(x)\Phi^3_{m_1}(y)}{x\bar{y}}\right] \tag{2.26}$$

where $\bar{x} \equiv (1-x)$. This simplifies, for example for $B \to \pi\pi$, to

$$H_i(M_1M_2) \quad = \quad \frac{f_B f_\pi}{m_B \lambda_B F_0^\pi(0)} \int_0^1 dx \int_0^1 dy \left[\frac{\phi_\pi(x)\phi_\pi(y)}{\bar{x}\bar{y}} + r_\chi^\pi \frac{\phi_\pi(x)\phi^3_\pi(y)}{x\bar{y}}\right] \tag{2.27}$$

since the asymptotic twist-3 amplitude $\phi^3_\pi = 1$ (for all pseudoscalar mesons), and the pion distribution amplitude is symmetric in exchange $x \leftrightarrow \bar{x}$. The first integral in the bracket in (2.27) is finite. However the second, involving the twist-3 amplitude (where the explicit power suppression can be seen), is logarithmically divergent. BBNS introduce a model-dependent parameterisation of this divergence by defining

$$X_H^M \equiv \int_0^1 \frac{dy}{1-y}\phi^3_M(y) = \int_0^1 \frac{dy}{1-y} \tag{2.28}$$

This parameter represents the soft-gluon interactions with the spectator quark and is expected to be of the order $X_H^M \sim \ln \mu_b/\Lambda_{QCD}$. It is also treated as universal, i.e. the same value for all cases, so there is no dependence on M or the index i of the contribution in which it arises. It is written in the form

$$X_H = (1 + \rho_H \, e^{i\varphi_H}) \ln \frac{m_B}{\Lambda_h} \tag{2.29}$$

The second source of non-factorisable contributions to QCD factorisation is the evaluation of the annihilation topologies as in Figure 2.5.

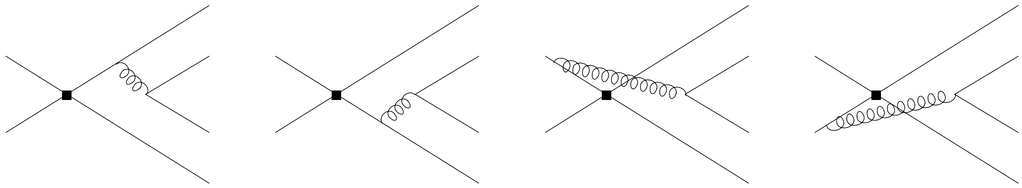

Figure 2.5: Power suppressed annihilation contributions.

Their contribution can be numerically significant, especially in $B \to \pi K$. The calculational difficulty arises in the appearance of endpoint singularities even for the leading twist contributions, which cannot be dealt with in the hard-scattering formalism. Since there is no consistent way of treating these contributions, an approximated model ignoring these soft endpoint divergences is used on top of the QCD factorisation setup in order to estimate the size of the annihilation contributions. The contributions are added at the amplitude level, via a new transition operator T_p^{ann} giving a new set of coefficients, $b_i(M_1 M_2)$.

$$\langle \pi\pi | \mathcal{H}_{eff} | \bar{B} \rangle = \frac{G_F}{\sqrt{2}} \sum_{p=u,c} \lambda_p \langle \pi\pi | T_p + T_p^{ann} | \bar{B} \rangle \tag{2.30}$$

The divergences that appear are treated in a similar way to the power corrections for the hard-spectator diagrams, and are written in terms of an analogous complex parameter X_A, introduced via

$$\int_0^1 \frac{dy}{y} \to X_A \qquad \int_0^1 dy \frac{\ln y}{y} \to -\frac{1}{2}(X_A)^2 \tag{2.31}$$

where again X_A can be simplified under the assumption of universality, so the value is independent of the identity of the meson or the weak decay vertex, and is parameterised by

$$X_A = (1 + \rho_A \, e^{i\varphi_A}) \ln \frac{m_B}{\Lambda_h} \tag{2.32}$$

2.3.3 Isospin decompositions for $B \to \pi\pi$

For our study of the non-factorisable corrections to charmless B-decays in Chapter 4, we decompose the $B \to \pi\pi$ decay amplitudes in terms of their *isospin amplitudes*. The factorisable contributions to these are calculated within the QCD factorisation framework, so it is useful at this point to discuss the decomposition of the decay amplitudes into their isospin components.

In $B \to \pi\pi$ decays, the final state $(\pi\pi)$ can only have total isospin of $I = 0$ or $I = 2$. This implies that the three decay amplitudes, $B^0 \to \pi^+\pi^-$, $B \to \pi^0\pi^0$ and $B^+ \to \pi^+\pi^0$, have only two decay paths, with change in total isospin between the initial and final state of $\Delta I = 1/2$ or $\Delta I = 3/2$. They must therefore obey a triangle relation [49]

$$\sqrt{2}\mathcal{A}(B^+ \to \pi^+\pi^0) - \mathcal{A}(B^0 \to \pi^+\pi^-) - \sqrt{2}\mathcal{A}(B^0 \to \pi^0\pi^0) = 0 \tag{2.33}$$

and similarly for the CP-conjugate decays. Assuming isospin invariance in the matrix elements $\mathcal{A}(B \to \pi\pi) \equiv \langle \pi\pi | \mathcal{H}_{eff} | B \rangle$, we can decompose the decay amplitudes into two isospin amplitudes $A_{3/2}$ and $A_{1/2}$ (where the index corresponds to the change in isospin). Explicitly we have:

$$\begin{aligned}
\sqrt{2}\mathcal{A}(B^+ \to \pi^+\pi^0) &= 3A_{3/2} \\
\mathcal{A}(B^0 \to \pi^+\pi^-) &= A_{3/2} - A_{1/2} \\
\sqrt{2}\mathcal{A}(B^0 \to \pi^0\pi^0) &= 2A_{3/2} + A_{1/2}
\end{aligned} \tag{2.34}$$

with equivalent expressions in terms of $\bar{A}_i$ for the charge-conjugate decays. We can break the isospin amplitudes down further into contributions from two weak amplitudes,

$$\begin{aligned}
A_i &= \lambda_u^* A_i^u + \lambda_c^* A_i^c \\
\bar{A}_i &= \lambda_u A_i^u + \lambda_c A_i^c
\end{aligned} \tag{2.35}$$

with $\lambda_q = V_{qb}V_{qd}^*$. The phase difference between λ_u and λ_c is related to the angle γ of the unitarity triangle:

$$\frac{\lambda_u}{\lambda_c} = -\sqrt{\bar{\rho}^2 + \bar{\eta}^2}\, e^{i\gamma} \tag{2.36}$$

As was first reported in [50], it is straightforward to use the explicit expressions for the decay amplitudes (B.1) to obtain the following expressions for the factorisable part of the isospin amplitudes:

$$
\begin{aligned}
A^u_{1/2} &= \frac{A_{\pi\pi}}{6}\left[4a_1 - 2a_2 + 6(a^u_4 + r^\pi_\chi a^u_6) + 3(a_7 - a_9) + 3(a^u_{10} + r^\pi_\chi a^u_8)\right] \\
A^c_{1/2} &= \frac{A_{\pi\pi}}{2}\left[2(a^c_4 + r^\pi_\chi a^c_6) + (a_7 - a_9) + (a^c_{10} + r^\pi_\chi a^c_8)\right]
\end{aligned}
$$

$$
\begin{aligned}
A^u_{3/2} &= -\frac{A_{\pi\pi}}{6}\left[2a_1 + 2a_2 - 3(a_7 - a_9) + 3(a^u_{10} + r^\pi_\chi a^u_8)\right] \\
A^c_{3/2} &= -\frac{A_{\pi\pi}}{2}\left[-(a_7 - a_9) + (a^u_{10} + r^\pi_\chi a^u_8)\right] \qquad (2.37)
\end{aligned}
$$

with

$$
A_{\pi\pi} = i\frac{G_F}{\sqrt{2}} m_B^2 F_0^{B\to\pi}(0) f_\pi \qquad r^\pi_\chi = \frac{2m_\pi^2}{2m_b m_q} \qquad (2.38)
$$

2.4 Limitations to QCD factorisation

The predominant problem with the factorisation framework is that it is only explicitly valid in the heavy quark limit – the master formula (2.4) is exact only as $m_b \to \infty$. However, as we know m_b is ~ 5 GeV it is justifiable to examine the validity of this limit. The power corrections in the $\Lambda_{\rm QCD}/m_b$ expansion are often difficult to calculate, and include non-factorisable corrections that cannot yet be determined in a model-independent manner.

The expected size of the non-factorisable corrections is $\mathcal{O}(\Lambda_{QCD}/m_b) \sim 10\%$, yet as we will show in detail in Chapter 4, the power corrections can be and are often required to be, considerably larger than this estimate.

The power-suppressed terms can be large with respect to the leading order contribution thanks to various different sources of suppression – such as small values of Wilson coefficients, CKM factors or colour suppression. Numerical enhancement of the power-suppressed terms themselves can also occur, where the coefficients can be larger than suggested by power counting, e.g., the chirally enhanced terms in coefficients $a_6(\pi\pi)$ or $a_8(\pi\pi)$ discussed in Sections 2.3.1 and 2.3.2.

Comparing the predictions from QCD factorisation to the available experimental data gives very good agreement in many cases. For charmless B decays however, the correspondence between prediction and data gives what has been called "The $B \to \pi\pi$ and $B \to \pi K$ puzzles". We can consider two independent ratios of CP-averaged branching fractions:

$$R^{\pi\pi}_{+-} = 2\left[\frac{\mathrm{BR}(B^\pm \to \pi^\pm\pi^0)}{\mathrm{BR}(B^0 \to \pi^+\pi^-)}\right]\frac{\tau_{B^0}}{\tau_{B^+}} \qquad R^{\pi\pi}_{00} = 2\left[\frac{\mathrm{BR}(B^0 \to \pi^0\pi^0)}{\mathrm{BR}(B^0 \to \pi^+\pi^-)}\right]$$

The branching ratio for $B \to \pi^+\pi^-$ is unexpectedly small compared to the prediction, and $B \to \pi^0\pi^0$, unexpectedly large. $B^\pm \to \pi^\pm\pi^0$ is however in agreement with the theory estimates. The experimental values, using the HFAG averages, are $R^{\pi\pi}_{+-} \sim 2.2$, $R^{\pi\pi}_{00} \sim 0.32$. Using the default parameters the QCD factorisation estimates are somewhat different: $R^{\pi\pi}_{+-} \sim 1.25$, $R^{\pi\pi}_{00} \sim 0.03$. Even using the "favoured scenario" for the parameters and with enhanced annihilation contributions we find: $R^{\pi\pi}_{+-} \sim 1.8$, $R^{\pi\pi}_{00} \sim 0.13$ [3]. An analogous situation exists for $B \to \pi K$ where moderate discrepancies occur in some branching ratios, such as the ratio of $B \to \pi^\mp K^\pm$ and $B^\pm \to \pi^\pm K^0$.

There is a reasonable agreement for the $B \to \pi\pi$ CP asymmetry predictions from QCD factorisation. There is however difficulty in making conclusive statements regarding this due to the discrepancies between the experimental measurements from BaBar and Belle. This can be seen graphically in the presentation of our results in Chapter 4, where we clarify and quantify the discrepancies between the predictions and measurements.

Chapter 3

Light-cone meson distribution amplitudes

A light from the shadows shall spring

J.R.R. Tolkien

This chapter is devoted to the study of distribution amplitudes of light mesons, where we derive new models characterised by a small number of parameters directly related to experimental observables – this is the first new result of this thesis. We discuss how these new models are constructed and how they are more descriptive than the current expressions of light meson distribution amplitudes. We also show how we can numerically evolve the new model distribution amplitudes in the scale μ, to exactly reproduce the leading order scaling behaviour of the usual approximated DA. Finally, within the framework of QCD factorisation, we study the effect of these model DAs on important 2-body non-leptonic B-decays such as $B \to \pi\pi$.

3.1 General framework

The basic equation to describe bound states in relativistic quantum field theory is known as the *Bethe-Salpeter* equation, which was first formulated in the 1950's [51, 52]. The leading twist distribution amplitude of a meson is related to this wave function by integrating out the dependence on the transverse momentum $p_\perp$,

$$\phi(u) \sim \int_{p_\perp^2 < \mu^2} d^2 p_\perp \, \phi(u, p_\perp) \tag{3.1}$$

The light-cone distribution amplitudes were originally introduced in the context of hadronic electromagnetic form factors and the pseudoscalar-photon transition form factor [53–57], but have attracted interest in B physics due to their appearance in QCD sum rules on the light-cone [46, 58–66], form factors [67, 68], and their use in factorisation for B decay amplitudes [1, 2].

Using the formalism introduced in Section 2.2.2, we can define the distribution amplitude for a general pseudoscalar meson P in terms of the matrix element of a non-local operator near the light-cone. We have

$$\begin{aligned}\langle 0|\bar{q}_1(x)\gamma_\mu\gamma_5[x,-x]q_2(-x)|P\rangle \;=\;& i f_P p_\mu \int_0^1 du\, e^{i\xi px}\left[\phi_P(u) + \frac{1}{4}\, m_P^2 x^2 \mathbb{A}_P(u) + O(x^4)\right] \\ &+ \frac{i}{2}\, f_P m_P^2 \,\frac{1}{px}\, x_\mu \int_0^1 du\, e^{i\xi px}\, \left[\mathbb{B}_P(u) + O(x^2)\right]\end{aligned} \tag{3.2}$$

where $\xi = 2u - 1$ and $[x, y]$ is the Wilson line defined in (2.7). In equation (3.2), ϕ_P is the leading twist-2 distribution amplitude, whereas $\mathbb{A}_P$ and $\mathbb{B}_P$ contain contributions from higher-twist operators. The corresponding definitions of vector meson DAs can be found in [69, 70].

The theory of meson DAs is well understood [41, 69–72], and suggests their parameterisation in terms of a *partial wave expansion* in conformal spin (see Section 3.2), allowed due to the conformal invariance of QCD. This expansion is in terms of contributions with different conformal spin, which do not mix with each other under a change of scale. This is true to leading logarithmic accuracy, but is no longer the case at higher order, as the underlying symmetry is anomalous. The leading-twist distribution amplitude $\phi(u)$, for both pseudoscalar and vector mesons has a conformal expansion given in terms of *Gegenbauer polynomials* $C_n^{3/2}$,

$$\phi(u, \mu^2) = 6u(1-u) \sum_{n=0}^{\infty} a_n(\mu^2) C_n^{3/2}(2u-1) \tag{3.3}$$

The Gegenbauer polynomials are generalisations of the associated Legendre polynomials; the first few are

$$\begin{aligned} C_0^{3/2}(x) &= 1 \\ C_1^{3/2}(x) &= 3x \\ C_2^{3/2}(x) &= \frac{3}{2}(-1+5x^2) \end{aligned}$$

The coefficients a_n in (3.3) are Gegenbauer moments, and renormalise multiplicatively to leading logarithmic accuracy

$$a_n(Q^2) = a_n(\mu^2) \left(\frac{\alpha_s(Q^2)}{\alpha_s(\mu^2)} \right)^{(\gamma_0^{(n)} - \gamma_0^{(0)})/(2\beta_0)} \tag{3.4}$$

where $\beta_0 = 11 - (2/3)n_f$. For pseudoscalar and longitudinally polarised vector mesons, the one-loop anomalous dimension $\gamma_0^{(n)}$, given by [73]

$$\gamma_0^{(n)} = 8C_F\left(\psi(n+2)+\gamma_E-\frac{3}{4}-\frac{1}{2(n+1)(n+2)}\right) \tag{3.5}$$

and for transversely polarised vector mesons

$$\gamma_0^{(n)} = 8C_F\left(\psi(n+2)+\gamma_E-\frac{3}{4}\right) \tag{3.6}$$

For π, ρ, ω, η, η' and ϕ, G-parity ensures that $a_{\text{odd}}=0$ and that the DA is symmetric under $u \leftrightarrow 1-u$, whereas for K and K^* the nonzero values of a_{odd} induce an antisymmetric component of the DA. $a_0 \equiv 1$ is fixed by normalisation

$$\int_0^1 \phi(u,\mu^2)=1$$

and all the other a_n are intrinsically nonperturbative quantities. As they do not mix under renormalisation to leading order accuracy, equation (3.3) is well suited to construct models for ϕ: truncating the series after the first few terms yields a parameterisation of the DA that is "stable" under a change of scale, except for the numerical values of a_n. Despite there being no small expansion parameter, such a *truncated conformal expansion* is often a meaningful approximation to the full distribution amplitude. An advantage of this expansion is that the contributions of higher conformal spins to the convolution integrals involving the LCDA (and therefore also the physical amplitudes) are suppressed by the highly oscillating behaviour of the partial waves. This suggests a construction of models for the DAs based on a truncated conformal expansion, where only the first few waves are included.

We now move on to discuss the construction of the distribution amplitude via the conformal expansion using the conformal invariance of QCD.

3.2 Conformal symmetry

3.2.1 The conformal group

The *conformal group* is defined as the group of general co-ordinate transformations of 4-D Minkowski space that conserve the interval $ds^2 = g_{\mu\nu}dx^\mu dx^\nu$ up to a change of scale – i.e. transformations that preserve angles and leave the light-cone invariant. Transformations of this type are: scale transformations ($x^\mu \to \lambda x^\mu$), inversions ($x^\mu \to x^\mu/x^2$), translations ($x^\mu \to x^\mu + c$) and Lorentz rotations. The conformal group is the maximal extension of the Poincaré group that leaves the light cone invariant [74]. In four dimensions the full conformal group has 15 generators, which are denoted by

$\mathbf{P}_\mu$	4 translations
$\mathbf{M}_{\mu\nu}$	6 Lorentz rotations
$\mathbf{D}$	dilatation
$\mathbf{K}_\mu$	4 special conformal transformations

An important subgroup of the full conformal group is the *collinear subgroup*, which (as we will see later) is the most relevant in the study of QCD. Denoted $SL(2,\mathbb{R})$, this subgroup is made up of a special case of the *special conformal transformation*

$$x^\mu \to x^{\mu\prime} = \frac{x^\mu + a^\mu x^2}{1 + 2a \cdot x + a^2 x^2} \tag{3.7}$$

for a^μ light-like; this can be reduced to

$$x_- \to x'_- = \frac{x_-}{1 + 2a x_-} \tag{3.8}$$

which maps the light-ray onto itself in the x_- direction. Transformations of this type together with the dilations and translations along the x_- direction make up the collinear subgroup.

Transformations of $SL(2,\mathbb{R})$ are governed by four generators $\mathbf{P}_+$, $\mathbf{M}_{-+}$, $\mathbf{D}$ and $\mathbf{K}_-$. These are most often presented in the linear combinations [75]:

$$\begin{aligned}
\mathbf{L}_+ &= \mathbf{L}_1 + \mathrm{i}\mathbf{L}_2 = -\mathrm{i}\mathbf{P}_+ \\
\mathbf{L}_- &= \mathbf{L}_1 - \mathrm{i}\mathbf{L}_2 = \tfrac{\mathrm{i}}{2}\mathbf{K}_- \\
\mathbf{L}_0 &= \tfrac{i}{2}(\mathbf{D} + \mathbf{M}_{-+}) \\
\mathbf{E} &= \tfrac{i}{2}(\mathbf{D} - \mathbf{M}_{-+})
\end{aligned} \tag{3.9}$$

so that the algebra of $SL(2,\mathbb{R})$ is written

$$[\mathbf{L}_0, \mathbf{L}_\mp] = \mp\mathbf{L}_\mp \qquad [\mathbf{L}_-, \mathbf{L}_+] = -2\mathbf{L}_0 \tag{3.10}$$

These generators act on fundamental fields $\Phi(x)$ which are equivalent to primary fields in conformal field theory. If we consider the parton model of hadron states, the hadron is replaced by partons moving collinearly in some direction $\vec{n}_\mu$. We can then consider only the fields confined to the light-cone

$$\Phi(x) \to \Phi(\alpha n)$$

with α a real number. Additionally, we choose the field Φ as an eigenstate of the spin operator so that is has a fixed spin projection s in +direction. The action of the generators can be described in terms of differential operators acting on the primary field. $\phi(\alpha) \equiv \phi(\alpha n)$

$$\begin{aligned}
[\mathbf{L}_+, \Phi(\alpha)] &= -\partial_\alpha \Phi(\alpha) \equiv L_+\Phi(\alpha), \\
[\mathbf{L}_-, \Phi(\alpha)] &= (\alpha^2\partial_\alpha + 2j\alpha)\Phi(\alpha) \equiv L_-\Phi(\alpha), \\
[\mathbf{L}_0, \Phi(\alpha)] &= (\alpha\partial_\alpha + j)\Phi(\alpha) \equiv L_0\Phi(\alpha) \\
[\mathbf{E}, \Phi(\alpha)] &= \frac{1}{2}(l-s)\Phi(\alpha)
\end{aligned} \tag{3.11}$$

The generator $\mathbf{E}$ measures the *collinear twist* of the field, defined as the dimension minus spin projection in + direction. The field $\Phi(\alpha x)$, with a fixed spin projection on the lightcone ($x^2 = 0$) is an eigenstate of the quadratic Casimir operator L^2, defined by

$$L^2 \equiv L_0^2 + L_1^2 + L_2^2 = L_0^2 + L_-L_+ \qquad \left[L^2, L_i\right] = 0 \tag{3.12}$$

so that

$$L^2\Phi(\alpha) = \sum_i [\mathbf{L}_\mathrm{i}, [\mathbf{L}_\mathrm{i}, \Phi(\alpha)]] = j(j-1)\Phi(\alpha) \tag{3.13}$$

Here $j = \frac{1}{2}(l+s)$ and is referred to as the *conformal spin*, where l is the canonical mass dimension of the field and s the (Lorentz) spin. Consequently, we see that the field $\Phi(\alpha)$ is transformed according to representations of the collinear conformal group $SL(2,\mathbb{R})$, specified by the conformal spin j.

3.2.2 Conformal symmetry in QCD

QCD is conformally invariant at leading order, but is broken at next-to-leading-order by the inclusion of quantum corrections. However, the conformal spin is seen as a good quantum number in hard-processes up to small corrections of order α_s^2. The non-local operators of QCD can be written in terms of *conformal operators*. We can construct a complete basis of local operators on $SL(2,\mathbb{R})$ from $\Phi(0)$ by applying the "raising" operator $\mathbf{L}_+$ k-times.

$$
\begin{aligned}
\mathcal{O}_0 &= \Phi(0) \\
\mathcal{O}_k &= [\mathbf{L}_+, \ldots, [\mathbf{L}_+, [\mathbf{L}_+, \Phi(0)]]] = (-\partial_+)^k \, \Phi(\alpha)|_{\alpha=0}
\end{aligned}
$$

The primary fields $\Phi(\alpha)$ can be formally expressed as a Taylor series expansion of local conformal operators

$$
\Phi(\alpha) = \sum_{k=0}^{\infty} \frac{(-\alpha)^k}{k!} O_k \tag{3.14}
$$

This is a simple example of a *conformal tower*. It is possible to construct conformal towers for general operators built of a number of primary fields and derivatives [75]. We can define a local conformal operator $\mathbb{O}_n$ that transforms under the collinear conformal subgroup. This is equivalent to demanding the operator satisfies

$$
\begin{aligned}
\left[\mathbf{L}^2, \mathbb{O}_\mathrm{n}\right] &= j(j-1)\,\mathbb{O}_n \\
\left[\mathbf{L}_0, \mathbb{O}_\mathrm{n}\right] &= j\,\mathbb{O}_n \\
\left[\mathbf{L}_-, \mathbb{O}_\mathrm{n}\right] &= 0
\end{aligned}
$$

The tower of operators can be built by repeatedly applying the raising operator, as above

$$
\begin{aligned}
\mathbb{O}_{n,n} &= \mathbb{O}_n \\
\mathbb{O}_{n,n+k} &= \underbrace{[\mathbf{L}_+, \ldots, [\mathbf{L}_+, [\mathbf{L}_+}_{k}, \ \mathbb{O}_n]]] = (-\partial_+)^k \, \mathbb{O}_n
\end{aligned}
$$

It is possible to construct explicitly a general local conformal operator as [74]

$$\mathbb{O}_n^{j_1,j_2}(x) = \left[\Phi_{j_1}(x)\, P_n^{(2j_1-1,2j_2-1)}\left(\frac{\overrightarrow{\partial}_+ - \overleftarrow{\partial}_+}{\overrightarrow{\partial}_+ + \overleftarrow{\partial}_+}\right)\Phi_{j_2}(x)\right] \tag{3.15}$$

where $P_n^{a,b}(x)$ are Jacobi polynomials and the superscripts indicate the conformal spins of the constituent fields.

Returning to QCD, we can extract different conformal operators related to the different spin and dimension of the constituent quark or gluon fields. For a quark $\sim$ anti-quark operator at the leading twist we have the relevant local conformal operator $\mathbb{O}_n^{1,1}$, given by

$$\mathbb{O}_n^{1,1}(x) = (i\partial_+)^n \left[\bar{\psi}(x)\,\gamma_+\, C_n^{3/2}\left(\overleftrightarrow{D}_+/\partial_+\right)\,\psi(x)\right] \tag{3.16}$$

where the Gegenbauer polynomials are a special case of the Jacobi polynomials $P_n^{1,1} = C_n^{3/2}$.

3.2.3 Conformal partial wave expansion

The aim of the partial wave expansion is to make full use of the underlying symmetry of the theory in order to simplify the dynamics of the problem. In the case of QCD, we make use of the conformal invariance to create a partial wave expansion in conformal spin. The conformal expansion of the LCDA is analogous to the partial wave expansion for a spherically symmetric potential in quantum mechanics. Here, the rotational symmetry allows the separation of angular and radial degrees of freedom. The angular dependence is encoded in the spherical harmonics $Y_l^m(\theta,\phi)$ which form an irreducible representation of $O(3)$, and the radial information is governed by an evolution equation, namely the 1-d Schrödinger equation in $R(r)$.

In QCD, the partial-wave expansion decomposes the distribution amplitude into longitudinal and transverse degrees of freedom. The dependence on the longitudinal momentum is expressed in terms of orthogonal polynomials which form irreducible representations of $SL(2,\mathbb{R})$. For a general two-body wavefunction, these polynomials are the Jacobi polynomials. For conformal spins $j_1 = j_2$, we obtain the Gegenbauer polynomials, defined by the generating function

$$\frac{1}{(1-2xt+t^2)^\lambda} = \sum_{n=0}^{\infty} C_n^{(\lambda)}(x)t^n \tag{3.17}$$

A multiple-particle state that is built of primary fields can be expanded in terms of irreducible representations of $SL(2,\mathbb{R})$ with increasing conformal spin. The lowest possible conformal spin for the multi-particle state equals the sum of spins of the constituents, and its wavefunction is simply a product of non-degenerate one particle states. This lowest state defines what is known as the *asymptotic* distribution amplitude, as it is reached at the formal limit of $q^2 \to \infty$. This state is expressed, in the general case, as

$$\phi_{as}(u_1, u_2 \dots u_m) = \frac{\Gamma(2j_1 + \cdots + 2j_m)}{\Gamma(2j_1)\dots\Gamma(2j_m)} u_1^{2j_1-1} u_2^{2j_2-1} \dots u_m^{2j_m-1} \tag{3.18}$$

where u_i is the momentum fraction of the i^{th} constituent, and the normalisation is chosen so that $\int [du_i]\phi_{as}(u_i) = 1$.

Light-cone meson distribution amplitudes

The distribution amplitude for the pion $\phi_\pi(u)$ is an expansion over an infinite series of Gegenbauer polynomials, with multiplicatively renormalisable coefficients

$$\phi_\pi(u,\mu^2) = 6u(1-u)\sum_{n=0}^{\infty} a_n(\mu^2) C_n^{3/2}(2u-1) \tag{3.19}$$

The Gegenbauer polynomials form an orthonormal set on the interval $0 < u < 1$ with weight function $u(1-u)$ and satisfy the orthogonality condition

$$\int_0^1 du\, u(1-u)\, C_n^{3/2}(2u-1) C_m^{3/2}(2u-1) = \delta_{mn} N_n \tag{3.20}$$

with

$$N_n = \frac{(n+1)(n+2)}{4(2n+3)} \tag{3.21}$$

The renormalisation group equation for $\phi_\pi(u,\mu^2)$ is known as the *Efremov-Radyushkin-Brodsky-Lepage* (ER-BL) evolution equation [55, 57]

$$\mu^2 \frac{d}{d\mu^2}\phi_\pi(u,\mu^2) = \int_0^1 dv V(u,v,\alpha_s)\phi_\pi(v,\mu^2) \tag{3.22}$$

The evolution kernel $V(u,v,\alpha_s)$ has been calculated perturbatively to next-to-leading order in α_s [76, 77]

$$V(u,v,\alpha_s) = \frac{\alpha_s}{2\pi} V_0(u,v) + \frac{\alpha_s^2}{4\pi^2} V_1(u,v) \tag{3.23}$$

The pion distribution amplitude can be expressed as matrix elements of renormalised local operators

$$\langle 0|\bar{d}(0)\gamma_+\gamma_5(i\overleftrightarrow{D}_+)^n u(0)|\pi^+(p)\rangle = if_\pi (p_+)^{n+1}\int_0^1 du(2u-1)^n \phi_\pi(u,\mu^2) \tag{3.24}$$

so the relevant conformal operators (3.16) are then [74]

$$O_n(x) = (i\partial_+)^n \left[\bar{d}(x)\gamma_+\gamma_5 C_n^{3/2}\left(\overleftrightarrow{D}_+/\partial_+\right) u(x)\right] \tag{3.25}$$

Due to the flavour structure of this operator, there is no mixing with operators involving two-gluon fields, nor with operators of three or more fields, as these appear at higher twist. Thus the operators of (3.25) do not mix at the leading order, and are multiplicatively renormalised. The evolution equation (3.22) can then be solved by a conformal spin expansion

$$\phi_\pi(u,\mu^2) = \sum_{n=0}^{\infty} \frac{u(1-u)}{N_n} C_n^{3/2}(2u-1)\langle\langle O_n(\mu^2)\rangle\rangle \tag{3.26}$$

where

$$\langle\langle O_n(\mu^2)\rangle\rangle = \int_0^1 du\, C_n^{3/2}(2u-1)\, \phi_\pi(u,\mu^2) \tag{3.27}$$

The sum runs over even values of n to ensure symmetry of the pion DA, due to charge conjugation invariance: $\phi_\pi(u) = \phi_\pi(1-u)$. We can construct the Gegenbauer moments, $a_n(\mu^2)$, using the reduced matrix elements of the conformal operators given in (3.27), such that

$$\begin{aligned} a_n(\mu^2) &= \frac{2(2n+3)}{3(n+1)(n+2)} \langle\langle O_n(\mu^2)\rangle\rangle \\ &= \frac{2(2n+3)}{3(n+1)(n+2)} \int_0^1 du\, C_n^{3/2}(2u-1)\, \phi_\pi(u,\mu^2) \end{aligned} \tag{3.28}$$

3.3 Non perturbative input

In general, not much is known about the amplitudes of these partial waves and hence the numerical values of the moments a_n. There is some information available on the lowest moments of the π DA, but much less for the other mesons. For the π and η mesons, there is some experimental information available on the $\pi(\eta)\gamma\gamma^*$ transition form factor [78], which can be used to extract the values of the first two amplitudes. The $\gamma\gamma^* \to \pi$ form factor factorises into a partonic hard scattering amplitude and a soft hadronic matrix element parameterised by the pion DA ϕ_π. The leading twist expression for $F_{\pi\gamma}$ is given by [79, 80]:

$$
\begin{aligned}
F_{\pi\gamma}(q^2) &= \frac{4}{\sqrt{2}} \int_0^1 dx\, \phi_\pi(x, q^2)\, T^H_{\gamma\to\pi}(x, q^2) \\
&= \frac{4}{\sqrt{2}q^2} \int_0^1 dx\, \frac{\phi_\pi(x, q^2)}{x}\, (1 + \mathcal{O}(\alpha_s))
\end{aligned}
\tag{3.29}
$$

using $\phi_\pi(x) = \phi_\pi(1-x)$ and since the amplitude for the subprocess $\gamma\gamma^* \to \pi$ (labelled $T^H_{\gamma\to\pi}$) is

$$
T^H_{\gamma\to\pi}(x, q^2) = \frac{1}{(1-x)q^2}\, (1 + \mathcal{O}(\alpha_s))
$$

This means that the $\gamma - \pi$ transition form factor approximately probes the sum of the Gegenbauer moments via

$$
\int_0^1 dx\, \frac{\phi_\pi(x)}{x} = 1 + \sum_n a_n \tag{3.30}
$$

By making some assumption (such as truncating this series after $n = 4$) it is possible to extract information about the moments.

On the theory side, there exist a few lattice calculations for the second moment of the π DA; some quite dated [81–83], and a recent retry [84, 85]. Unfortunately, these results are still preliminary and cannot yet be used in phenomenological applications. Other theoretical calculations have been done using QCD sum rules for both pseudoscalar and vector mesons; these are reviewed below.

3.4 Previous constructions of ϕ_π

This section briefly reviews and consolidates the previous calculations (and constructions) of the pion DA and its moments a_n.

The earliest calculation of one of the moments of the pion DA was that of a_2 by Chernyak and Zhitnitsky (CZ) [41]. They developed a model of the pion DA based on local QCD sum rules whereby ϕ_π is expanded in terms of local operators from which the a_n can be extracted. The form of the DA is strongly peaked at the endpoints, due to the approximation of the vacuum quark distribution by a delta function and derivatives of, the non-perturbative contributions to the sum rule forcing the DA to be end-point concentrated. The DA is shown graphically later in this section in Figure 3.1, and is described by a model wavefunction of

$$\phi_\pi^{CZ}(u) = 30u(1-u)(1-2u)^2 \tag{3.31}$$

which corresponds to the numerical result

$$a_2(0.5\text{GeV}) = 2/3 \tag{3.32}$$

The drawback of extracting the a_n in this way is that the expansion of an intrinsically non-local quantity, namely the pion DA, in terms of contributions from the local operators causes an increased sensitivity to the non-perturbative effects. The coefficients of the condensates in the sum rule increase with n and can in fact dominate over the perturbative contributions for a large enough value of n. This implies that this method should be reliable for at least $n = 2$ but not for large n. They also obtained the result

$$\phi\,(1/2, 1/2\,\mathrm{GeV}) = 0 \tag{3.33}$$

neglecting all $a_{n\geq 4}$. This however is an artifact of the neglect of higher order moments.

This method was improved by Braun and Filyanov [29], who found that $\phi(1/2)$ was required to be non-zero; they found a constraint on $\phi(1/2)$ at the scale of 1 GeV of

$$\phi\,(1/2, 1\,\mathrm{GeV}) = 1.2 \pm 0.3 = \frac{3}{2} - \frac{9}{4}a_2(1) + \frac{45}{16}a_4(1) \tag{3.34}$$

They also re-determined the first two moments using the CZ procedure:

$$a_2(1\mathrm{GeV}) = 0.44 \qquad a_4(1\mathrm{GeV}) = 0.25$$

Other calculational methods have also been used to determine the moments of the DA. For example, the most recent calculation is from Ball and Zwicky [46, 58] using light-cone sum rules, who have determined the first two moments as

$$a_2(1\mathrm{GeV}) = 0.115 \qquad a_4(1\mathrm{GeV}) = -0.015$$

Another alternative method is to use sum rules with *non-local condensates*, as developed in [86–90]. This method constructs the DA by connecting the dynamic properties of the pion with the QCD vacuum structure. This allows for the fact that quarks and gluons can travel through the QCD vacuum with non-zero momentum k_q, which implies a non-zero average virtuality,

$\langle k_q^2 \rangle = \lambda_q^2$, using the ratio

$$\lambda_q^2 = \frac{\langle \bar{q}\sigma g G g \rangle}{2\bar{q}q} \tag{3.35}$$

The most recent calculations using this technique was by Bakulev, Mikhailov and Stefanis (BMS) [87], who used a virtuality of $\lambda_q^2 = (0.4 \pm 0.1)\mathrm{GeV}^2$ and extracted the values of a_2 to a_{10} from the non-local condensate sum rules. The non-local quark condensate represents a partial resummation of the operator product expansion to all orders, for the vacuum expectation value of the (non-local) operator $\langle \bar{q}(0)E[0,z]q(z)\rangle$. This is expressed in terms of analytic functions $F_{S,V}$, whose derivatives are related to condensates of the corresponding dimension

$$M(z) \equiv \langle \bar{q}(0)E[0,z]q(z)\rangle = \frac{\langle \bar{q}(0)q(0)\rangle}{4}\left[F_S(z^2) - \frac{i\hat{z}}{4}F_V(z^2)\right] \tag{3.36}$$

$E[0,z]$ is an appropriate Wilson line operator, taken in an appropriate gauge so that the path-ordered exponential equals unity. The lowest order condensates are found via standard QCD sum rules [91], and are

$$Q^3 = \langle \bar{q}q \rangle \qquad Q^5 = ig_s\langle \bar{q}G^{\mu\nu}\sigma_{\mu\nu}q\rangle \qquad Q^6 = \langle (\bar{q}q)^2 \rangle \tag{3.37}$$

The functions $F_{S,V}$ are given in terms of a virtuality distribution which describes the distribution of the vacuum fields in terms of λ_q^2

$$F_{S,V}(z^2) = \int_0^\infty e^{\alpha z^2/4} f_{S,V}(\alpha)d\alpha \tag{3.38}$$

where

$$\int_0^\infty f_{S,V}(\alpha)\,d\alpha = \begin{cases} 1 & \mathrm{S} \\ 0 & \text{V and chiral limit} \end{cases} \tag{3.39}$$

In the BMS approach, this distribution is modelled by performing an expansion where the large average virtuality (compared to the relevant hadronic scale) is included in only the first term of the series, instead of the usual expansion of the non-local condensate in terms of local condensates $\langle\bar{q}q\rangle$, $\langle\bar{q}D^2q\rangle\ldots$. This corresponds to taking the form of the virtuality distribution as $f_S(\alpha)=\delta(\alpha-\lambda_q^2/2)$ and $f_V\sim\alpha_s Q^3\delta'(\alpha-\lambda_q^2/2)$ [90].

The pion distribution amplitude can then be connected directly to the non-local condensates by means of a sum rule

$$\begin{aligned} f_\pi^2\phi_\pi^{BMS}(x) &= \int_0^{s_0}\rho^{pert}(x,s)e^{-s/M^2}ds+\frac{\alpha_s\langle GG\rangle}{24\pi M^2}\Phi_G(x,M^2) \\ &\quad +\frac{16\pi\alpha_s\langle\bar{q}q\rangle^2}{81M^4}\sum_{i=S,V,T_j}\Phi_i(x,M^2) \end{aligned} \tag{3.40}$$

The s and M are Borel parameters and the Φ_i are local condensates, with i running over all scalar, vector and tensor types. Using this sum rule provides values for the first ten Gegenbauer moments of the pion distribution amplitude; for $n>4$, the a_n were found to be $\sim 10^{-3}$ and so were neglected in their calculations. The non-zero moments were found to be

$$a_2(1.16\text{GeV})=0.19 \qquad a_4(1.16\text{GeV})=-0.13 \tag{3.41}$$

Finally, the extraction of the moments a_2 and a_4 from the photon-pion transition form factor (as discussed above), has been developed and refined by a succession of authors [92–95], culminating in the constraint

$$a_2(1\text{GeV})+a_4(1\text{GeV})=0.1\pm 0.1 \tag{3.42}$$

The moments of the DA which are obtained in all of these models are summarised in the table below, where the moments are all normalised to a scale of $q^2 = 1$ GeV^2

Model	a_2	a_4
AS	0	0
CZ	0.56	0
BF	0.44	0.25
BMS	0.20	-0.14
BZ	0.115	-0.015

The models of the DAs are shown for comparison in Figure 3.1.

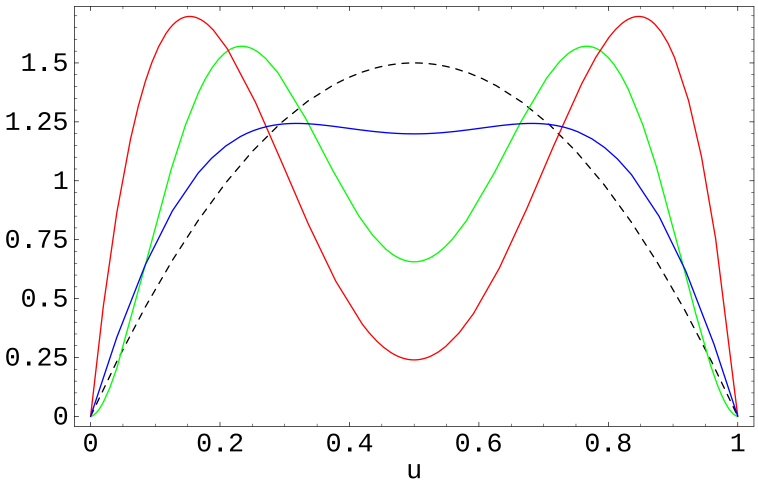

Figure 3.1: Model pion distribution amplitudes for comparison between asymptotic (dotted), BZ (blue), BMS (red) and CZ (green), all taken as scale $q^2 = 1$ GeV^2.

3.5 New models for LCDA

Here we discuss the main new result of this chapter, where we introduce new models for the leading-twist distribution amplitudes of the π and the K based on the fall-off behaviour of the nth Gegenbauer moment of these amplitudes, a_n in n, which is assumed to be power-like [5]. The models are formulated in terms of a few parameters, notably the first inverse moment of the DA (which for the π is directly related to experimental data) and the strength of the fall-off of the a_n, and can be summed to all orders in the conformal expansion, parameterising the full DA at a certain energy scale. Although we focus on the pseudoscalar mesons π and K, the models we propose are equally well applicable to vector mesons ρ, ω, K^* and ϕ.

3.5.1 Motivation

For many processes involving distribution amplitudes it is usually argued that a truncated conformal expansion would be sufficient for the calculation of physical amplitudes so long as the perturbative scattering amplitude is "smooth" — the reason being the highly oscillatory behaviour of higher order Gegenbauer polynomials. In order to quantify this statement, consider the simplest case of one meson in the initial or final state, so that the convolution integral reads

$$I = \int_0^1 du\, \phi(u) T(u) \tag{3.43}$$

where T is the perturbative scattering amplitude.

This can be separated into three cases:

(i) T is nonsingular for $u \in [0, 1]$,

(ii) T has an integrable singularity at one of the endpoints,

(iii) T contains a non-integrable singularity at one of the endpoints.

As a typical example for case (i), consider $T(u) = \sqrt{u}$, which yields

$$\int_0^1 du\,\phi(u)\sqrt{u} = \sum_{n=0}^{\infty} \frac{(-1)^n 36(n+1)(n+2)}{(2n-1)(2n+1)(2n+3)(2n+5)(2n+7)}\,a_n$$

This result implies a strong fall-off $\sim 1/n^3$ of the coefficients of higher Gegenbauer moments a_n: assuming $a_i \equiv 1$ for all i, already the first three terms in the sum account for 98.8% of the full amplitude. In reality the convergence will be even better as all existing evidence points at $|a_n| \ll 1$ for $n \geq 1$.

As an example for case (ii) consider $T(u) = \ln u$, giving

$$\int_0^1 du\,\phi(u)\ln(u) = -\frac{5}{6}\,a_0 + \sum_{n=1}^{\infty} \frac{(-1)^{n-1}}{n(n+3)}\,3a_n$$

The singularity at $u = 0$ evidently worsens the convergence of the series; again assuming $a_i \equiv 1$, the first three terms now overshoot the true result by 35%. In order to approximate the full amplitude to within 5% one now has to include nine terms, but the convergence will again be better in practise, thanks to the fall-off of a_n with n.

Case (iii) is more complicated and depends on the asymptotic behaviour of the a_n. For $T(u) = 1/u$, for instance, one obtains

$$\int_0^1 du\,\phi(u)\,\frac{1}{u} = 3\sum_{n=0}^{\infty}(-1)^n a_n \tag{3.44}$$

Here the amplitude is finite only if the a_n fall off sufficiently fast in n. For stronger endpoint divergences the coefficients multiplying the a_n start to grow in n and for $T \sim 1/u^2$ the integral diverges, even for the asymptotic DA, which would indicate a breakdown of factorisation for that process.

This discussion suggests that models of ϕ, based on a conformal expansion truncated after the first few terms, can be used appropriately for cases (i) and (ii), but are less reliable for case (iii). Convolutions with $T \sim 1/u$ are very relevant both in hard perturbative QCD e.g. $\gamma\gamma^* \to \pi$ (Section 3.3), and in decays such $B \to \pi\pi$. The a_n can have different weighting in the different convoluted amplitudes, and have the highest impact for the convolutions of type (iii). Instead of basing a parameterisation of ϕ on a_2 and a_4 (taking all $a_{n>4} = 0$), it is not unreasonable to use the case in (3.44), where all a_n enter with the highest possible weight factor. This is the basic idea behind our models of leading-twist DAs.

3.5.2 Model construction

In beginning to construct a model of the (leading-twist) pion DA we consider the two properties that any viable model must fulfil. Firstly, the large-q^2 behaviour must be satisfied for all light-meson DAs, in that the distribution amplitude must tend to the asymptotic form $\phi_\pi(u, \mu^2 \to \infty) = 6u(1-u)$. Also, in order for QCD factorisation in B decays to make sense the first inverse moment, $\int_0^1 du\, \phi_\pi(u)/u$, which as we have seen is related to the $\pi\gamma\gamma^*$ transition form factor, must exist. Both these conditions are fulfilled for models based on a truncated conformal expansion, which has in addition the prediction that for $u \to 0, 1$, $\phi \sim u(1-u)$, independently of the factorisation scale. This prediction is in general, not fulfilled for models that are not truncated at fixed order in the conformal expansion, as shown below.

As was introduced in equation (3.30), the first inverse moment of the pion

DA ϕ_π is related to the sum of all the Gegenbauer moments. We define this as our first "important parameter", Δ, via:

$$\int_0^1 du \frac{\phi(u,\mu^2)}{3u} \equiv \Delta(\mu^2) = 1 + \sum_{n=1}^{\infty}(-1)^n a_n(\mu^2) \tag{3.45}$$

If this sum is to be convergent then the a_{2n} must fall-off in n sufficiently fast (recalling that for the π, all odd-numbered a_n vanish due to G-parity). If we assume an asymptotic equal-sign behaviour for the moments with large n, then the slowest possible fall-off is power-like $a_{2n} \sim 1/n^p$, with p slightly larger than 1. When the distribution amplitude is defined with a power-like fall-off it is possible to explicitly sum over the Gegenbauer moments. This is done using the generating function for the Gegenbauer polynomials:

$$f(\xi,t) = \frac{1}{(1-2\xi t + t^2)^{3/2}} = \sum_{n=0}^{\infty} C_n^{3/2}(\xi)\, t^n \tag{3.46}$$

To show this, we begin from the full conformal expansion for the pion distribution amplitude, suppressing notation for the μ^2-dependence for compactness and defining $\bar{u} \equiv (1-u)$. We define the moments with a power-like fall-off as

$$a_n = \frac{1}{(n/b+1)^a} \tag{3.47}$$

for n even. This gives us an expression for the DA (for even n) of

$$\begin{aligned} \phi^+(u) &= 6u\bar{u} \sum_{n=0}^{\infty} C_n^{3/2}(2u-1)\, a_n \\ &= 6u\bar{u} \sum_{n=0}^{\infty} C_n^{3/2}(2u-1) \left[\frac{1}{(n/b+1)^a}\right] \end{aligned}$$

where ϕ^+ denotes the same-sign behaviour of the Gegenbauer moments. We can quite easily extend this across all values of n, giving

$$\phi^+(u) = 3u\bar{u}\sum_{n=0}^{\infty} C_n^{3/2}(2u-1)\left(1+(-1)^n\right)\left(\frac{b}{b+n}\right)^a$$

We can express the (a, b) dependent part of this equation in terms of an analytic integral equation

$$\left(\frac{b}{b+n}\right)^a = \frac{1}{\Gamma(a)}\int_0^1 dt\,(-\ln t)^{a-1}\,t^{n/b}$$

giving

$$\phi^+(u) = \frac{3u\bar{u}}{\Gamma(a)}\int_0^1 dt\,(-\ln t)^{a-1}\sum_{n=0}^{\infty} C_n^{3/2}(2u-1)\left(1+(-1)^n\right)t^{n/b}$$

The sum can be split into two parts

$$\sum_{n=0}^{\infty} C_n^{3/2}(2u-1)\,t^{n/b} + \sum_{n=0}^{\infty} C_n^{3/2}(2u-1)\,(-t)^{n/b}$$

which can be directly related to the generating function given in equation (3.46), and gives a final expression for the DA of

$$\tilde{\phi}^+_{a,b}(u) = \frac{3u\bar{u}}{\Gamma(a)}\int_0^1 dt(-\ln t)^{a-1}\left(f\left(2u-1, t^{1/b}\right) + f\left(2u-1, -t^{1/b}\right)\right) \tag{3.48}$$

Using an analogous method we can obtain a re-summed DA with alternating-sign behaviour of the Gegenbauer moments,

$$a_n = \frac{(-1)^{n/2}}{(n/b+1)^a} \quad \text{for } n \text{ even}$$

of

$$\tilde{\phi}^{-}_{a,b}(u) = \frac{3u\bar{u}}{\Gamma(a)} \int_0^1 dt(-\ln t)^{a-1} \left(f\left(2u-1, it^{1/b}\right) + f\left(2u-1, -it^{1/b}\right) \right) \tag{3.49}$$

From equation (3.45) we can find the corresponding values of Δ

$$\Delta^{+}_{a,b} = (b/2)^a \zeta(a, b/2) \qquad \Delta^{-}_{a,b} = (b/4)^a (\zeta(a, b/4) - \zeta(a, 1/2 + b/4)) \tag{3.50}$$

where $\zeta(a, s) = \sum_{k=0}^{\infty} 1/(k+s)^a$ is a generalisation of the Riemann zeta function known as the Hurwitz zeta function. In order to obtain models for arbitrary values of Δ we split off the asymptotic DA and write

$$\phi^{\pm}_{a,b}(\Delta) = 6u\bar{u} + \frac{\Delta - 1}{\Delta^{\pm}_{a,b} - 1}\left(\tilde{\phi}^{\pm}_{a,b}(u) - 6u\bar{u}\right) \tag{3.51}$$

valid for $a \geq 1$ and $b > 0$. This equation implies that the asymptotic DA is recovered for $\Delta = 1$ and also from $\phi^{+}_{a,b}$ in the limit $a \to 1$. Examples of these DAs for various values of a, b are shown in Figures 3.2 and 3.3 in the next section.

The fall off of the a_n in inverse powers of n gives a compact, closed expression for the DA using equation (3.51). This sort of fall-off behaviour is in fact intrinsic to QCD, which we can see if we consider the behaviour of the moments $a_n(\mu^2)$ under a change of scale. Taking the models defined at the hadronic scale $\mu \sim 1.2$GeV, we know the a_n scale with μ according to equation (3.4). For large n we have

$$\gamma_0^{(n)} \overset{n\to\infty}{\approx} 8C_F \ln n + O(1)$$

and

$$a_n(Q^2) \overset{n\to\infty}{\approx} \frac{1}{n^{4C_F/\beta_0 \ln(1/L)}}\, a_n(\mu^2)$$

with $L = \alpha_s(Q^2)/\alpha_s(\mu^2)$. This shows that the leading-order scaling induces a power-like fall-off of the a_n, at least for large n. Another consequence of this is that as $Q^2 \to \infty$ ($L \to 0$) the suppression of the higher order moments is power-like so that

$$\tilde{\phi}^{\pm}(Q^2 \to \infty) = \tilde{\phi}^{\pm}(a \to \infty) = 6u(1-u)$$

Hence the DAs $\phi^{\pm}_{a,b}$ defined in (3.51) approach the asymptotic DA in this limit, so both of the necessary conditions for the DA construction are satisfied.

3.5.3 Properties of model DAs

Once the parameters Δ, a and b are specified at a certain reference scale, the model DA can be evolved to a different scale via the evolution equation (3.22), using the method which we describe in Section 3.6 – which shows how the evolution equation can be solved numerically to leading logarithmic accuracy. The procedure for the full analytic evolution of a DA expressed as a conformal expansion is included for completeness in Appendix C.

After evolution to higher scales, the DA is no longer described by the function $\phi^{\pm}_{a,b}(\Delta)$ with a simple suitably chosen set of Δ, a and b. This lack of "form-invariance" under changes of scale is not however disadvantageous to our model. We determine the value of Δ at some low scale around $\mu = 1.2\text{GeV}$ (chosen according to the analysis of [87]) and ideally the other parameters a, b could then be fixed from some experimental or theoretical determination. There is an analogy to this elsewhere in QCD, for the *parton distribution function*, which has a parameterisation fixed at a low scale (typically ~ 2

GeV), but has parameters which are fitted to experimental data obtained at a large variety of scales [96–98].

Figures 3.2 and 3.3 show that the two models ϕ^+ and ϕ^- have quite a dissimilar functional dependence on the momentum fraction u, notably that ϕ^- becomes non-analytic at $u = 1/2$ for values of $a \leq 3$. The spike at $u = 1/2$ characteristic for ϕ^- causes these models to significantly deviate from the asymptotic distribution amplitude even for Δ close to 1.

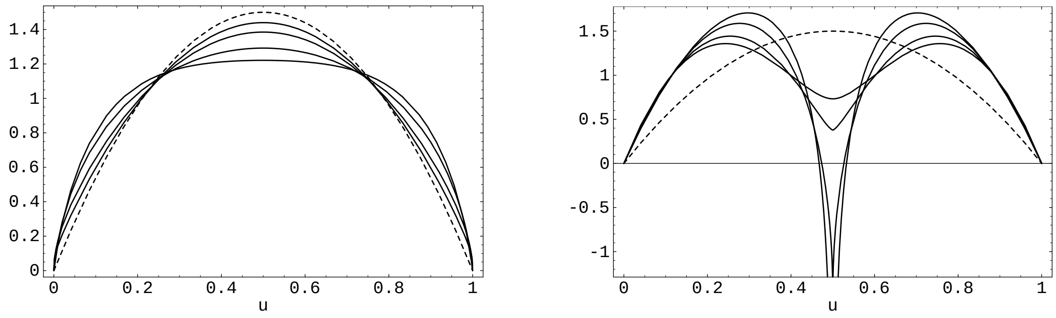

Figure 3.2: Left: Examples for model DAs $\phi^+_{a,b}$ as functions of u, for $a = 1.5, 2, 3, 4$, and constant $b = 2$ and $\Delta = 1.2$ (solid curves). For $a \to 1$, $\phi^+_{a,b}$ approaches the asymptotic DA. Right: the same for $\phi^-_{a,2}$. The asymptotic DA is also shown for comparison (dashed curve).

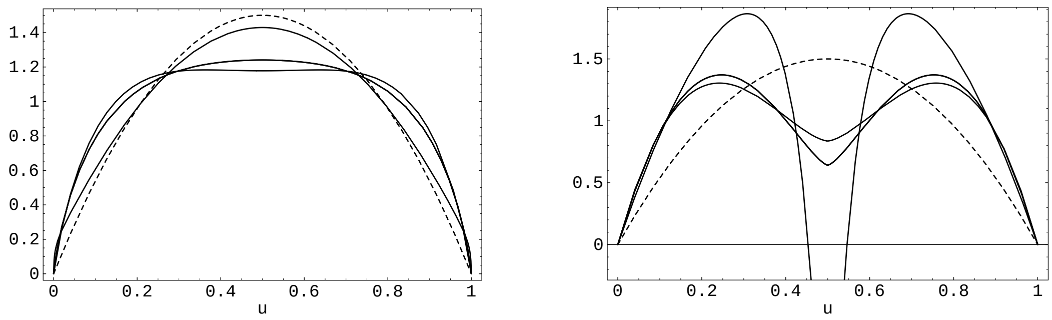

Figure 3.3: Left: Examples for model DAs $\phi^+_{a,b}$ as functions of u, for $b = 0.1, 1, 10$, and constant $a = 3$ and $\Delta = 1.2$ (solid curves). Right: the same for $\phi^-_{3,b}$. The asymptotic DA is also shown for comparison (dashed curve).

What we can also discern from the form of $\phi_{a,b}$ is that it is much more sensitive to variation in the fall-off parameter a, than b. Since the experimental data available are too scarce to constrain all of the parameters of the model we fix $b \equiv 2$. Using the set of model DAs $\phi_{a,b}$ we can find the possible values of the lowest non-zero Gegenbauer moments a_2 and a_4. For $a = 1$, ϕ approaches the asymptotic DA with $a_2 = a_4 = 0$; at $a \to \infty$ the models approach the standard NLO fixed order conformal expansion with $a_2 = \Delta - 1$ and $a_4 = 0$.

As discussed above, for models based on the truncated conformal expansion, the endpoint behaviour of the DA (as $u \to 0, 1$) is assumed to follow $\phi \sim u(1-u)$. This is no longer true for our new models for all possible values of a. For example, for the model ϕ^+, we have

$$\begin{aligned}
\phi^+ &\sim \sqrt{u(1-u)} && \text{for a} = 2 \\
\phi^+ &\sim u(1-u)\ln u(1-u) && \text{for a} = 3 \\
\phi^+ &\sim u(1-u) && \text{for a} > 3
\end{aligned}$$

We see that the linear endpoint behaviour is only obtained for models with higher values of a. This is not however a drawback to the model. The original argument in the literature for this endpoint behaviour was put forward in [41] from the calculation of DA moments via QCD sum rules:

$$\langle \xi^n \rangle = \int_0^1 du\, \xi^n \phi(u) \overset{n \to \infty}{\sim} \frac{1}{n^2}$$

This is a result of a leading order calculation of the perturbative contributions to the QCD sum rule. The NLO result [99, 100] does not have the same dependence, instead following

$$\phi \sim u(1-u)\ln^2\left(u/(1-u)\right)$$

which is equivalent to $a_n \sim (1/n^3)$. The large-n behaviour of the non-perturbative terms cannot be determined from the sum rules, but there is no reason why it should not follow the behaviour of NLO perturbation theory or some other scaling.

3.5.4 Constraints on model parameters

The asymptotic distribution amplitude is recovered for all models with $\Delta = 1$ and with ϕ^+ in the limit of $a \to 1$. We must impose the constraint that $a \geq 1$, otherwise the models $\phi^{\pm}_{a,b}$ will not vanish at the endpoints $u = 0, 1$. In order to constrain our parameters, we can now introduce the experimental restrictions on our parameter set Δ, a, b. As discussed above, we fix $b \equiv 2$ and we also fix our reference scale as $\mu = 1.2$ GeV. The available experimental data for the π, as summarised in [87], points to a value of Δ around 1.1 at the scale $\mu \approx 1.2\,\text{GeV}$.

If we require a_2 to be positive, which as seen in Section 3.4 is a reasonable conclusion from all of the previous determinations, then we require $\Delta \geq 1$. We can infer an upper bound from experimental data or by imposing the requirement that $a_2 \leq 0.2$ – the upper bound as found by the most recent analyses. This corresponding bound on Δ is $\Delta \leq 1.2$ for ϕ^+, and is smaller again for ϕ^-. The final constraint we must consider is the allowed range of

$\phi_\pi(1/2)$ from light-cone sum rule analyses, which give [29]:

$$0.9 \leq \phi_\pi(1/2, 1\,\mathrm{GeV}) \leq 1.5$$

For $\Delta > 1$, $\phi(1/2)$ is always smaller than 1.5, so only the lower bound is relevant. The upper bound on $\Delta^\pm$ for various values of a (as implied by the lower bound $\phi_\pi(1.2) \geq 0.9$) is

a	2	3	4	5	6	∞
Δ^+_{max}	2.04	1.58	1.43	1.36	1.33	1.27
Δ^-_{max}	1.04	1.11	1.16	1.19	1.22	1.27

The constraint on Δ^+ is weaker than those discussed above, but for ϕ^- the minimum value of $\phi_\pi(1/2)$ poses a nontrivial constraint on Δ. Concentrating on the general characteristics of the distribution amplitudes in order to retain a generality for the other psuedoscalar and vector mesons, we do not refine these constraints further using specific data for the pion. It is therefore possible to draw up a set of general constraints on the (symmetric) part of our model DAs:

- $1 \leq \Delta \leq 1.2$ with $0 \leq a_2 \leq 0.2$ for $\phi^+_{a,2}$: this is based on the observation [41] that DAs of mesons with higher mass tend to become narrower,
- $1 \leq \Delta \leq \mathrm{Min}(1.2, \Delta^-_{\mathrm{max}})$ for $\phi^-_{a,2}$, with Δ^-_{max} given in the table above,
- $b = 2$, lacking further data.

3.5.5 Extension to ϕ_K

As mentioned before, we have to distinguish between those mesons for which the $a_{\rm odd}$ vanish due to G-parity, such as the π, and the strange mesons, for which the odd moments are in general non-zero and induce an antisymmetric part into the DA.

We can now consider the extension of our new model DAs to the leading-twist DA of the Kaon, ϕ_K. This differs from ϕ_π by the contribution of odd Gegenbauer moments. We can construct a model for this antisymmetric part in an analogous way as before, where we introduce $\Delta^{\rm asym}, c, d$ in place of Δ, a, b. Since there is almost no information at all about the form of the antisymmetric DAs we set $d \equiv 2$ immediately. We have

$$\begin{aligned}
\tilde{\psi}_c^+(u) &= \frac{3u\bar{u}}{\Gamma(c)} \int_0^1 dt(-\ln t)^{c-1} \left(f(2u-1, \sqrt{t}) - f(2u-1, -\sqrt{t}) \right) \\
\tilde{\psi}_c^-(u) &= \frac{3u\bar{u}}{i\Gamma(c)} \int_0^1 dt(-\ln t)^{c-1} \left(f(2u-1, i\sqrt{t}) - f(2u-1, -i\sqrt{t}) \right)
\end{aligned} \tag{3.52}$$

The models give a value of the first odd moment as $a_1 = (2/3)^c$. If we wish to redefine these expressions to account for arbitrary a_1, we can write

$$\psi_c^\pm = a_1 (3/2)^c \tilde{\psi}_c^\pm(u) \tag{3.53}$$

An example of such a model is shown in Figure 3.4. The scale evolution proceeds as for the symmetric part. There is very little information about the a_1 moment for the Kaon – not even the sign is known reliably [46]. From a heuristic standpoint it is expected $a_1 \geq 0$. This is because the DA is expected to be skewed towards larger values of u, since u denotes the momentum of

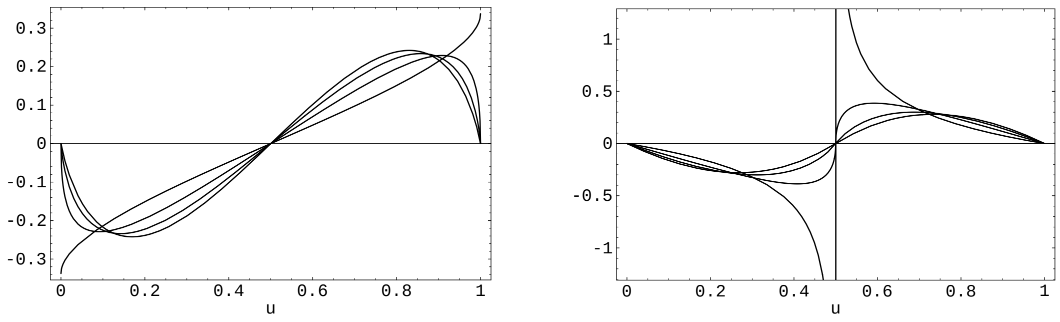

Figure 3.4: Models for the antisymmetric contributions to the twist-2 DA for $a_1 = 0.15$. ψ_c is shown as function of u for $c \in \{1, 2, 3, 4\}$. Left: ψ_c^+, Right: ψ_c^-. Like the symmetric models ϕ_a^-, ψ_c^- is non-analytic at $u = 1/2$ for $c \leq 3$.

the s-quark (the heavier quark) in the meson. The first calculation using QCD sum rules was from Chernyak and Zhitnitsky [41], who confirmed this intuition with a central value of

$$a_1^K(1\,\mathrm{GeV}) = 0.17 \tag{3.54}$$

This result was countered by the work of [99], who claimed to find a sign error in the CZ method as well as adding higher order radiative corrections; this gave a value of a_1 of

$$a_1^K(1\,\mathrm{GeV}) = -0.18 \tag{3.55}$$

It was reported in [46] that this re-analysis of the CZ sum rule calculation gave a problem with the q^2 dependence of the form factors. In light of these thoughts we use the original result from [41] and use the evolved value of $a_1 = 0.15$ at 1.2GeV. We can then combine the asymmetric and symmetric parts of the wavefunction to give a total DA for the K. We can write

$$\Delta^{\mathrm{tot},\pm} = \Delta + \Delta^{\mathrm{asym},\pm}$$

where Δ is the sum of the even-valued moments from the symmetric contributions to the DA, and we defined $\Delta^{\mathrm{asym},\pm}$

$$\begin{aligned}
\Delta^{\mathrm{asym},+} &= \int_0^1 du \frac{\psi_c^+(u)}{3u} = -a_1(3/2)^c \zeta(c, 3/2) \\
\Delta^{\mathrm{asym},-} &= \int_0^1 du \frac{\psi_c^-(u)}{3u} = -a_1(3/4)^c \left[\zeta(c, 3/4) - \zeta(c, 5/4)\right]
\end{aligned}$$

3.6 Numerical evolution of model DA

Using the evolution equation for the meson DA

$$\mu^2 \frac{\partial}{\partial \mu^2} \phi(u, \mu^2) = \int_0^1 dv\, V(u, v, \mu^2) \phi(v, \mu^2) \tag{3.56}$$

the kernel is given, to leading order in α_s, as

$$V(x, y, \mu) = C_F \frac{\alpha_s(\mu)}{2\pi} V_0(x, y) + O(\alpha_s^2)$$

with, for pseudoscalar mesons,

$$\begin{aligned}
V_0(x, y) &= V_{BL}(x, y) - \delta(x - y) \int_0^1 dz V_{BL}(z, y) \\
V_{BL}(x, y) &= \frac{1 - x}{1 - y} \left(1 + \frac{1}{x - y}\right) \Theta(x - y) + \frac{x}{y} \left(1 + \frac{1}{y - x}\right) \Theta(y - x)
\end{aligned}$$

Equation (3.56) is not well suited to the numerical evolution of ϕ, as it requires the use of an explicit formula for α_s, which is itself the leading order solution of a renormalisation group equation. In order to exactly reproduce the correct LO scaling behaviour of the Gegenbauer moments numerically, we can rewrite (3.56) in terms of a differential equation in α_s. To LO this is written as

$$-\frac{\beta_0}{2C_F}\,\alpha_s\,\frac{\partial}{\partial\alpha_s}\,\phi(x,\alpha_s) = \int_0^1 dy\, V_0(x,y)\phi(y,\alpha_s) \qquad (3.57)$$

which can be solved iteratively using Euler's method:

$$\phi(x,\alpha_s-\Delta\alpha_s) = \phi(x,\alpha_s) + \frac{2C_F}{\beta_0}\,\frac{\Delta\alpha_s}{\alpha_s}\int_0^1 dy V_0(x,y)\phi(y,\alpha_s)$$

We have checked that for $\Delta\alpha_s = 0.01$ and with 21 mesh points in x we correctly reproduce the known scaling behaviour of the truncated conformal expansion to within one per mille. We can show this for example, using the standard conformal expansion truncated at a_4

$$\phi(u,\alpha_s) = 6u(1-u)\left[1 + a_2(\alpha_s)C_2^{3/2}(2u-1) + a_4(\alpha_s)C_4^{3/2}(2u-1)\right]$$

using the values for the first two moments from Ball and Zwicky [46] given at $\mu = 1.2\text{GeV} \Rightarrow \alpha_s^{LO} = 0.6$ as $a_2(0.6) = 0.115$, $a_4(0.6) = -0.015$. Figure 3.5 shows the results for evolving this wavefunction up to a scale of 5.3 ($\alpha_s^{LO} = 0.26$) using the numerical method, and for the full analytical evolution using the formulae in Appendix C. As we can see clearly, both methods give equivalent results. The change of our model DAs with the scale μ is shown for an example model ($\phi^{\pm}_{3,3}$) in Figure 3.6.

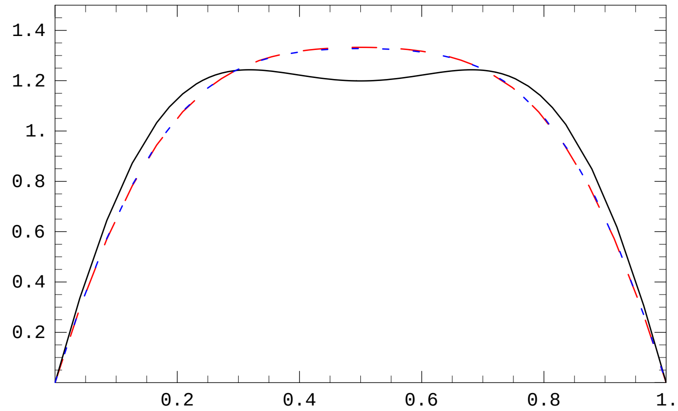

Figure 3.5: Numeric (dashed red line) and analytic evolution (dotted blue line) of sample DA from 1.2GeV to 5.3GeV; un-evolved DA shown for comparison.

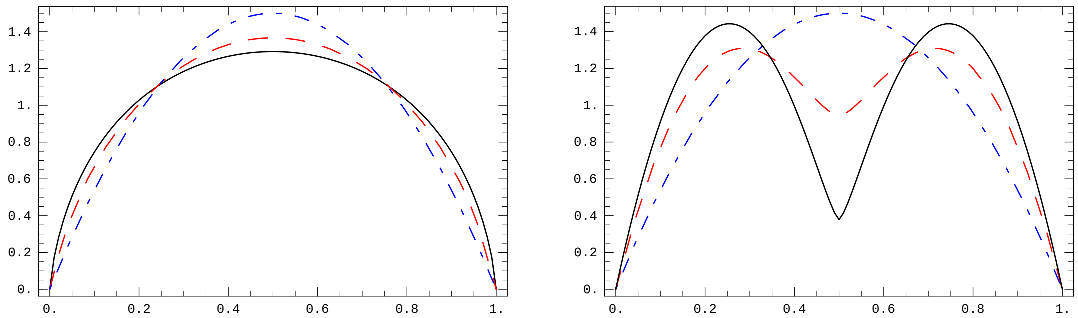

Figure 3.6: Evolution of model DAs. Left: $\phi^{+}_{3,3}(1.2)$ and Right: $\phi^{-}_{3,3}(1.2)$ from scale $\mu = 1.2$GeV (solid curves) to $\mu = 4.8$GeV (dashed red line). We also show the asymptotic curve for comparison (dot-dash blue line).

3.7 Application to $B \to \pi\pi$

It is at this point that we can consider the effects of the leading-twist DA on the non-leptonic B decays calculated within QCD factorisation. As shown in Chapter 2, the matrix elements determining the $B \to \pi\pi$ decay amplitudes are written as convolution integrals involving the leading twist DA. We discussed in Section 2.4 how the recent experimental data from the non-leptonic B decays (specifically $B \to \pi\pi$) imply the failure of QCD factorisation to explain the branching ratios and CP asymmetry measurements. This section investigates the effect of a non-standard DA on the predictions of QCD factorisation.

In this study, we use the full QCD factorisation formulae for the factorisable contributions (including the calculated $1/m_b$ corrections) and also include the model-dependent corrections for the hard-scattering terms (parameterised by the complex number X_H) which we include at the "default level" of $X_H = \ln(m_\pi/\Lambda_h) \sim 2.4$ [2]. We do not however include the non-factorisable weak annihilation terms. We use the input parameters as quoted in [3] except for that of the leading-twist ϕ_π, which we replace by our model parameter and the $B \to \pi$ transition form factor which we take from light-cone sum rules as found in [46].

We begin by considering the time-dependent CP asymmetry in $B \to \pi^+\pi^-$, which is defined as

$$A_{CP}^{\pi\pi} = \frac{\Gamma(\bar{B}_0 \to \pi^+\pi^-) - \Gamma(B_0 \to \pi^+\pi^-)}{\Gamma(\bar{B}_0 \to \pi^+\pi^-) + \Gamma(B_0 \to \pi^+\pi^-)} = S_{\pi\pi}\sin(\Delta m t) + C_{\pi\pi}\cos(\Delta m t) \tag{3.58}$$

where the mixing-induced and direct asymmetries ($S_{\pi\pi}$ and $C_{\pi\pi}$ respectively) depend on the unitarity triangle angles β and γ via

$$S_{\pi\pi} = \frac{2\,\mathrm{Im}\lambda_{\pi\pi}}{1+|\lambda_{\pi\pi}|^2} \qquad C_{\pi\pi} = \frac{1-|\lambda_{\pi\pi}|^2}{1+|\lambda_{\pi\pi}|^2} \tag{3.59}$$

with

$$\lambda_{\pi\pi} = e^{-2i\beta}\frac{e^{-i\gamma}+P/T}{e^{i\gamma}+P/T} \tag{3.60}$$

In practise, we calculate the CP asymmetry via its parameterisation in

Wolfenstein parameters, so that the CKM factors read

$$e^{\pm i\gamma} = \frac{\bar{\rho} \pm i\bar{\eta}}{\sqrt{\bar{\rho}^2 + \bar{\eta}^2}} \qquad e^{-2i\beta} = \frac{(1-\bar{\rho})^2 - \bar{\eta}^2 - 2i\bar{\eta}(1-\rho)}{(1-\bar{\rho})^2 + \bar{\eta}^2} \tag{3.61}$$

Although the penguin-to-tree ratio P/T is highly suppressed, it is not negligible and can be expressed via QCD factorisation in terms of CKM phases and pure strong interaction parameters.

$$\begin{aligned} \frac{P}{T} &= \frac{re^{i\phi}}{\sqrt{\bar{\rho}^2 + \bar{\eta}^2}} \\ &= \left(\frac{1}{\sqrt{\bar{\rho}^2 + \bar{\eta}^2}}\right) \frac{\left(a_4^c(\pi\pi) + r_\chi^\pi a_6^c(\pi\pi)\right) + \left(a_{10}^c(\pi\pi) + r_\chi^\pi a_8^c(\pi\pi)\right)}{a_1(\pi\pi) + \left(a_4^u(\pi\pi) + r_\chi^\pi a_6^u(\pi\pi)\right) + \left(a_{10}^u(\pi\pi) + r_\chi^\pi a_8^u(\pi\pi)\right)} \end{aligned} \tag{3.62}$$

P/T is then given by a ratio of polynomials in the Gegenbauer polynomials a_n with complex coefficients. This enables us to write the time-dependent CP asymmetry as

$$S_{\pi\pi} = \frac{2\bar{\eta}\left[\bar{\rho}^2 + \eta^2 - r^2 - \bar{\rho}(1-r^2) + (\bar{\rho}^2 + \bar{\eta}^2 - 1)\, r\cos\phi\right]}{\left[(1-\bar{\rho}^2) + \bar{\eta}^2\right]\left[\bar{\rho}^2 + \bar{\eta}^2 + 2r\bar{\rho}\cos\phi\right]} \tag{3.63}$$

In the limit where P/T is zero this reduces to $S_{\pi\pi} = \sin 2\alpha$.

The variation of the CP asymmetry in terms of Δ is shown in Figure 3.7. The left-hand figure shows the variation within the physical region for Δ, and shows that both S_{+-} and the direct asymmetry C_{+-} are largely independent of Δ. The right-hand figure shows the level of enhancement required to approach a 10% change in the value of the asymmetry, and that there is an increased effect for larger value of a. The effect is only significant for unrealistically large values of Δ. The current experimental results [101, 102]

$$S_{\pi\pi} = -0.30 \pm 0.17 \pm 0.03 \quad (\text{BaBar})$$
$$S_{\pi\pi} = -0.67 \pm 0.16 \pm 0.06 \quad (\text{Belle})$$

can only be accommodated using very extreme values of Δ. For example, taking a model with same-sign fall-off, to reproduce the BaBar result with $a = 2$ would require a value of $\Delta > 10$ to be within the 1σ band and $\Delta = 20$ to approach the central value. This also produces unphysical values for the Gegenbauer moments, $a_2(2.2\text{ GeV}) = 7.7$ and $a_4(2.2\text{ GeV}) = 0.5$. Obtaining a value of $S_{\pi\pi} = -0.67$ is not possible for values of $\Delta \geq 1$, which is required to keep a_2 positive.

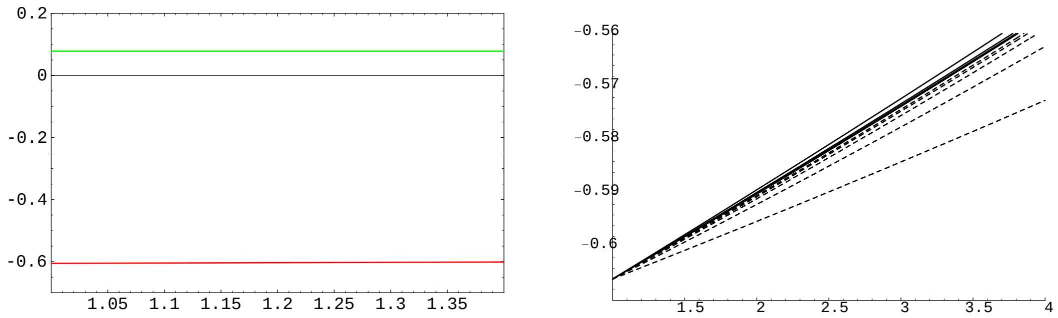

Figure 3.7: CP asymmetries in $B \to \pi^+\pi^-$ decays in QCD factorisation. Left: In physical region of Δ, C_{+-} (green) and S_{+-} (red). Right: S_{+-} as a function of Δ for $a = 2, 3 \ldots 6$, shown for models with same-sign fall-off (dashed) and alternating fall-off (solid lines). Curves converge as a increases.

We now move on to study the effect of the model DAs on the $B \to \pi\pi$ branching fractions. We find that the effect is significantly more pronounced on the branching ratios than for the CP asymmetries, as there is no longer the near cancellation of terms that occurs in the calculation of A_{CP}. Considering first the decay of $B \to \pi^+\pi^-$, the central value from QCD factorisation (for the asymptotic DA) is found to be

$$\mathrm{BR}(B \to \pi^+\pi^-) = 5.5 \times 10^{-6} |0.25 e^{i \cdot 15^\circ} + e^{-i\gamma}|^2 \tag{3.64}$$

where $\gamma = 60^\circ \pm 7^\circ$ [103], and the explicit dependence of the branching ratio on the Gegenbauer moments is again a polynomial in a_n. Figure 3.8 shows the variation of the branching ratios for the model DAs compared with the current experimental data. These graphs show that large increases away

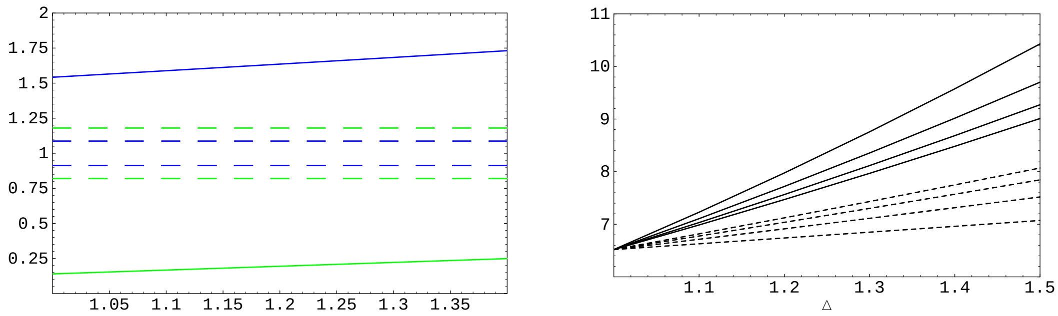

Figure 3.8: Left: Ratio of CP-averaged branching ratios for $B \to \pi\pi$ decays as compared with experimental result as a function of Δ, for model DA $\phi^+_{2,2}$; $B^0 \to \pi^+\pi^-$ (blue) and $B^0 \to \pi^0\pi^0$ (green). Right: Example of $\Gamma(B \to \pi^+\pi^-)$ (units 10^{-6}) as a function of Δ for $a = 2, 3 \ldots 5$ for same-sign fall-off (dashed lines) and alternating (solid lines). Curves converge for increasing a.

from the asymptotic value are possible by increasing Δ within its physical range. However, we see that in the case of $\pi^0\pi^0$ (where unlike $\pi^+\pi^-$, the enhancement is toward the experimental value) it is still not possible to reach the 1σ error bound within the allowed range of Δ.

This study does not aim to be a full error analysis and the graphs presented here are illustrative of the discrepancies that exist in the $\pi\pi$ system for QCD factorisation predictions. These results show that the lack of agreement between the predictions and the experimental results is not a result of the uncertainties from the leading-twist distribution amplitude, not even with our model DA with parameters well outside the allowed range. An alternative explanation of these discrepancies, namely the over-neglect of suppressed non-factorisable corrections, is discussed next in Chapter 4.

Chapter 4

Non-factorisable corrections to charmless B-decays

It does not do to leave a live dragon out of your calculations

"The Hobbit", J.R.R. Tolkien

This chapter is devoted to a study of the non-factorisable corrections to non-leptonic charmless decays of the B-meson. This subset of decays is a crucial testing ground for QCD factorisation (QCDF). As we have access to increasingly accurate measurements in the flavour sector, it is essential to exploit the data to better understand the limitations and potential "pitfalls" with QCDF. Indeed, before we enter the era of LHC physics we ideally need to have complete grasp of the theoretical framework of B decays, as it is expected this sector will provide complementary, indirect evidence for new physics searches. As we discussed in Chapter 2, QCDF is only marginally consistent with the data on charmless B-decays, and investigation is warranted to study the source of this discrepancy.

It is known that the factorisable contributions to exclusive B decays can be estimated using the formalism of QCD factorisation which is exact in the heavy quark limit, $m_b \to \infty$. Contributions that cannot be treated in this framework, i.e. the "non-factorisable" corrections, vanish in this limit, and are in general treated as unknown hadronic parameters.

Our study specifically scrutinises the $B \to \pi\pi$ system in the context of these unknown non-factorisable corrections. A previous analysis of non-factorisable corrections was presented in [50], but we consider a different approach to the problem, and specifically quantify our comparison of the theory – data agreement. We begin by removing the model dependence from the QCDF predictions and including "generic" non-factorisable (NF) contributions which aim to replicate both the known and unknown NF corrections. Our aim is to determine the general size and nature of the NF corrections and test what exactly is required to reconcile the predictions with the experimental data.

Our study analyses three separate scenarios for the inclusion of non-factorisable effects; in each scenario the sizes and phases of the NF contributions are varied. We also test a scenario which includes an enhanced *"charming penguin"* contribution, which we discuss in the following sections. We analyse the level of NF corrections required to bring each of the branching fractions and CP asymmetries within the $B \to \pi\pi$ system in line with their experimental measurements. Finally, we give a short discussion on the implication of our results on the predictions for $B \to \pi K$, on which analysis is currently underway [104].

4.1 Non-factorisable effects in $B \to \pi\pi$

The continued improvement of experimental data on the charmless B decays, most notably for $B \to \pi\pi$, has culminated in a large enough number of results (with sufficient accuracy) to fully constrain all the QCD parameters relevant for describing this system. There are now six available measurements for the three $B \to \pi\pi$ channels, for the branching ratios $\mathrm{BR}(B \to \pi^+\pi^-)$ [105, 106], $\mathrm{BR}(B \to \pi^+\pi^0)$ [105,107] and $\mathrm{BR}(B \to \pi^0\pi^0)$ [107,108], and for the three CP asymmetry measurements S_{+-}, C_{+-} [101, 102] and C_{00} [107, 108]. The CP asymmetries are defined in equation (3.59). We use the most recent data (as of September 2005) from BaBar and Belle, as well as the combined results from the Heavy Flavour Averaging Group (HFAG)[1]. Although this system is well known experimentally, there are still some discrepancies between the two B-factory experiments, most notably in the measurement of $B \to \pi^0\pi^0$, and increasingly in the measurement of $B \to \pi^+\pi^-$. These are shown for illustration in Figure 4.1 and the CP asymmetries for $\pi^+\pi^-$ in Figure 4.2.

As discussed in Section 2.4, there are discrepancies between these results and the QCDF predictions, leading to the coined "$B \to \pi\pi$ problem". In Chapter 3 we examined the effect of the uncertainty in the hadronic input parameters – specifically that of the light-cone distribution amplitude of the pion – on the $B \to \pi\pi$ observables. We determined that the resummed models can significantly affect the branching ratios and can account for both moderate and large deviations from the asymptotic DA. However, these models cannot cause enough enhancement to bring agreement between theory and data, within the physical range of the model input parameters. It is logical therefore, to examine the next large source of uncertainty in the theoretical

[1] http://www.slac.stanford.edu/xorg/hfag/index.html

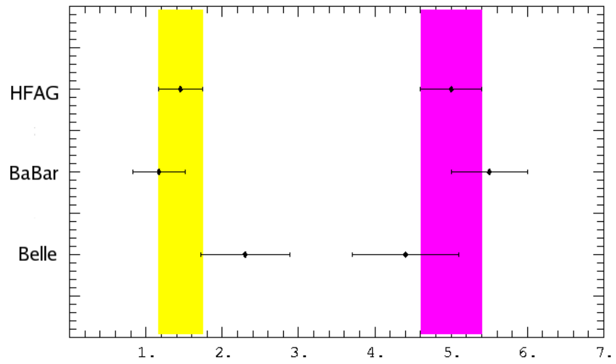

Figure 4.1: Plot of experimental results for $B \to \pi\pi$ branching fractions in units of 10^{-6}: From left to right $B \to \pi^0\pi^0$ (Yellow), and $B \to \pi^+\pi^-$ (Magenta). HFAG error bounds are shown for comparison: $\mathrm{BR}(B \to \pi^0\pi^0) = (1.45\pm0.29)\times10^{-6}$ and $\mathrm{BR}(B \to \pi^+\pi^-) = (5.0\pm0.4)\times10^{-6}$.

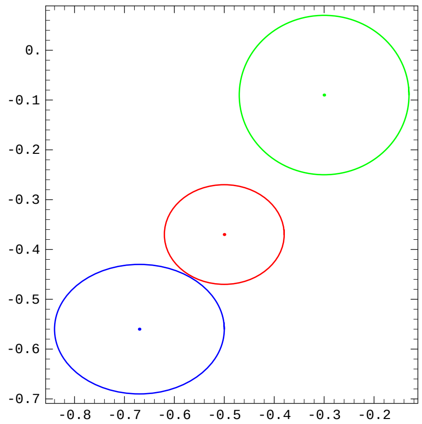

Figure 4.2: Plot of experimental results for $B \to \pi\pi$ CP asymmetries from HFAG (Red), Belle (Blue) and BaBar (Green). The horizontal axis shows $S_{\pi\pi}$ and the vertical axis $C_{\pi\pi}$.

predictions: non-factorisable corrections.

The large quantity of experimental data makes this system ideal to test our hypothesis that non-factorisable contributions can have a large effect on predictions of charmless B decays. Annihilation contributions to $B \to \pi\pi$ are expected to be small in QCDF, and this is supported by attempts of direct calculation of these topologies via QCD sum rules [109]. If this is the case, then the enhanced NF contributions would be predominantly from hard-gluon exchange, as parameterised by the non-perturbative parameter

X_H. This is supported to some degree by the results of factorisation fits to charmless data [110]. This study fits both X_H and X_A to all the experimental data on charmless decays and finds best-fit values for X_H well outside the expected range. In our analysis we do not distinguish between the different sources of NF correction, instead categorising them according to their contribution to the $B \to \pi\pi$ isospin amplitudes. Using the decomposition presented in Section 2.3.3, we find that additional contributions will be required mainly for the $\Delta I = 1/2$ amplitude.

4.2 Charming penguins

The *charming penguin* is a non-perturbative $\mathcal{O}(\Lambda_{QCD}/m_b)$ correction from enhanced penguin diagrams containing charm loops (Figure 4.3). It was first introduced by Ciuchini et al. in 1997 [111, 112], who added long-distance contributions to decay amplitudes to improve agreement of fits to experiment. The charming penguin originates from a non-perturbative penguin contraction of the leading operators in the effective Hamiltonian, namely those with $\mathcal{O}(1)$ Wilson coefficients Q_1 and Q_2, i.e., when the c and $\bar{c}$ annihilate. It is expected to give large contributions in some decay channels, notably $B \to K^+\pi^-$ and $B^+ \to K^0\pi^+$, where the factorised amplitudes are colour or Cabbibo suppressed with respect to the penguins.

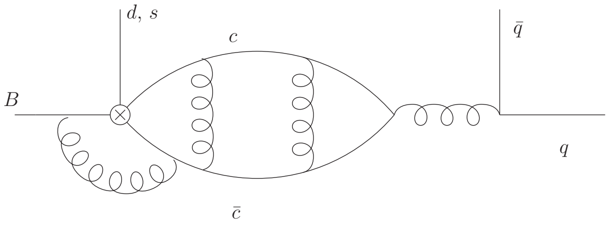

Figure 4.3: Example of a charming penguin.

The evidence and support for a charming penguin contribution has fluctuated since their introduction in [111]. The original parameterisation was in terms of a diagrammatic deconstruction into renormalisation group invariant quantities or topologies [113]. For example the leading (tree) contributions are described by emission topologies E_1 and E_2 which are scheme independent combinations of Wilson coefficients and matrix elements related to the current-current operators Q_1 and Q_2, as shown in Figure 4.4.

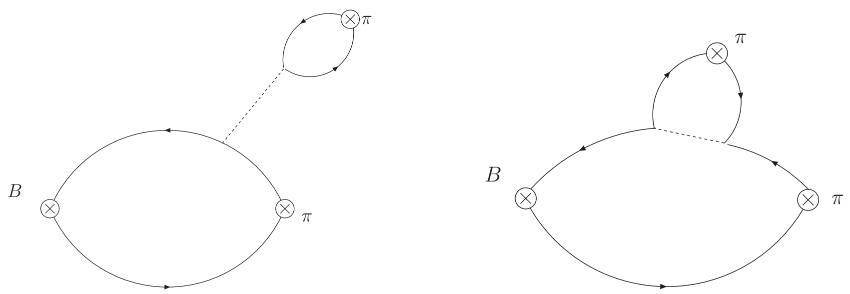

Figure 4.4: Emission diagrams. Left: colour allowed (DE) topology; Right: colour suppressed (CE) topology. The dashed line represents the four-fermion operator.

The charm and *GIM penguin* followed a topology of the type in Figure 4.5. The charming penguin has only the charm quark in the loop; the GIM penguins are those where the diagrams always appear in the combination of $u-c$.

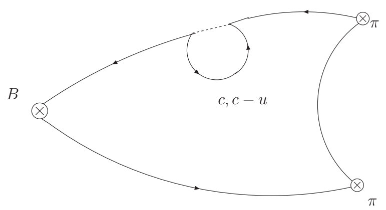

Figure 4.5: Example of charming and GIM penguin topologies (CP).

This description was later updated to include further diagrams (annihilation and penguin contractions) in addition to the original diagram, to give two phenomenological parameters $\widetilde{P}_1$ and $\widetilde{P}_1^{\rm GIM}$ for the charming and GIM penguins respectively. Fits of the charming penguins to $K\pi$ and $\pi\pi$ decays gave promising results [114]. However, when QCD factorisation was introduced and the non-factorisable corrections were shown to be calculable in perturbation theory, the charming penguin fell out of favour. It should be noted that since the charm penguins are expected to have a size equivalent to a $\Lambda_{\rm QCD}/m_b$ correction they are not in fact in conflict with the QCDF results in the $m_b \to \infty$ limit. If we call into question the size of the power-suppressed corrections to the $\Lambda_{\rm QCD}/m_b$ expansion and expect – and in fact demand – some of the non-factorisable contributions to be large, the charming penguin can provide significant additional contributions at this order.

The current QCD factorisation predictions (specifically for the $B \to \pi\pi$ and $B \to \pi K$ decays) do not satisfactorily explain the current experimental data. Both the $B \to \pi\pi$ and $B \to \pi K$ decays may require significant levels of power-suppressed corrections. It is therefore quite possible that the charming penguin can provide additional enhancement, enough to bring the predictions into agreement with the current experimental results.

Charming penguins are not Cabbibo enhanced in $B \to \pi\pi$ decays, unlike the case for $B \to \pi K$. It is naively expected that, along with the other $\mathcal{O}\left(\Lambda_{\rm QCD}/m_b\right)$ corrections, the charming penguin contributions should be small. However, as we show in our study, the predictions for the $B \to \pi\pi$ branching fractions cannot be brought into agreement with the experimental data without significant non-factorisable corrections. Since the charming penguin is of the same order as the $\mathcal{O}\left(\Lambda_{\rm QCD}/m_b\right)$ effects, there is no reason why a sizable contribution should not exist in these decays.

The charming penguin parameter $\widetilde{P}_1$, and the GIM-penguin parameter $\widetilde{P}_1^{\rm GIM}$

were expressed as a complex number fitted to experiment by Ciuchini et al., and added to the factorisable amplitudes via

$$P_1 = a_4^c A_{\pi\pi} + \widetilde{P}_1 \qquad P_1^{\mathrm{GIM}} = (a_4^c - a_4^u) A_{\pi\pi} + \widetilde{P}_1^{\mathrm{GIM}}$$

where the notation is from QCD factorisation, as found in Appendix B.

There is some disagreement over the inclusion of charming penguins within the factorisation framework. The parameter $\widetilde{P}_1$ contains not only the charming penguin contribution but additionally the annihilation and penguin contractions of the penguin operators. Ciuchini et al. suggest that all chirally suppressed terms should be dropped and replaced with this term (these correspond to dropping the coefficients a_6^p from QCD factorisation). The proponents of QCD factorisation however, argue that the "charming penguin" contribution is completely described by the penguin annihilation contributions and non-perturbative corrections to the coefficient a_4^c, i.e those contained in a_6^c. They argue that a large non-perturbative penguin enhancement is implausible, and that any modification required to bring theory predictions into agreement with data should be attributed to weak annihilation rather than charming penguins [2].

As our study does not include any of the model-dependent calculations of the $\mathcal{O}(\Lambda_{\mathrm{QCD}}/m_b)$ terms suggested by BBNS, to obtain a charming penguin enhancement we need additional contributions. We do not replace all of the chirally-suppressed terms as suggested by Ciuchini et al., and instead take the charm penguin to be in addition to the QCDF penguin diagrams (i.e. keep the calculable part of a_6^c, but remove any dependence on terms proportional to X_H). We can then allow for the possibility of the charming penguin explicitly as an enhancement of the coefficient $\alpha_4^c = a_4^c + r_\chi a_6^c$.

4.3 $B \to \pi\pi$ Analysis

We use the expansion of the $B \to \pi\pi$ decay amplitudes in terms of the two isospin amplitudes $A_{1/2}$ and $A_{3/2}$. We construct three different scenarios for inclusion of non-factorisable corrections and enhancements on top of the factorisable amplitude as calculated within QCD factorisation. We include only the (fully) factorisable parts from QCDF, i.e. we do not include the hard-scattering or annihilation contributions incorporated in the model-dependent parameters X_H and X_A (Section 2.3.2). NF corrections are then added according to the prescriptions of our three scenarios, so we can determine the size and nature of corrections needed to reconcile with the experimental data.

In each scenario we allow the size and phases of the NF contributions to each isospin amplitude to vary independently. The full set of $B \to \pi\pi$ branching ratios and CP asymmetries are calculated for each of the combinations of NF contributions we consider. We take a defined set of input parameters which are also varied within their allowed ranges in order to further optimise the agreement between theory and experiment. Our input parameters are a combination of CKM phases, the $B \to \pi$ form factor and Δ from the parameterisation of the pion wavefunction using the models developed in Chapter 3.

	Input ranges
Δ	$1.1\leq \Delta \leq 1.3$
$F^{B\to\pi}$	0.26 ± 0.04
R_u	0.399 ± 0.08
γ	$60.3°\pm 6.8°$

We consider primarily the data from the HFAG which averages over all of the current data available for each channel. However, we consider the data from BaBar and Belle separately where it is required, if the discrepancy between the two experiments is significant. Each of our scenarios is constructed with a "base" of the fully calculated factorisable part of the $B \to \pi\pi$ isospin amplitudes, as found using from QCDF. Different combinations of non-factorisable corrections and charming penguins are then added.

We add a percentage non-factorisable contribution to each of the isospin amplitudes individually. The amplitude $A_{3/2}$ is tree dominated with a tiny contribution from electroweak penguins; the expressions for the isospin amplitudes given in equation (2.37) show that the amplitude $A^c_{3/2}$ contains only contributions from electroweak penguins. We can therefore safely assume that there will be no significant non-factorisable contribution to this particular amplitude. This is supported by the good agreement between the QCD factorisation prediction and the measurement for the decay $B \to \pi^+\pi^0$.

The non-factorisable corrections are added then as

$$\begin{aligned} A_{3/2} &= A^F_{3/2} + \lambda^*_u\,|A^{u\,F}_{3/2}|\,N_{3/2}\,e^{i\,d_{3/2}} \\ A_{1/2} &= A^F_{1/2} + \lambda^*_u\,|A^{u\,F}_{1/2}|\,N^u_{1/2}\,e^{i\,d_u} + \lambda^*_c\,|A^{c\,F}_{1/2}|\,N^c_{1/2}\,e^{i\,d_c} \end{aligned} \tag{4.1}$$

where the notation is intuitive: the superscript F denotes the pure factorisable amplitudes, the $N_{\Delta I}\, e^{i\, d_{\Delta I}}$ is the size of the non-factorisable contribution ($0 \leq N_{\Delta I} \leq 1$), with arbitrary phase $d_{\Delta I}$. The level of non-factorisable corrections is expected to be of the order of $\bar{\Lambda}/m_b \sim 10\%$, where $\bar{\Lambda}$ measures the kinetic energy of the b quark within the B meson. As a conservative estimate, we allow corrections of up to 20% as our "normal" expected level, i.e taking each $N \leq 0.2$. As an indicator for the enhanced corrections we allow double this estimate with up to 40% non-factorisable corrections. Anything beyond this limit would be approaching the point where the factorisation scheme itself would begin to break down. The QCD factorisation scheme is based upon the calculation of order α_s corrections, so any terms suppressed by $1/m_b$ should not be much larger than $\alpha_s m_b$, otherwise it would not make sense to include small calculable terms and to neglect large incalculable terms.

We also consider the possibility of additional contributions from charming penguin diagrams, which are not accounted for in the calculation of the factorisable amplitudes. The charming penguin contribution arises purely in the isospin amplitude $A^c_{1/2}$, and as such, can be parameterised as an enhancement to the factorisation coefficient α^c_4

$$\alpha^c_4 = a^c_4 + r_\chi a^c_6 \rightarrow \alpha^{c\,eff}_4 = R\,\alpha^c_4$$

where R is some complex factor $R = |R|e^{i\varphi}$ with $|R| > 1$. This will have an effect on both the decay amplitudes for $BR(B \rightarrow \pi^+\pi^-)$ and $BR(B \rightarrow \pi^0\pi^0)$, but there is no effect on $BR(B \rightarrow \pi^+\pi^0)$ which has no contribution from $A^c_{1/2}$.

The scenarios are summarised as follows:

- Scenario I: QCD factorisation + expected level of non-factorisable corrections at $\leq 20\%$

- Scenario II: QCD factorisation + enhanced non-factorisable corrections at $\leq 40\%$

- Scenario III: QCD factorisation + expected non-factorisable corrections at $\leq 20\%$ and charming penguin contribution

In order to quantify the "quality" of each of these scenarios we construct a χ^2 statistic, where the form factor $F_0^{B\to\pi}(0) \equiv F^\pi$ and the phases of the non-factorisable contributions (NF) are left as fitting parameters. The absolute size of the NF correction and the CKM parameters R_u and γ are taken as fixed, and the fitting is performed separately over differing values of the pion distribution amplitude parameter Δ. We define

$$\chi^2 = \sum_{i=1}^{6} \frac{[y_i - x_i]^2}{\sigma_i^2}$$

where y_i are the theory predictions, and x_i are the data values with their associated error σ_i, calculated by combining statistical and systematic errors in quadrature. The index i runs over the 6 available experimental measurements of the CP-averaged branching ratios and CP asymmetries: $\{\Gamma^{+-}$, Γ^{00}, Γ^{+0}, S_{+-}, C_{+-}, $C_{00}\}$. We then numerically minimise the χ^2 while scanning over the three phases and applying the constraint $F^\pi < 0.3$. We perform this separately for the BaBar, Belle and HFAG averaged data sets. The goodness-of-fit then follows the χ^2 probability distribution with 2 degrees of freedom (equal to the number of measurements minus the number of fitted parameters). We express the goodness-of-fit as χ^2/n_d, where the closer the value to 1, the better the fit.

4.4 Results

We now present and discuss the results of the analysis for the $B \to \pi\pi$ system for each of the specified scenarios in turn.

4.4.1 Scenario I

In this scenario we calculate the CP-averaged branching ratios and CP asymmetries for $B \to \pi\pi$ decays with the expected level of non-factorisable corrections ($\leq 20\%$). We find that it is very difficult to reconcile the predictions for all of the observables with their experimental measurements within the experimental error bounds. We varied all of the input parameters within their allowed ranges and found a set of optimum inputs (shown in Table 4.1) which gave the best agreement between theory and experiment; the results were approximately the same for all data sets. The two CKM parameters optimised at their input values but the DA parameter Δ required its maximum allowed contribution to best optimise the agreement. For the form factor we used the best-fit value as calculated from the minimisation of the χ^2 function on the full set of $B \to \pi\pi$ data.

Δ	F^{π}	R_u	γ
1.3	0.22	0.399	60.3°

Table 4.1: Optimum input parameter; R_u, γ are the default central values ($R_u = \sqrt{\bar{\rho}^2 + \bar{\eta}^2}$) for 20% non-factorisable corrections.

Since the optimum scenario is clearly obtained for the maximum possible NF correction, we specified the size of the contributions as $N = 0.2$ for each amplitude and scanned over all possible phase combinations. We then calculated the ratio of the theory over experimental results for the branching fractions and the CP asymmetries. The most illustrative results are of $B \to \pi^+\pi^-$ against $B \to \pi^0\pi^0$ and for $S_{\pi\pi}$ against $C_{\pi\pi}$. Considering first the branching ratios, the value of $\mathrm{BR}(B \to \pi^+\pi^0)$ is quite well reproduced, but the $\pi^+\pi^-$ and $\pi^0\pi^0$ branching fractions show considerable discrepancy. This is illustrated for the HFAG result in Figure 4.6 and also separately for the data sets from BaBar and Belle in Figure 4.7 and Figure 4.8 respectively, highlighting the large impact of the differing measurements of $\mathrm{BR}(B \to \pi^+\pi^-)$.

The ellipses shown in Figures 4.6 to 4.8, are the 2σ and 3σ error ellipses. These are calculated from the experimental results under the assumption of no correlation between the branching ratios, and using the measured correlations for the CP asymmetries [101, 102]. These curves correspond to confidence regions (confidence level across 2 degrees of freedom) of $\sim 84\%$ and $\sim 95\%$ respectively.

These figures clearly show that with a 20% non-factorisable correction, it is not possible to reproduce the experimental data within the 2σ error bound, and not even to 3σ using the Belle data alone. Using the HFAG data and maximal contribution of $\Delta = 1.3$, the χ^2 minimisation yields a value of $F^\pi = 0.22$ with χ^2/r of $4.41/2$. For the BaBar data alone we also obtain $F^\pi = 0.22$ but with a much improved fit and $\chi^2/r = 0.850/2$.

We observe that in increasing the parameter Δ from the asymptotic value ($\Delta = 1$) to its physically allowed maximum ($\Delta = 1.3$) we find a steadily decreasing χ^2 value, and correspondingly increasing best-fit value of F^π. The distribution of the χ^2 values as a function of the form factor is plotted for 20% NF corrections, for the full range of possible phases in Figure 4.9. This shows clearly the minimum χ^2 in agreement with the numerical minimisation

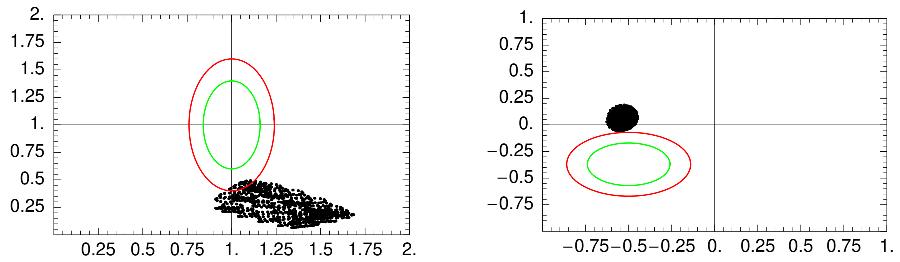

Figure 4.6: Theory/Experimental ratio using HFAG data for Γ^{+-} against Γ^{00} (left) and CP asymmetry $S_{\pi\pi}/C_{\pi\pi}$ (right). Error ellipses shown at 2σ and 3σ.

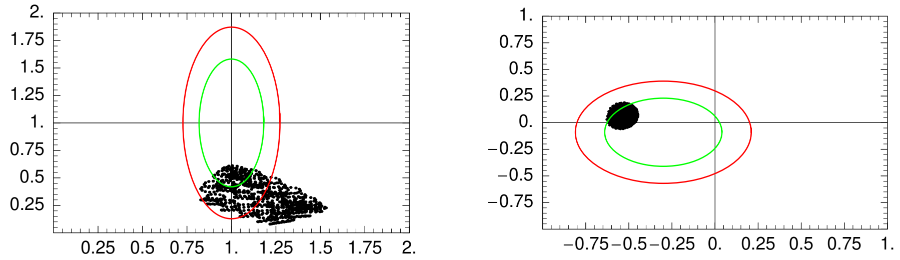

Figure 4.7: As Figure 4.6 using only BaBar data set.

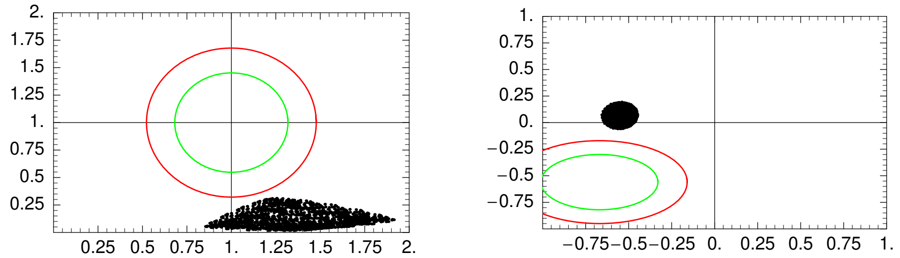

Figure 4.8: As Figure 4.6 using Belle data set.

requiring $F^{\pi} \sim 0.22$.

4.4.2 Scenario II

In a direct extension of Scenario I, we repeat our study with a further enhanced non-factorisable contribution beyond that of the expected levels. We again use the factorisable isospin amplitudes calculated within QCDF, but now add up to 40% non-factorisable corrections. As may be expected, this reproduces the experimental data quite well. We find the optimum parameter set to be similar to that from Scenario I; the agreement is not greatly

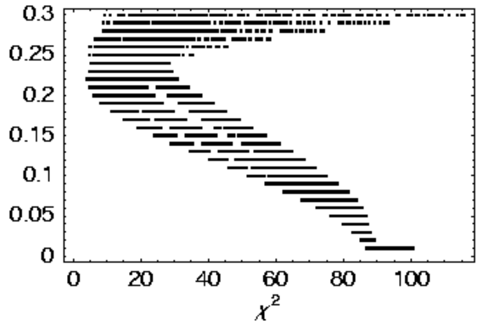

Figure 4.9: Dependence of minimum χ^2 on F^π for $\Delta = 1$ and 20% NF correction.

improved from changing the CKM input, but it is improved by the maximisation of Δ and use of the best-fit form factor. For a 40% NF correction, the χ^2 minimisation gives a value of $F^\pi = 0.23$ at $\chi^2/r = 2.0/2$ when using the maximum correction of $\Delta = 1.3$. As in Scenario I, we see that the χ^2 improves as we increase Δ, and the best-fit form factor increases correspondingly, around the value of $F^\pi \sim 0.23$. This is illustrated in Figure 4.10.

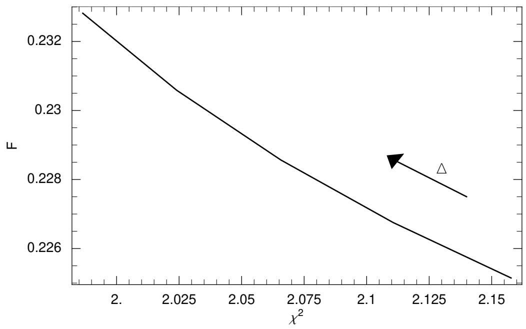

Figure 4.10: Dependence of minimum χ^2 on F^π with increasing Δ for 40% NF correction.

We find that there is a range of allowed values of from $0.21 \leq F^\pi \leq 0.23$ which give good agreement with the data. We illustrate the best possible agreement (for both a 30% and 40% non-factorisable correction) using the BaBar data set in Figure 4.11.

The results using the HFAG data are shown in Figure 4.12. In this case the

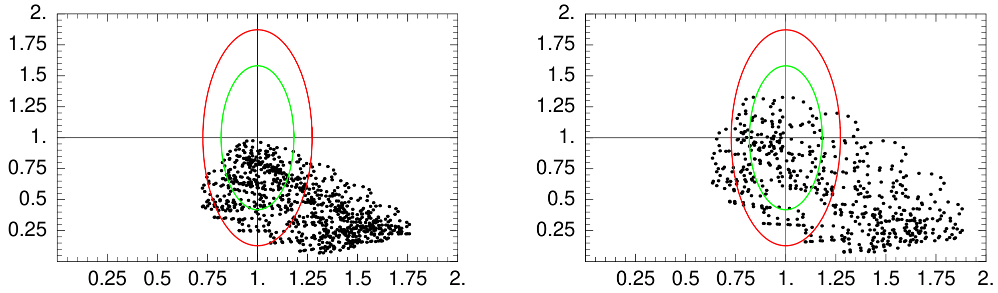

Figure 4.11: The $BR(B \to \pi^+\pi^-)$, $BR(B \to \pi^0\pi^0)$ agreement for the best-fit case for 30% NF correction (left) and 40% (right), both using BaBar data.

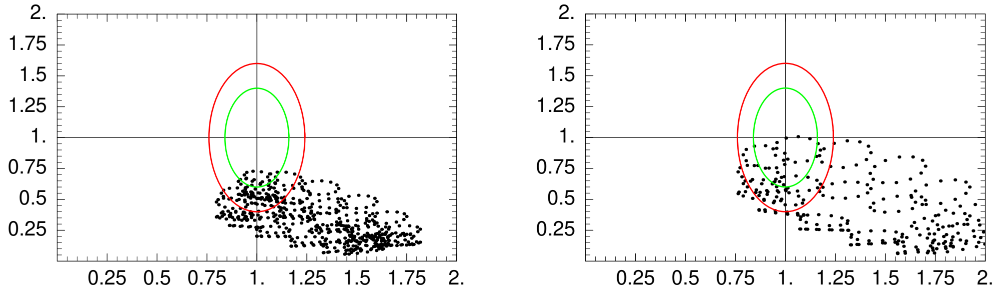

Figure 4.12: The $BR(B \to \pi^+\pi^-)$, $BR(B \to \pi^0\pi^0)$ agreement for the best-fit case for 30% NF correction (left) and 40% (right), using HFAG data.

experimental results are further away from the theory predictions, primarily due to the Belle measurement of BR($B \to \pi^0\pi^0$). We see that the enhanced levels of NF corrections of around 30% can bring the theory values close to the experimental averages, at least to within the 3σ error, although larger corrections are needed to approach 2σ agreement. The optimum for Δ is again found to be maximal, $\Delta = 1.3$, and for the form factor $F^\pi = 0.22$ and $F^\pi = 0.23$ for the 30% and 40% cases respectively.

4.4.3 Scenario III

Our third scenario involves adding contributions from charming penguins in addition to the expected non-factorisable correction ($\leq 20\%$) to the QCDF base. As discussed above, we expect this to impact on the values of the branching ratios for $B \to \pi^0\pi^0$ and $B \to \pi^+\pi^-$. For illustration, Figure 4.13 shows the possible enhancement of these branching ratios for various sizes of charming penguin contribution.

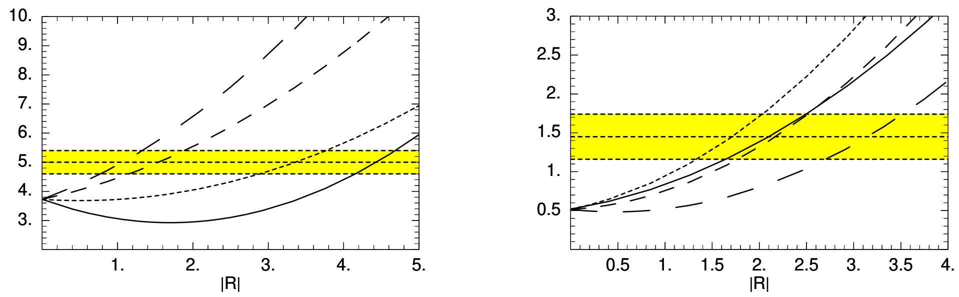

Figure 4.13: Dependence of $BR(B \to \pi^+\pi^-)$ (left) and $BR(B \to \pi^0\pi^0)$ (right) on charming penguin parameter R, in units of 10^{-6}; curves shown for constant φ of 0 (long-dashed), $\pi/4$ (short-dashed), $\pi/2$ (dotted) and π (solid). The experimental result and 1σ error from HFAG is shown for comparison.

This is presented for the expected 20% non-factorisable correction and our "best-fit" set of parameters (Δ, F^π and NF phases for each branching ratio), as found in the analysis with no charming penguin contribution (Scenario I). The figure shows that it should indeed be possible to improve the agreement between the theory and experimental results for both branching ratios simultaneously, with a level of 20% non-factorisable corrections.

To better gauge and quantify the level of enhancement that is needed, we again compare the agreement of the ratio of $B \to \pi^+\pi^-$ and $B \to \pi^0\pi^0$ branching fractions, and the $B \to \pi^+\pi^-$ CP asymmetry. The results are shown below in Figure 4.14 and Figure 4.15 for sample values of $|R| = 1, 1.5, 2$, scanning over possible phases $0 \leq \varphi \leq 2\pi$ and using the combined HFAG dataset.

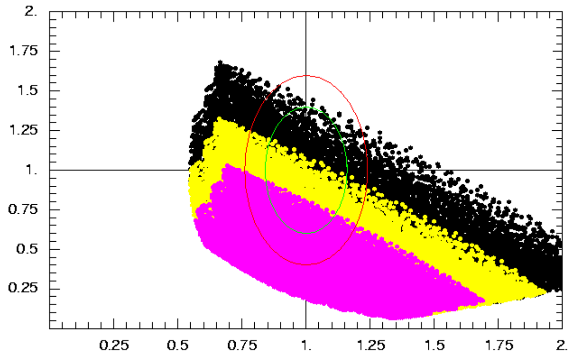

Figure 4.14: Theory/Experimental ratio using HFAG data for Γ^{+-} against Γ^{00} with charming penguin contribution of $|R| = 1$ (magenta), $|R| = 1.5$ (yellow) and $|R| = 2$ (Black), scanning over all possible phases φ.

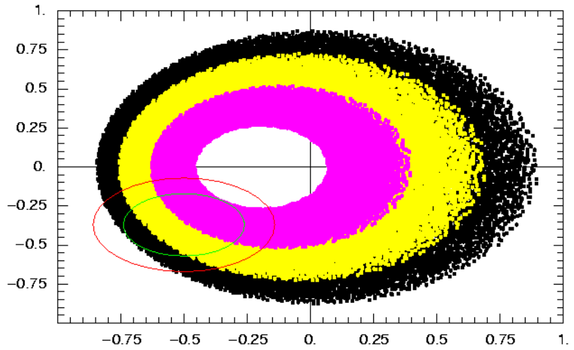

Figure 4.15: As above for CP asymmetry $S_{\pi\pi}/C_{\pi\pi}$.

Similarly to our previous scenarios, we find that the input parameters optimise for the maximal contribution $\Delta = 1.3$ and with $F^{\pi} = 0.22$. The figures show that considerable enhancement is possible, even for small values of $|R|$, and that it is possible to reproduce the data very well. It is clear however that there must be restrictions on the size and the phase of the parameter R, in order not to overshoot the experimental bounds – especially in the case of the CP asymmetry. Any contribution of magnitude $|R| > 2$ would be difficult to reconcile with the data.

As can be seen in the figures, using any magnitude of enhancement between $|R| = 1$ and $|R| = 2$ can reproduce the data extremely well for both the branching ratios and for the CP asymmetry; however, the required phase does not agree for both. The best-fit for the branching ratios requires $\varphi \sim 120°$, and for the CP asymmetries $\varphi \sim 300°$. It is the value of $C_{\pi\pi}$, that dictates the best-fit value for the CP plot, as it is very sensitive to the phase of the additional charming penguin contributions. Using our χ^2 minimisation technique we found the best-fit to all six experimental results, requiring a charming penguin contribution of $R = 2e^{i260°}$, resulting in a (minimum) $\chi^2 = 0.44$; this is shown below in Figure 4.16.

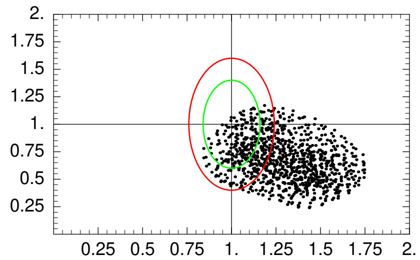

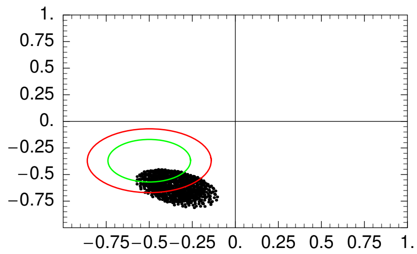

Figure 4.16: Best fit agreement from χ^2 minimisation to full data set with charming penguin contribution of $R = 2e^{i260°}$, using HFAG data with $\Delta = 1.3$, $F^{\pi} = 0.22$.

4.5 Discussion and comments

In this chapter we have presented an analysis of the non-factorisable corrections to $B \to \pi\pi$ and shown how the experimental data can be used to guide and constrain the levels of contribution needed to gain agreement between data and theory. Before discussing the full implications of our results, it is useful to compare the size of the model-dependent QCD factorisation parameterisation of the non-factorisable effects to our generic non-factorisable contributions. Consider first the corrections arising from the hard-spectator diagrams, where the divergences from the chirally enhanced twist-3 contributions to kernel T_i^{II} are parameterised by complex parameter X_H:

$$H_i(\pi\pi) = \frac{N_i f_B f_\pi}{m_B \lambda_B F_0^\pi(0)} \left[3 r_\chi^\pi \Delta X_H \right]$$

with $N_i = 0$ (i = 6, 8), -1 (i = 5, 7) or 1 otherwise. These contributions enter into each of the factorisation coefficients $a_i^{II}(\pi\pi)$. We can extract the contributions proportional to X_H in both of the isospin amplitudes $A_{1/2}$ and $A_{3/2}$ and obtain

$$\begin{aligned} (A^p_{1/2})_{HS} &= B_{\pi\pi} \frac{m_B}{\lambda_B} \frac{C_F \pi \alpha_s(\mu_h)}{2N_c^2} \mathbb{C}_{1/2}\ r_\chi^\pi \Delta X_H \\ (A^p_{3/2})_{HS} &= -B_{\pi\pi} \frac{m_B}{\lambda_B} \frac{C_F \pi \alpha_s(\mu_h)}{2N_c^2} \mathbb{C}_{3/2}\ r_\chi^\pi \Delta X_H \end{aligned}$$

with $B_{\pi\pi} = i\frac{G_F}{\sqrt{2}} f_B f_\pi^2$, and the $\mathbb{C}_{\Delta I}$ are combinations of Wilson coefficients given as

$$\begin{aligned} \mathbb{C}_{1/2} &= \delta_{pu}(4C_2 - 2C_1) + 6C_3 - 3C_8 + 3C_9 - 3C_{10} \\ \mathbb{C}_{3/2} &= \delta_{pu}(2C_2 + 2C_1) + 3C_8 + 3C_9 + 3C_{10} \end{aligned}$$

Comparing this contribution to the expression for our generic non-factorisable correction (4.1), we can estimate what size of correction corresponds to the "default" estimate of $X_H \sim \ln(m_b/\Lambda_h) \sim 2.4$ [2]. For $\Delta = 1$ and equal size contributions from $N^u_{1/2}$ and $N^c_{1/2}$, we estimate that using the BBNS model for X_H equates to a non-factorisable correction of $\sim 8\%$.

We can perform a similar decomposition for the other main source of non-factorisable corrections – the annihilation contributions – parameterised by the parameter X_A in the BBNS model. There is no correction to the $A_{3/2}$ isospin amplitude (and correspondingly no annihilation contribution to the $B \to \pi^+\pi^0$ decay), and the correction to $A_{1/2}$ can be expressed

$$(A^p_{1/2})_{ann} = B_{\pi\pi}\frac{2C_F}{N_c^2}\left[A_1^i \mathbb{C}_1 + A_3^f \mathbb{C}_3\right]$$

with $\mathbb{C}_i$ again combinations of Wilson coefficients

$$\begin{aligned}
\mathbb{C}_1 &= \delta_{pu}C_1 + C_3 + 2C_4 + 2C_6 - \tfrac{1}{2}C_9 + \tfrac{1}{2}C_{10} + \tfrac{1}{2}C_8 \\
\mathbb{C}_3 &= C_5 + N_c C_6 - \tfrac{1}{2}C_7 - \tfrac{1}{2}N_c C_8
\end{aligned}$$

and the amplitudes A_1^i and A_3^f, calculated with asymptotic distribution amplitudes and assuming SU(3) flavour symmetry, are

$$\begin{aligned}
A_1^i &= 2\pi\alpha_s\left[9(X_A - 4 + \frac{\pi^2}{3}) + r_\chi^\pi X_A^2\right] \\
A_3^f &= 12\pi\alpha_s\, r_\chi^\pi(2X_A^2 - X_A)
\end{aligned}$$

We can see the explicit power-suppression of these terms relative to the leading gluon exchange contributions via the fact that the weak annihilation terms are proportional to f_B rather than $f_B\, m_B/\lambda_B$. By comparing these expressions with the isospin expansions of (4.1) and using the default value of $X_A \sim \ln(m_b/\Lambda_h) \sim 2.4$, we obtain a corresponding size for the generic non-factorisable correction of $\sim 5\%$.

From these estimates it becomes very clear how this size of contribution cannot reproduce the experimental data. This would correspond to an overall NF contribution less than the moderate (20%) correction we tested in Scenario I, which in itself could not reconcile the predictions with the experimental data.

It was the marginal agreement of the QCDF predictions with the $B \to \pi\pi$ data that originally motivated us to test the consequences of enhancing the non-factorisable corrections to a moderate (20%) and extreme (40%) level. Our results show clearly that even for extremal values of our input parameters, the best-fit scenarios do not provide reasonable agreement between theory and experiment until at least 30% contributions are used. In the case of the combined HFAG data, a 40% contribution is required to obtain a reasonable 2σ agreement. This also highlights the problems with the discrepancies between the BaBar and Belle measurements.

Our final scenario incorporated the possibility of the charming penguin as an additional non-factorisable effect. We found that significant enhancement of the branching ratios is possible, but that a considerable contribution with $|R| > 2$ is not supported by the data. There are also a number of questions which must be addressed if we are to consider this contribution as a realistic contender for a significant, neglected $1/m_b$ correction. Firstly, the required best-fit phase of the charming penguin parameter R does not naturally agree for both the branching ratios and the CP asymmetries simultaneously. The best-fit agreement (shown in Figure 4.16) is however reasonable, although yet more NF corrections would be needed to gain a 1σ agreement with the data.

Secondly, we must ensure that the size of the contribution suggested by our results is appropriate with respect to the leading QCD factorisation terms. To check this, we can determine the relative size of the charming penguin contribution to the relevant isospin amplitude, $A_{1/2}$, compared with the factorisable contribution. For the maximum allowed charming penguin contribution $|R| = 2$, the ratio of the charming penguin contribution to the QCDF contribution is ~ 0.3, and for a moderate contribution of $|R| = 1.5$, we find a ratio of ~ 0.15. We can compare this to the relative size of our generic non-factorisable corrections, for example with equal phases and $|N_{1/2}^{u,c}| = 0.2$, which provides a correction 15% the size of the purely factorisable terms.

It would seem that the enhancement from the charming penguin must be approached with caution, as even a moderate increase, $|R| = 1.5$, gives an overall contribution equal to the size of the non-factorisable corrections coming from all of the annihilation and hard-spectator topologies. This suggests the implementation of the charming penguins in this way can provide a relative size contribution too large for them to be realistic additional NF contributions. We should then increase the constraint on the value of R, restricting the maximum contribution to be $|R| \sim 1.2$. The theoretical agreement to the $B \to \pi\pi$ observables would still receive significant improvement from the additional contributions, although not enough to bring both the branching ratios and CP asymmetries into 2σ agreement using only a 20% generic NF contribution. The best-fit agreement to the HFAG data with this constraint is shown in Figure 4.17.

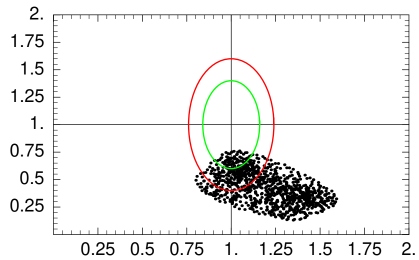

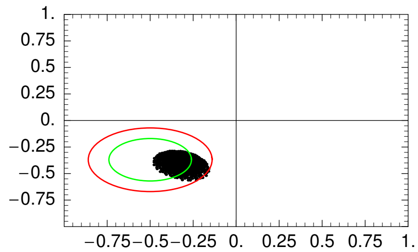

Figure 4.17: Best fit agreement from χ^2 minimisation to full data set with charming penguin contribution of $R = 1.2e^{i269^\circ}$, using HFAG data with $\Delta = 1.3$, $F^\pi = 0.22$.

Finally we can consider the application of this work to other charmless decays, as the techniques and results that we determined for $B \to \pi\pi$ can be applied to $B \to \pi K$ [104]. An isospin decomposition can be performed in an analogous way to $B \to \pi\pi$; there are now six independent isospin amplitudes

$$A^p_{3/2,1} \qquad A^p_{1/2,1} \qquad A^p_{1/2,0}$$

with $p = u, c$. The factorisable contribution can again be determined from QCDF, and the non-factorisable contributions defined as corrections to the above amplitudes. These corrections can be related to the non-factorisable corrections to $B \to \pi\pi$ via $SU(3)$ flavour symmetry.

It is possible in principle to use the best-fit data found from the $B \to \pi\pi$ case for $\Delta(\pi)$ and $F_0^{B\to\pi}$. The separate πK input parameters, $\Delta(K)$ and a_1^K (from the ϕ_K distribution amplitude), $F_0^{B\to K}$, and the CKM factors R_u and γ, can be varied within their allowed ranges.

There is experimental information available for four πK branching ratios ($\pi^0 K^+, \pi^+ K^0, \pi^0 K^0, \pi^- K^+$), four direct CP asymmetries C_{+0}, C_{0+}, C_{00} and C_{-+} and one indirect CP asymmetry for $B \to \pi^0 K^0$. Using this information, the level of non-factorisable corrections needed to bring the predictions for the πK system into agreement with the data can be tested and constrained. The possibility of charming penguins also has more significance in this system, as they are expected to have a significant contribution to the decays $B \to K^+\pi^-$ and $B^+ \to K^0\pi^+$.

Chapter 5

Exclusive radiative B-decays

It is wisdom to recognise necessity when all other courses have been weighed, though as folly it may appear to those who cling to false hope...

"The Lord of the Rings", J.R.R. Tolkien

Radiative penguin transitions such as $b \to s\gamma$ or $b \to d\gamma$ are examples of flavour changing neutral currents. They are rare decays, arising only at 1-loop in the Standard Model and are a valuable test of predictions of flavour physics, enabling us to test the detailed structure of this sector at the level of radiative corrections.

There has been much work and speculation regarding the phenomenology of FCNC processes, as they are ideal candidates for indirect searches for new physics phenomena e.g. as reviewed in [115,116]. The process $b \to s\gamma$ allows a large parameter space for new physics and has undergone scrutiny by a number of authors [117–121]; this process is seen as ideal to constrain the possible new physics effects, assisted by available experimental data on both the inclusive process $B \to X_s\gamma$ and the exclusive channel $B \to K^*\gamma$. The $b \to d\gamma$ process is suppressed with respect to $b \to s\gamma$ by the CKM factor $\lambda_t = V_{tb}V_{td}^*$, and the exclusive modes have previously had only experimental upper bounds from the B factories. In June of this year however, Belle announced new measurements of $B \to \rho\gamma$ and $B \to \omega\gamma$ [122]. These new data for $b \to d$ decays and updated results for the $b \to s$ processes present an ideal opportunity to perform an analysis of the radiative B decays, allowing us to both test the predictions of the Standard Model and examine the sensitivity of $b \to (d,\, s)\gamma$ to new physics.

In this chapter, we consider the exclusive channels $B \to (\rho,\, \omega)\gamma$ and $B \to K^*\gamma$ within the Standard Model, based on the formulation of $B \to V\gamma$ decays in QCD factorisation from Bosch and Buchalla [4]. We construct ratios of these branching fractions in order to limit the theoretical uncertainties in the predictions. We also examine the effect of the uncertainty from the distribution amplitudes of the vector mesons – the ρ, ω or K^* – by using our new resummed DA model as developed in Chapter 3. By testing the branching fractions against our DA parameter Δ, we can determine how much of an effect the LCDA has upon the final predictions for these decay channels. Using the ratio of the $B \to (\rho,\, \omega)\gamma$ and $B \to K^*\gamma$ branching fractions we show how the CKM ratio $|V_{td}/V_{ts}|$ can be extracted, and obtain an estimate of this quantity using the QCDF predictions.

We then go on to motivate an analysis of $B \to V\gamma$ decays within generic supersymmetric models with the so-called *mass insertion approximation* [123]. We then determine the constraints on such a generic MSSM model for both $b \to d\gamma$ and $b \to s\gamma$ transitions, using all the available experimental data from the B factory experiments.

5.1 $B \to V\gamma$ in QCD factorisation

A model-independent framework for the analysis of the radiative decays has been presented in [4]; we summarise the important points and calculational formulae here. The method presents an expansion in the heavy-quark limit, giving expressions valid at leading order in a $\Lambda_{\rm QCD}/m_b$ expansion. There are contributions from power-suppressed annihilation topologies, particularly relevant for the $B \to \rho\gamma$ decays, where they are numerically enhanced by large Wilson coefficients. We implement these corrections following the method of [124].

The process, shown in Figure 5.1, is dominated by the electromagnetic penguin operator $Q_{7\gamma}$. The annihilation diagram shown is important in $B \to \rho\gamma$, specifically for the charged decays.

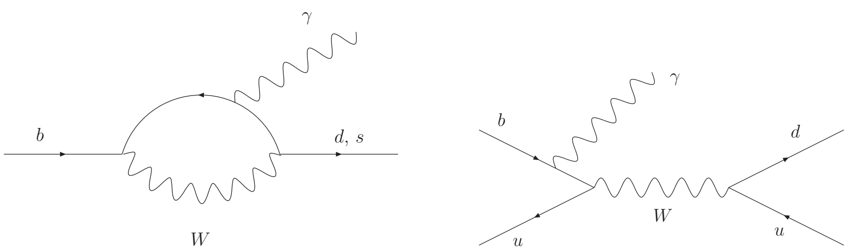

Figure 5.1: Loop diagram for $b \to d\gamma$ and the annihilation diagram for $B^- \to \rho^-\gamma$.

The decay amplitudes are expressed following a similar procedure as in QCDF for decays into two mesons, i.e. in terms of Wilson coefficients and hadronic matrix elements, which are then calculated using a factorisation formula. The matrix elements for the radiative processes are found using a factorisation formula valid up to corrections of order $(\Lambda_{\rm QCD}/m_b)$

$$\langle V\gamma(\epsilon)|Q_i|\bar{B}\rangle = \left[F^{B\to V}(0)T_i^I + \int_0^1 d\xi\, dv\, T_i^{II}(\xi, v)\, \Phi_B(\xi)\Phi_V(v)\right]\cdot \epsilon \quad (5.1)$$

where ϵ is the photon polarisation four-vector. For the matrix element of the operator Q_7, the formula (5.1) becomes trivial: The kernel T_i^I is a purely kinematic function and the spectator term is absent, so the only dependence on non-perturbative input parameters that remain is from the $B \to V$ transition form factor. At the leading order, this is the only contribution to the $B \to V\gamma$ decay. At the next-to-leading order we gain additional contributions from the other $\Delta B = 1$ operators, dominated by Q_1 and Q_8.

The matrix elements of the additional operators can be expressed in terms of the calculable matrix element for $\langle Q_7 \rangle$. There are two contributions, one from the hard-scattering kernel T_i^I for vertex corrections, and the other from T_i^{II} which includes the hard-spectator corrections. These are given by

$$\begin{aligned} \langle Q_{1,8} \rangle^I &= \frac{\alpha_s(m_b) C_F}{4\pi} \langle Q_7 \rangle G_{1,8} \\ \langle Q_{1,8} \rangle^{II} &= \frac{\alpha_s(\mu_h) C_F}{4\pi} \langle Q_7 \rangle H_{1,8} \end{aligned}$$

The type-I contributions depend on $G_i(s_p)$, which are simple functions of $s_p = m_p^2/m_b^2$ (for $p = u, c$) given explicitly in [4]. The spectator contributions are incorporated into the functions H_i, and are more interesting than the type-I functions:

$$H_1(s_p) = -\frac{2\pi^2}{3N_c} \frac{f_B f_V^\perp}{F^V m_B^2} \int_0^1 d\xi \frac{\Phi_B(\xi)}{\xi} \int_0^1 dv\, h(1-v, s_p)\, \Phi_\perp(v)$$

$$H_8 = \frac{4\pi^2}{3N_c} \frac{f_B f_V^\perp}{F^V m_B^2} \int_0^1 d\xi \frac{\Phi_B(\xi)}{\xi} \int_0^1 dv\, \frac{\Phi_\perp(v)}{v}$$

The hard-scattering function $h(u, z)$ is given as

$$h(u, z) = \frac{4z}{u^2}\left[Li_2\left(\frac{2}{1-\sqrt{\frac{u-4z}{u}}}\right) + Li_2\left(\frac{2}{1+\sqrt{\frac{u-4z}{u}}}\right)\right] - \frac{2}{u} \tag{5.2}$$

and is real for values of $u \leq 4z$, and complex for $u > 4z$. For $z \to 0$ (for example the up-quark contribution $z_u \sim 0$), the function is regular and becomes

$$h(u, 0) = -\frac{2}{u}$$

The distribution amplitude for the B-meson is parameterised as before using the first inverse moment

$$\int_0^1 d\xi \frac{\Phi_B(\xi)}{\xi} = \frac{m_B}{\lambda_B}$$

These type-II contributions also include a dependence on the light-cone distribution amplitude of the vector meson of the $B \to V\gamma$ decay, specifically, for the *transversely polarised vector mesons*, $\phi_\perp$. The vector meson is described at leading twist, by two distribution amplitudes $\phi_\parallel$ and $\phi_\perp$ corresponding to longitudinally and transversely polarised mesons. The vector meson in $B \to V\gamma$ decays is to leading power transversely polarised, and hence can be described by $\phi_\perp$, as any contributions from $\phi_\parallel$ are suppressed.

As with the pseudoscalar mesons, the distribution amplitude $\phi_\perp$ can be treated using a conformal expansion that is often truncated at the moment a_2. In our analysis, we wish to examine the effects of a non-standard DA on the radiative decays, so we use our resummed model DA in place of this truncated expansion. For definiteness we use the model $\phi^+_{3,3}(\Delta)$, where $\Delta = 1$ reduces to the asymptotic DA. This model applies to the mesons symmetric in the fractional momentum u, i.e. π, ρ, ω. Where we consider the K^* channels, there is a non-zero anti-symmetric part to the meson wavefunction which we can also model using our resummed DA models. This is constructed in an analogous way to the symmetric DA, as discussed in Chapter 3. We use the model $\psi_4^+(a_1)$, which allows for the inclusion of an arbitrary value of the first anti-symmetric Gegenbauer moment a_1^K. We take the value of a_1^K from our discussion on ϕ_K unless otherwise stated. The value of Δ for the K^* wavefunction is the sum of the symmetric and antisymmetric parts, i.e.

$$\Delta^{\text{tot},+} = \Delta + \Delta^{\text{asym},+}$$

with $\Delta^{\text{asym},+} = -a_1(3/2)^c\zeta(c, 3/2)$. Hereafter, we will refer to the total Δ^{tot} as Δ and imply the inclusion of the anti-symmetric part.

Finally we combine all of the contributions to the $B \to V\gamma$ decay into a factorisation coefficient, written as [4]

$$\begin{aligned} a_7^p(V\gamma) = C_{7\gamma}^{\text{NLO}} \quad &+ \quad \frac{\alpha_s(m_b)C_F}{4\pi}\left[C_1^{(0)}(m_b)\, G_1(s_p) + C_8^{(0)\,\text{eff}}(m_b)\, G_8\right] \\ &+ \quad \frac{\alpha_s(\mu_h)C_F}{4\pi}\left[C_1^{(0)}(\mu_h)\, H_1(s_p) + C_8^{(0)\,\text{eff}}(\mu_h)\, H_8\right] \end{aligned} \tag{5.3}$$

The Wilson coefficients $C_1^{(0)}$ and $C_8^{(0)\,\text{eff}}$ as indicated, are taken at leading order.

The decay amplitudes are then expressed as follows, keeping both the charm and up-quark contribution

$$A(B \to V\gamma) = \frac{G_F}{\sqrt{2}}\left[\sum_p \lambda_p^{(q)} a_7^p(V\gamma)\right]\langle V\gamma|Q_7|\bar{B}\rangle \tag{5.4}$$

giving the final $B \to V\gamma$ branching ratios as

$$\mathrm{BR}(\bar{B} \to V\gamma) = \tau_B \frac{G_F \alpha_e m_B^3 m_b^2}{32\pi^4}\left(1 - \frac{m_V^2}{m_B^3}\right)^3 \left|\sum_p \lambda_p^{(q)} a_7^p(V\gamma)\right|^2 c_V^2 \left|F^V\right|^2 \tag{5.5}$$

where $q = s$ for $V = K^*$ and $q = d$ for $V = \rho$; $c_V = 1$ for K^*, ρ^- and $c_V = 1/\sqrt{2}$ for ρ^0. The CP-conjugate branching ratios are obtained by replacing $\lambda_p^{(q)} \to \lambda_p^{(q)*}$; in our analysis we take all branching ratios as CP-averaged.

The annihilation contributions can be included in the factorisation coefficient a_7^p via

$$a_7^p \longrightarrow a_7^p + a_{ann}^p$$

The dominant annihilation contributions are suppressed by one power of $\Lambda_{\mathrm{QCD}}/m_b$, but can still be calculated within QCD factorisation, (a proof to $\mathcal{O}(\alpha_s)$ can be found in [124]). These can give a sizable contribution to the radiative decays, such as $B \to \rho\gamma$, where the contributions originating from operators Q_1 and Q_2 are enhanced by large Wilson coefficients C_1 and C_2. These have small impact on the $B \to K^*$ decays due to CKM suppression, however this decay can receive a large contribution from the operator Q_6 [125]. The annihilation contributions are also sensitive to the flavour of the light quark of the B-meson, and so differentiate between decays of the $B^0\,(\bar{B}^0)$ and the $B^\pm$, and additionally are dependent on the distribution amplitude $\phi_\perp$. Since this is clearly important to our analysis, we describe the contributions a_{ann}^p in more detail in Appendix B.

There is no indication for large power corrections beyond these calculable annihilation terms [4, 126].

5.2 Analysis and comparison with Belle data

For channels that have low statistics such as the rare radiative processes, the experimental measurements often combine different individual channels in order to improve the significance, and allow a signal to be discovered. Belle is to date the only experiment to have released an actual measurement of the $b \to d\gamma$ processes [122], where they combine the data from three channels $\rho^0\gamma$, $\rho^+\gamma$, $\omega\gamma$. The average is defined as [127]

$$\mathrm{BR}\left[B \to (\rho,\omega)\gamma\right] = \frac{1}{2}\left\{\mathrm{BR}(B^+ \to \rho^+\gamma) + \frac{\tau_{B^+}}{\tau_{B^0}}\left[\mathrm{BR}(B^0 \to \rho^0\gamma) + \mathrm{BR}(B^0 \to \omega\gamma)\right]\right\}$$

We can also define an isospin-averaged branching ratio $\mathrm{BR}(B \to K^*\gamma)$ which is used frequently

$$\mathrm{BR}(B \to K^*\gamma) = \frac{1}{2}\left\{\mathrm{BR}(B^+ \to K^{*+}\gamma) + \frac{\tau_{B^+}}{\tau_{B^0}}\mathrm{BR}(B^0 \to K^{*0}\gamma)\right\} \tag{5.6}$$

We can predict the branching fractions or CP asymmetries for the $B \to V\gamma$ decays directly from these averages using the QCD factorisation formulae of Section 5.1. We can also find the ratio of these averaged branching fractions which is fitted directly from the experimental data. We define, using the CP-averaged branching fractions [127, 128]

$$\begin{aligned} R\left[(\rho,\omega)\gamma/K^*\gamma\right] &= \frac{\mathrm{BR}\left[B \to (\rho,\omega)\gamma\right]}{\mathrm{BR}(B \to K^*\gamma)} \\ &= \left|\frac{V_{td}}{V_{ts}}\right|^2 \frac{(1 - m_{(\rho,\omega)}^2/m_B^2)^3}{(1 - m_{K^*}^2/m_B^2)^3}\,\zeta^2\, c_\rho^2 \left|\frac{a_7^c((\rho,\omega)\gamma)}{a_7^c(K^*\gamma)}\right|^2 \left[1 + \Delta R\right] \end{aligned} \tag{5.7}$$

ζ denotes the form factor ratio $T_1^\rho(0)/T_1^{K^*}(0)$, which characterises the $SU(3)$ breaking in the transition form factors. The form factor $T_1(0)$ is one of seven independent form factors which describe all $B \to V$ decays, and is the only one relevant for the radiative $B \to V\gamma$ decay. It is defined in conjunction with two other form factors $T_{2,3}$ via [58]

$$\begin{aligned}
\frac{1}{c_V}\langle V(p)|\bar{q}\sigma_{\mu\nu}q^\nu(1+\gamma_5)b|B(p_B)\rangle = i\epsilon_{\mu\nu\rho\sigma}\epsilon^{*\nu}p_B^\rho\, p^\sigma\, 2T_1(q^2) \\
+ T_2(q^2)\left\{e_\mu^*(m_B^2 - m_V^2) - e^*q)(p_B+p)_\mu\right\} \\
+ T_3(q^2)(e^*q)\left\{q_\mu - \frac{q^2}{m_B^2 - m_V^2}(p_B+p)_\mu\right\}
\end{aligned}$$

The parameter ζ has been estimated using several methods, the most recent value is from Ball and Zwicky using light-cone sum rules [129] who find $\zeta^{-1} = 1.25 \pm 0.18$.

ΔR is given within QCD factorisation by [128]

$$\Delta R = 2\mathrm{Re}\,\delta a\left(\frac{R_u^2 - R_u\,\cos\gamma}{1 - 2R_u\,\cos\gamma + R_u^2}\right) \tag{5.8}$$

written in terms of $R_u = \sqrt{\bar{\rho}^2 + \bar{\eta}^2}$ and the CKM angle γ. δa is given by

$$\delta a = \frac{a_7^u((\rho,\omega)\gamma) - a_7^c((\rho,\omega)\gamma)}{a_7^c((\rho,\omega)\gamma)} \tag{5.9}$$

where the factors a_7 implicitly include the annihilation contributions, which contribute only at order $\Lambda_{\mathrm{QCD}}/m_b$. If the annihilation contributions to δa were neglected then $\delta = \mathcal{O}(\alpha_s)$. To obtain expression (5.9) we make use of the identity:

$$\lambda_c\, a_7^c + \lambda_u\, a_7^u = -\lambda_t\, a_7^c\left(1 - \frac{\lambda_u}{\lambda_t}\frac{a_7^u - a_7^c}{a_7^c}\right) \tag{5.10}$$

where the second term in the bracket in (5.10) is neglected for $B \to K^*\gamma$ as it provides a contribution of less than 1%. This results in the correction δa depending only on the factorisation coefficients from $(\rho, \omega)\gamma$.

The advantage of calculating the ratio of branching fractions in this way is to reduce the error from theoretical uncertainties. Firstly, from the theory parameters that cancel in taking the ratio, including parameters such as m_b which have a sizable associated uncertainty. Secondly, the quantity ΔR is a small correction with central values close to zero, primarily due to the smallness of the CKM factor f, multiplying $\mathrm{Re}(\delta a)$. The ranges of γ and R_u (as suggested in Chapter 4) imply $-0.1 \leq f \leq 0.03$. The contribution to ΔR specifically from the neutral decays is also small due to an accidental cancellation between the $\mathcal{O}(\alpha_s)$ and annihilation effects in δa. The two main sources of uncertainty remaining in the expression R_{th} are from ζ and ΔR.

We use our prediction for R_{th} in combination with the experimental results to constrain the possibility of new physics in the radiative decays, or in its absence, to determine the CKM factor $|V_{td}/V_{ts}|$. We can use R_{th} in the following ways – either to extract the value of $|V_{td}/V_{ts}|$ assuming ΔR is fully known, or to extract information about ΔR using the best-fitted value for the CKM ratio from another source.

We begin by analysing the individual branching ratios for $B \to \rho\gamma$ and $B \to K^*\gamma$ before going on to study the ratio R_{th}. We summarise the experimental results for the radiative decays in Table 5.1 [11, 122, 130, 131].

Decay channel	BaBar	Belle	Average
$B_{\rm exp}(B \to K^*\gamma)$	40.6 ± 2.6	43.0 ± 2.5	42.0 ± 1.7
$B_{\rm exp}(B^0 \to K^{*0}\gamma)$	$39.2 \pm 2.0 \pm 2.4$	$40.1 \pm 2.1 \pm 1.7$	40.1 ± 2.0
$B_{\rm exp}(B^+ \to K^{*+}\gamma)$	$38.7 \pm 2.8 \pm 2.6$	$42.5 \pm 3.1 \pm 2.4$	40.3 ± 2.6
$B_{\rm exp}(B \to (\rho,\,\omega)\gamma)$	< 1.9	$1.34^{+0.34+0.14}_{-0.31-0.10}$	
$R_{\rm exp}\,[(\rho\,\omega)\gamma/K^*\gamma]$		$0.032 \pm 0.008^{+0.003}_{-0.002}$	

Table 5.1: The CP-averaged branching fractions for exclusive $B \to K^*\gamma$ and $B \to \rho\gamma$, in units of 10^{-6} (with exception of R_{exp}) and using the combined branching fractions defined in the text.

5.2.1 $B \to (\rho, \omega)\gamma$

Using the formulae collected above we can obtain a theoretical estimate for the combined and individual branching ratios for $B \to \rho\gamma$. With a conservative estimate of the uncertainty on our values, and using the asymptotic distribution amplitude of the rho and omega mesons ($\Delta(\rho) = \Delta(\omega) = 1$), we find $\mathrm{BR}(B^\pm \to \rho^\pm\gamma) = (1.52 \pm 0.45) \times 10^{-6}$ and $\mathrm{BR}(B^0 \to \rho^0\gamma) = (0.72 \pm 0.22) \times 10^{-6}$. We also find, for the combined weighted averages

$$\mathrm{BR}(B \to (\rho,\,\omega)\gamma) = (1.60 \pm 0.48) \times 10^{-6}$$

which is above, but within the error bounds of the current experimental measurements. We take the values of the form factors as $F^\rho = 0.267 \pm 0.021$ and $F^\omega = 0.242 \pm 0.022$ [58]. The error on the branching ratio is estimated by taking into account the dominant uncertainties on the input parameters: F^ρ, F^ω, λ_B, m_b, m_c, f_B and the CKM inputs. Adding these in quadrature leads to an error estimate of $\mathcal{O}(30\%)$ for the $B \to \rho\gamma$ channels.

The distribution amplitude for the rho meson required for the calculation of the hard-spectator and annihilation contributions to the process is that for the transversely polarised mesons $\phi_\perp(u, \mu)$. The leading twist DA (both the transverse and longitudinal) is often expressed as a truncated conformal expansion, where there is a prediction for $a_2^{\perp}$ from QCD sum rules [69, 70] of $a_2^{\perp}(\rho, 1\text{GeV}) = 0.2 \pm 0.1$. In this analysis we replace the conformal expression of $\phi_{\perp}(\rho)$ with our resummed DA model. The suggested region for Δ was examined in [58], and is based on the indication from all available calculations that $a_2 > 0$. This demands, as for $\phi(\pi)$, that $\Delta > 1$. Using the model DA with $a = 3$ suggests $\Delta(\rho) = \Delta(\omega) = 1.15 \pm 0.10$. In light of this we use a "physical range" for Δ of $1 \leq \Delta \leq 1.4$.

We test the effect of our non-standard DA by plotting the dependence of the $b \to d\gamma$ branching ratios on the parameter Δ, as is shown in Figure 5.2.

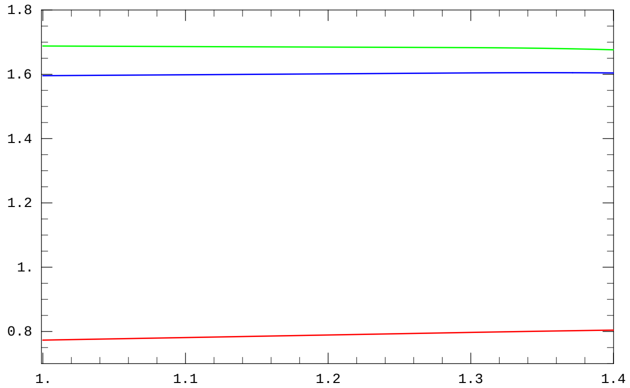

Figure 5.2: Branching fractions for $B \to \rho\gamma$ decays from QCD factorisation using our model DA $\phi_{3,3}^{+}$, in units of 10^{-6} and in possible physical region of Δ: $B^+ \to \rho^+\gamma$ (green), $B \to \rho^0\gamma$ (red) and the combined $B \to (\rho, \omega)\gamma$ (blue).

This figure shows that within this range the dependence on Δ appears relatively small. There is a downward trend in the $\rho^+\gamma$ case and conversely an upward trend in the $\rho^0\gamma$ case. These conspire to cancel in the combined branching fraction, leaving $B \to (\rho, \omega)\gamma$ free of any significant dependence on Δ and of uncertainty from the distribution amplitude. The actual change in the value of the branching ratio over the full (physical) range of Δ is of the order of 3% for $(\rho^0\gamma)$ and 1% for the combined ratio.

5.2.2 $B \to K^*\gamma$

The theoretical estimate for the $B \to K^*\gamma$ decays can be found in an analogous way to $B \to \rho\gamma$, using the definition of the weighted average from equation (5.6). We obtain an estimate for the $K^*\gamma$ branching ratio as $\mathrm{BR}(B \to K^*\gamma) = (5.49 \pm 1.64) \times 10^{-5}$, which is somewhat higher than, but within the error bounds of, the current experimental measurement. The considerable decrease between this value and that presented in [4] is predominantly due to the updated value of the form factor $F^{K^*} = 0.333 \pm 0.028$ [58] from its previous value of $F^{K^*} = 0.38 \pm 0.06$ [64].

We begin by considering the effect of the K^* distribution amplitude, by testing the dependence of the branching fractions on our non-standard DA. Unlike the ρ, we have the additional complication for the K^* meson of an anti-symmetric part to the distribution amplitude. The moments for the truncated conformal expression are largely unknown, although there have been predictions from QCD sum rules [58, 99]. This gives us:

$$a_1^\perp(K^*, 1\mathrm{GeV}) = 0.10 \pm 0.07 \qquad a_2^\perp(K^*, 1\mathrm{GeV}) = 0.13 \pm 0.08$$

We can examine the dependence on both the symmetric part of the K^* DA and on the leading anti-symmetric moment a_1^K. The value of the symmetric contribution to Δ for the K^* is estimated at $\Delta(K^*) = 1.12 \pm 0.10$ – we consider the wider range of $1 \leq \Delta(K^*) \leq 1.4$, in order to compare directly with the physical range used in the $\rho\gamma$ case. The dependence of the $B \to K^*\gamma$ branching ratios on Δ with a constant value of $a_1^K = 0.13$ is summarised in Figure 5.3. Although this graph suggests that the K^* branching ratios have a larger dependence that the $B \to \rho\gamma$ decays, the percentage change across the full range of Δ is in fact the same for both sets of decays. As before, we have a 1% change for the combined K^* decay and a 3% change for K^{*0}. This effect suggests that the discrepancies between the experimental values and the theory predictions can not be attributed to the uncertainty from the DA – increasing the contribution of the higher order moments of the DA by increasing Δ serves only to increase the prediction of the averaged K^* branching ratio.

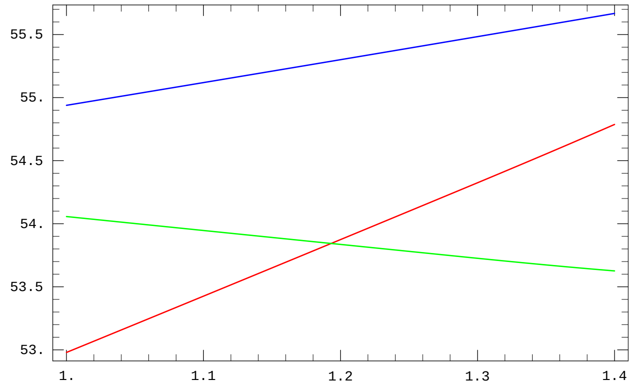

Figure 5.3: Branching fractions (in units of 10^{-6}) for $B \to K^*\gamma$ decays in QCD Factorisation using our model DA with antisymmetric part ψ_4, in the possible physical region of Δ and constant $a_1 = 0.13$; $B^+ \to K^{*+}\gamma$ (green), $B \to K^{*0}\gamma$ (red) and the combined $B \to K^*\gamma$ (blue).

Figure 5.4 shows the dependence of the $B \to K^*$ branching ratio on both Δ and a_1, and shows clearly that a higher value of the moment a_1 will lead to lower values of the branching ratio for all values of $\Delta(K^*)$, although the change is not considerable.

5.2.3 $R\left[(\rho,\omega)\gamma/K^*\gamma\right]$ and the extraction of $|V_{td}/V_{ts}|$

This section proceeds to build on the results from the individual branching fractions, by calculating the ratio $R_{\rm th}\left[(\rho,\omega)\gamma/K^*\gamma\right]$ as introduced above. As discussed, this is important for the extraction of information on the hadronic

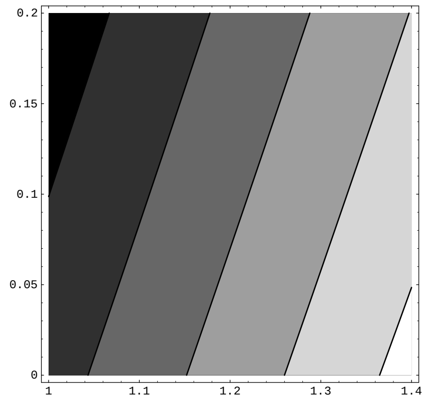

Figure 5.4: Density plot of BR($B \to K^*\gamma$) (with increasing values indicated by lighter shading) for variation in Δ (horizontal axis) and a_1 (vertical axis). Contours shown at $5.5, 5.52 \ldots 5.58 \times 10^{-5}$.

quantity ΔR and the value of the CKM ratio $|V_{td}/V_{ts}|$.

We begin by using equation (5.7), and the calculation of ΔR as in equations (5.8) and (5.9) to find the ratio of the $(\rho, \omega)\gamma$ and $K^*\gamma$ branching ratios. We use the asymptotic distribution amplitudes for $\phi_\perp(\rho)$, $\phi_\perp(\omega)$ and $\phi_\perp(K^*)$, and obtain an estimate of $R_{\rm th}$ as

$$R_{\rm th} = \frac{\mathrm{BR}(B \to (\rho, \omega)\gamma)}{\mathrm{BR}(B \to K^*\gamma)} = 0.030 \pm 0.008$$

which is in rather good agreement with the experimental measurement. The theoretical uncertainty remaining in $R_{\rm th}$ is dominated by the form factor ratio ζ, and the value of the quantity ΔR. We can use the ratio to extract a value of $|V_{td}/V_{ts}|$. Using $\zeta^{-1} = 1.25$ and our estimate of ΔR from QCD factorisation as $\Delta R = 0.006$, we obtain:

$$|V_{td}/V_{ts}| = 0.195 \pm 0.051$$

which is well within the SM range of $|V_{td}/V_{ts}| = 0.197 \pm 0.013$ [132]. We plot the dependence of $R_{\rm th}$ against $|V_{td}/V_{ts}|$ in Figure 5.5.

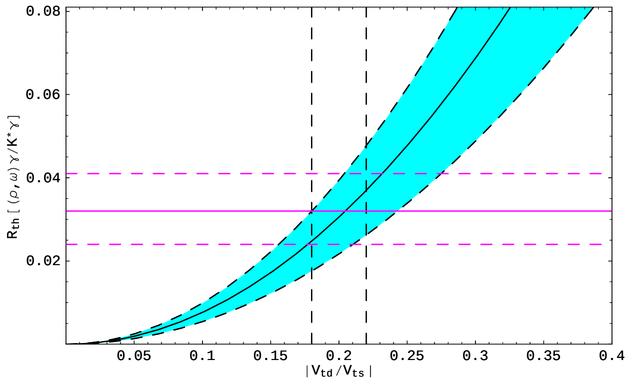

Figure 5.5: Plot of $R_{\rm th}\left[(\rho,\omega)\gamma/K^*\gamma\right]$ (within quoted $\pm 1\sigma$ errors) against $|V_{td}/V_{ts}|$ with current Belle experimental result and 1σ errors shown (horizontal band in magenta) and the SM best-fit for $|V_{td}/V_{ts}|$ (vertical band).

The constraints on the unitarity fit are continually improving, so we are approaching the stage of having consistent measurements for many of the CKM parameters. We can then in principle use the measured (fitted) value for $|V_{td}/V_{ts}|$ in order to examine the parametric uncertainties entering into $R_{\rm th}$.

We expect the dependence on the distribution amplitudes that enter into $R_{\rm th}$ to be small, even though there is dependence on $\Delta(\rho)$, $\Delta(K^*)$ and $a_1^{K^*}$. We approximate by taking $\Delta(\omega) = \Delta(\rho)$. Increasing the contribution from $\Delta(\rho)$ acts to increase the ratio, and increasing $\Delta(K^*)$ acts to decrease it. Since these effects are of the same magnitude, the overall effect is negligible.

The dependence of $R_{\rm th}$ on the form factor ratio is much greater and is illustrated in Figure 5.6. This shows the sensitivity to changes in the value of ζ^{-1} especially any movement towards lower values.

Our prediction for $R_{\rm th}\left[(\rho,\omega)\gamma/K^*\gamma\right]$ is close to the central value determined experimentally, showing clearly how well the uncertainties can be reduced by calculating the combined ratio. The parametric uncertainty in the individual

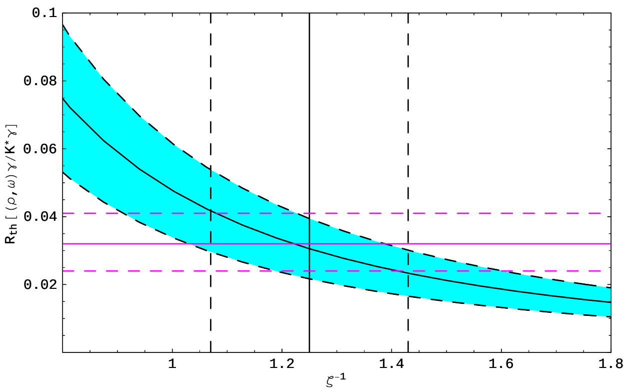

Figure 5.6: Plot of $R_{\text{th}}\,[(\rho,\omega)\gamma/K^*\gamma]$ (within quoted $\pm 1\sigma$ errors) against form factor ratio $\zeta^{-1} = T_1^{K^*}(0)/T_1^{\rho}(0)$ (vertical band) with current Belle experimental result and 1σ errors shown (horizontal band in magenta).

branching ratios is dominated by the dependence on the form factors which enter quadratically in the expressions for BR($B \to V\gamma$). The ratio R_{th} reduces the sensitivities to F^{ρ} and F^{K^*} by limiting the impact of the long-distance hadronic physics to the SU(3) breaking in the form factor ratio ζ. The other main uncertainty is from the QCDF prediction for ΔR; this is largely due to λ_B, as it is this that determines the strength of the weak annihilation contributions. This is especially relevant for the charged modes $B \to \rho^{\pm}\gamma$.

It is worth questioning however, why the individual branching ratios have high central values with respect to their experimental determinations, most notably, the $B \to K^*\gamma$ branching ratio. From the calculation of inclusive $B \to X_s\gamma$, which is in good agreement with the data, it is justifiable to conclude that the short distance physics is compatible with the Standard Model expectations [126]. This suggests two lines of reasoning: firstly, that the uncertainties which are removed when calculating the ratio R_{th} have a considerable effect on the branching ratio. We illustrate the sensitivity to the form factor F^{K^*} in the $K^*\gamma$ branching ratio in Figure 5.7. This shows how the experimental measurement leans towards a lower value for this result and how the reduction to the updated value from [58] leads to such a significant drop in the theory estimate of $\mathrm{BR}(B \to K^*\gamma)$.

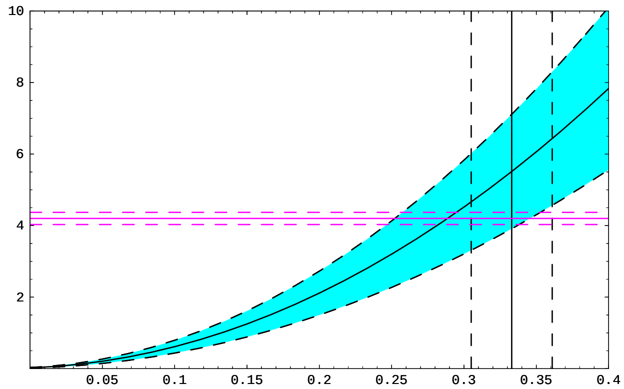

Figure 5.7: Plot of $\mathrm{BR}(B \to K^*\gamma)$ in units of 10^-5 (and within conservative estimated errors) against form factor $F^{K^*}(0)$ (vertical band) with current experimental average (horizontal band in magenta).

A second line of reasoning is to consider if there are any other factors contributing to the over-estimation of the branching ratios, which conspire to cancel in the combined ratio R_{th}. This could include errors from the calculation of ΔR, large power corrections which have been neglected, or new physics in the underlying $b \to (d, s)\gamma$ transitions.

We now go on to consider the possibility of new physics in the $B \to V\gamma$ decays. The errors on the experimental data are reducing to a level where it will be possible to impose considerable constraints on new physics models. As we discussed in the opening motivation of this chapter, the radiative decays (especially those involving the $b \to s$ transition) have long been seen as an excellent candidate for searches for new physics. We proceed to perform an analysis in a generic minimal supersymmetric model as an example of the most popular extension of the Standard Model. We show how effective constraints can be imposed on the parameter space for possible new physics effects in the radiative decays using the bounds from the experimental results.

5.3 Introduction and motivation for supersymmetry

Supersymmetry (SUSY) is the most popular low-energy extension of the standard model (see for example [133, 134]). Beyond the elegance of the symmetry itself, which unifies fundamental fermions and scalars, supersymmetric models have many virtues which can alleviate some of the issues within the Standard Model.

The main benefit that motivates many SUSY models is the resolution of the "hierarchy problem". In the Standard Model (SM) there are a number of corrections which lead to infinite contributions to a particular process – these are removed by renormalisation by introducing some cut-off energy Λ. Quadratic divergences appear in the contribution of heavy fermions to the Higgs self energy. These can be again be removed by renormalisation, but large corrections ($\sim m_f^2$) remain. Hence fine-tuning is required to ensure the small Higgs mass required in order to produce a vacuum expectation value of the correct size to give the observed W and Z boson masses. If we are envisioning that our theory contains the large scales of grand unification, namely the Planck scale ($m_{PL} \sim 10^{19}$GeV), then we have to ask how we can arrange for the Higgs mass term (and the corresponding electroweak scale) to be so much smaller then the underlying mass scale m_{PL}. Supersymmetry requires that each scalar particle has a fermionic "superpartner" (and vice versa) of the same mass so that all the quadratic divergences of the scalar mass terms will automatically vanish. These cancellations occur at every order in perturbation theory protecting the light scalar masses.

Supersymmetry is also a natural bridge to incorporate gravity, as implementing SUSY as a local gauge symmetry demands local co-ordinate covariance i.e linking to general relativity. Supersymmetry is also an integral requirement at some energy scale in most string theories [135].

If SUSY were to be manifest then all particles and their superpartners would be mass degenerate. Since to date, no state which can be identified as a superpartner has been observed, then we must have broken supersymmetry at our low energy scales. The mechanism for the SUSY breaking is unknown, but as we discuss below it has a large impact on phenomenology. We can give rough bounds for the masses of the superpartners; all of the masses must be over 100GeV (otherwise they should have been observed at LEP), but at least some masses have to be less than 1 TeV, in order to resolve the hierarchy problem.

5.3.1 Low energy MSSM

The Minimal Supersymmetric Standard Model (MSSM) is the simplest and most popular SUSY extension to the SM. The particle content is a set of supermultiplets, constructed from the SM states and their superpartners. The superpartners of the left and right handed quarks are denoted as left and right handed squarks even though the squarks are scalar and have no chiral structure. In summary we have the following:

		spin 0	spin $\frac{1}{2}$	$(SU(3)_c,\, SU(2),\, U(1)_Y)$
(s)quarks	Q	$(\tilde{u}_L,\, \tilde{d}_L)$	$(u_L,\, d_L)$	$(3, 2, \frac{1}{6})$
	U	$\tilde{u}^*_R$	u^+_R	$(\bar{3}, 1, -\frac{2}{3})$
	D	$\tilde{d}^*_R$	d^+_R	$(\bar{3}, 1, \frac{1}{3})$
(s)leptons	L	$(\tilde{\nu},\, \tilde{e}_L)$	$(\nu,\, e_L)$	$(1, 2, -\frac{1}{2})$
	E	$\tilde{e}^*_R$	e^+_R	$(1, 1, 1)$
higgs(inos)	H_u	(h^+_u, h^0_u)	$(\tilde{h}^+_u,\, \tilde{h}^0_u)$	$(1, 2, \frac{1}{2})$
	H_u	(h^0_d, h^-_d)	$(\tilde{h}^0_d,\, \tilde{h}^-_d)$	$(1, 2, -\frac{1}{2})$

The interactions among the scalar particles are governed by a superpotential W, where the dimensionless numbers $\mathbf{y_i}$ contain the Yukawa couplings of the SM fermion fields.

$$W = U\mathbf{y_u}QH_u + D\mathbf{y_d}QH_d + E\mathbf{y_e}LH_d + \mu H_u H_d \tag{5.11}$$

The gauge bosons of the Standard Model also get a fermionic superpartner generically called a gaugino. The *gluino* is the superpartner of the gluon, and hence carries colour charge. The remaining gauginos corresponding to superpartners of the W, Z and photon, combined with the higgsinos of the same quantum numbers all mix together to give four new physical states – two charged and two neutral fermions labelled *charginos* and *neutralinos* respectively.

Since SUSY cannot be manifest, we need to find a mechanism to break the symmetry. It is in principle possible to achieve spontaneous symmetry breaking of global SUSY, however it is very difficult to build a realistic model. The problems with the different spontaneous SUSY breaking scenarios include, for example, violation of mass sum rules between quarks and squarks or the need for additional field content beyond the MSSM. It is instead expected that SUSY is *softly* broken by dimensionful parameters such as squark mass terms. These explicit breaking terms are put in by hand, and can be thought of as originating from dynamics beyond the MSSM operating at some very high energy scale and "communicated" to the low energy sector via some (unknown) mechanism. The soft breaking Lagrangian contains a host of mass terms for scalar particles and gauginos, bi- and tri-linear scalar interactions, giving a total of 105 new physical parameters in its most general form. In general scenarios there is no reason why these parameters should be flavour-blind, but often in particular models many simplifying assumptions are made about the structure of the flavour sector. We consider the implications of this in the next section.

5.3.2 Implications for the flavour sector

Given the most general form of supersymmetry breaking as we have discussed above, there are many new parameters and contributions in the flavour sector which could impact on the phenomenology of flavour changing and CP violating processes. There is potential for many supersymmetric contributions to these processes, allowing them to arise at rates much higher than experimentally observed. This is however coupled with the very stringent constraints on any new physics, for example, from the fitting of the unitarity triangle – which combines all available experimental data on flavour and CP violation. The success with which this fit determines the CKM parameters to be in agreement with the Standard Model expectations shows where new large sources of flavour changing neutral currents or CP violation are not favoured in a possible new physics model.

There are a large number of different possible scenarios for SUSY breaking

[136], including the simplifying assumption of flavour universality at the high energy scale. This universality removes all of the terms which could lead to "dangerous" FCNC and CP-violating effects which are already excluded by experiment. For example, in the minimal supergravity (mSUGRA) model, which imposes gravity-mediated SUSY breaking, the canonical scenario has universal scalar masses

$$m^2_{\tilde{q}_{ij}} = \delta_{ij} m_0^2$$

However, even in this picture evolving the dynamics from the high energy ("GUT" scale) to the electroweak scale induces flavour non-universality due to the contribution from the Yukawa couplings [137], although they are expected to be small.

Alternatively, in other SUSY breaking scenarios, it is possible for the dynamics of the hidden sector to be communicated to the low energy theory in a flavour specific way – even before radiative corrections or the RGE evolution are included. This will allow flavour changing neutral currents which are in general not GIM-suppressed or CP invariant. This clearly will produce a very rich phenomenology with many new sources of flavour and CP physics.

5.3.3 Mass insertion approximation

To test the impact of a particular SUSY model on the flavour sector we would, ideally, diagonalise the squark mass matrices so we could calculate diagrams with the squark mass eigenstates. Without knowledge of the full mass matrices however, this is a rather difficult problem, as the matrices are related to the parameters of the soft SUSY breaking Lagrangian in a non-trivial manner. We instead utilise the fact that the flavour changing effects originate from the off-diagonal elements of the squark (sfermion) mass matrices. If the off-diagonal elements are small relative to the diagonal entries we can use the *mass insertion approximation* [123]. This enables us to simply compute ratios of the off-diagonal entries over the diagonal elements of the squark mass matrices and compare with the bounds we can derive from experimental data.

In order to allow the most general method of SUSY breaking and flavour structure, we can consider a "generic" R-parity conserving MSSM. We parameterise the FCNC and left-right squark mixing by taking the squark mass matrices as both flavour universal and real. This mass matrix is written with the off-diagonal elements denoted $(\Delta_{AB})_{ij}$, where AB stands for LL, RR, LR, RL and denotes the helicity of the squarks. For example, m^2_{LL} can be written

$$m^2_{LL} = \begin{pmatrix} (m^2_{LL})_{11} & (\Delta_{LL})_{12} & (\Delta_{LL})_{13} \\ (\Delta_{LL})_{21} & (m^2_{LL})_{22} & (\Delta_{LL})_{23} \\ (\Delta_{LL})_{31} & (\Delta_{LL})_{32} & (m^2_{LL})_{33} \end{pmatrix}$$

We can then constrain the perturbations from universal scalar masses $m^2_{\tilde{f}}$ by normalising the off-diagonal elements by a common mass, normally taken as the average scalar mass $m^2_{\tilde{f}}$. The mass insertions are defined as

$$(\delta^d_{AB})_{ij} = \frac{(\Delta_{AB})_{ij}}{m^2_{\tilde{f}}} \tag{5.12}$$

For the $b \to d$ transition the relevant insertions are $(\delta^d_{AB})_{13}$ and for the $b \to s$ transitions $(\delta^d_{AB})_{23}$. The universal scalar mass is often taken as an approximate mass scale, such as the average squark mass $m_{\tilde{f}} \sim 500$ GeV.

Different realisations of the MSSM will be characterised by different sets of soft breaking terms which in turn induce different sets and combinations of mass insertions. We classify the effect of these different MSSM models on δ_{ij}^d in terms of the helicities AB = LL, RR, LR, RL. We consider for the most part cases where a single helicity mass insertion dominates, but also test some cases where two of the mass insertions are sizable (a double mass insertion). This allows us to find the leading contributions to various processes by considering diagrams with a single (or double) mass insertion and express the phenomenological bounds in a model-independent way.

5.4 Gluino contributions in generic MSSM

We add supersymmetric contributions to the Standard Model expressions using an effective Hamiltonian induced by gluino exchange as first derived in [138] using the mass insertion approximation. Gluino exchange is the dominant contribution and we do not consider charged Higgs, chargino or neutralino exchanges. This is a good approximation in a preliminary analysis of this nature as these contributions are proportional to the weak coupling rather than α_s as for the gluino contributions, and so can be safely neglected.

Two classes of diagrams contribute to the $\Delta B = 1$ processes, namely penguin and box diagrams, which give both additional contributions to the existing Standard Model operators Q_i, and induce new operators $\widetilde{Q}_i$ obtained from the Q_i under the exchange L $\leftrightarrow$ R. The gluino contributions which interfere with the SM contributions (i.e those from operators Q_i) are combined at the level of the Wilson coefficients. The contributions from the remaining new operators $\widetilde{Q}_i$ are added separately since they do not interfere with the SM amplitude.

The Wilson coefficients for the SUSY operators act to modify the initial conditions of the SM operators at the scale $\mu = M_W$. For the radiative processes, we only need to consider the relevant contributions, namely to $C_7^{(0)\,\mathrm{eff}}$ and $C_8^{(0)\,\mathrm{eff}}$:

$$\begin{aligned} C_7 &= \frac{\alpha_s \pi}{m_{\tilde{q}}^2}\left[\left(\delta_{13}^d\right)_{LL}\frac{8}{3}M_3(x) + \left(\delta_{13}^d\right)_{LR}\frac{m_{\tilde{g}}}{m_b}\frac{8}{3}M_1(x)\right] \\ C_8 &= \frac{\alpha_s \pi}{m_{\tilde{q}}^2}\left[\left(\delta_{13}^d\right)_{LL}\left(-\frac{1}{3}M_3(x) - 3M_4(x)\right)\right. \\ &\qquad\qquad \left. + \left(\delta_{13}^d\right)_{LR}\frac{m_{\tilde{g}}}{m_b}\left(-\frac{1}{3}M_1(x) - 3M_2(x)\right)\right] \end{aligned} \tag{5.13}$$

where the $M_i(x)$ are functions of $x = m_{\tilde{g}}^2/m_{\tilde{q}}^2$ obtained from the calculation of the gluino penguins [138], ($m_{\tilde{q}}$ is the average squark mass and $m_{\tilde{g}}$ is the gluino mass). In all of the following analysis we use equal values for the average squark and gluino masses, i.e. $x = 1$. The co-efficients for $\widetilde{Q}_7$ and $\widetilde{Q}_8$ are obtained from these under the exchange L $\leftrightarrow$ R.

In considering the SUSY contributions to $B \to V\gamma$ the Standard Model contribution is added to the gluino contribution and we determine the possible constraints on the flavour-violating sources in the squark sector. The bounds we determine on the δ_{13}^d and δ_{23}^d insertions are only indicative as they are extracted ignoring the error of the theory calculation. We also indicate the bound on the parameter space when the 1σ theory error is included.

5.5 New physics in $b \to d$ transitions

Although the constraints on the flavour sector are quite stringent there is still room for new physics to affect the flavour sector. Using the new results for the $B \to \rho\gamma$ decays we can constrain the possibility of new physics in a generic supersymmetric model using the mass insertion approximation introduced above. Constraints on δ^d_{13} derived from the $\bar{B}_d$—B_d mass difference ΔM_d and the CP asymmetry in $B \to J/\psi K_s$ were determined in [139]. This study found that with NLO evolution, for a single mass insertion and $m_{\tilde{q}} \sim m_{\tilde{g}}$, the limits on δ^d_{13} are of the order of 10^{-1} for the LL or RR insertions, and $\sim 10^{-2}$ for LR, RL.

We expect the radiative $b \to d$ decays to show a similar hierarchy, as the LR and RL insertions are those most effectively constrained by measurements of $B \to \rho\gamma$ as they enter into the Wilson coefficients with the factor $(m_{\tilde{g}}/m_b)$. The LL and LR insertions contribute to the same operator that is responsible for the $B \to V\gamma$ decay in the SM, and so yield a SUSY contribution which interferes with the SM. As a consequence, the rates tend to be larger than the RR (and RL) cases since these insertions do not add to the leading SM amplitude. The consequences of this in light of our high central values for the SM amplitudes, are that the resulting parameter spaces for the RR and RL insertions will be more constrained than the LL and LR ones.

With these considerations in mind, we use the gluino contributions to $\Delta B = 1$ transitions and the constraints from the newly measured radiative processes to constrain the δ^d_{13} insertions. We can then determine if the measurement of the $B \to \rho\gamma$ decay can put stringent limits on the possible SUSY models that may have impact on the $b \to d$ sector.

We consider single mass insertions for each helicity combination, and double mass insertions for a left-right symmetric case: $(\delta^d_{13})_{LL} = (\delta^d_{13})_{RR}$ and $(\delta^d_{13})_{RL} = (\delta^d_{13})_{LR}$ as motivated in a number of SUSY models e.g. left-right supersymmetric models.

5.5.1 Constraints on δ^d_{13}

Using the full SM + SUSY contribution to the $B \to \rho\gamma$ processes, we can determine the allowed parameter space in the δ^d_{13} plane using the available experimental results. We use both the $B \to (\rho, \omega)\,\gamma$ branching fraction and the ratio $R\,[(\rho, \omega)\gamma/K^*\gamma]$ as these were fitted separately from the Belle data set [122], so we can apply the constraints concurrently. We begin by considering a single mass insertion with an average squark mass of $m_{\tilde{q}} =$ 500GeV. For constraints based on the ratio $R_{\rm th}$ we take all insertions to $B \to K^*\gamma$ to be zero in the first instance.

The absolute value of the $B \to (\rho,\, \omega)\gamma$ branching ratio is plotted against the absolute value of the mass insertion (for each single mass insertion dominating in turn) in Figure 5.8.

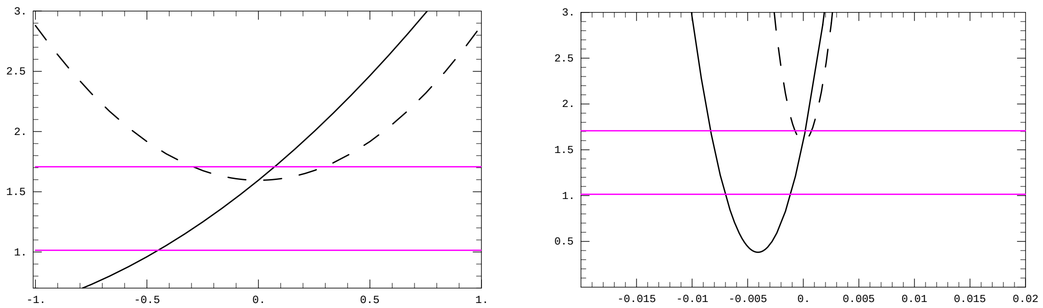

Figure 5.8: Left: Dependence of BR($B \to (\rho,\, \omega)\gamma$) with gluino contributions on the single mass insertion $|(\delta^d_{13})_{LL}|$ (solid line) and $|(\delta^d_{13})_{RR}|$ (dashed line) with $m_{\tilde{q}} = m_{\tilde{g}} =$ 500GeV. Experimental 1σ bounds shown for comparison. Right: same for $|(\delta^d_{13})_{LR}|$ (solid) and $|(\delta^d_{13})_{RL}|$ (dashed).

The difference between the LL and RR cases is due to the way the gluino contribution interferes with the Standard Model. For the case where the $(\delta^d_{13})_{LL}$ insertion dominates, the supersymmetric contribution is to the same operator responsible for the $B \to \rho\gamma$ decay. This interference in general causes the decay to proceed at a larger rate than that of the RR case. For the RR case where no interference with the Standard Model is present, the results will be symmetric around $(\delta^d_{13})_{RR} = 0$, and similarly for $(\delta^d_{13})_{RL}$.

The allowed values for the LR and RL insertions are expected to be much smaller than for the LL or RR insertions as they enter into the Wilson coefficients with factor $(m_{\tilde{g}}/m_b)$. Hence $(\delta^d_{13})_{LR}$ and $(\delta^d_{13})_{RL}$ will be the most effectively constrained. The high central value of SM amplitude for BR$(B \to (\rho, \omega)\gamma)$ will lead to a minimal allowed area of parameter space for the RR and RL insertions. If the error on the SM amplitude is taken into account the constraints the parameter space would clearly be less stringent.

The full constraints on the parameter space for the four single mass insertions are shown in Figure 5.9, where we extract the bounds on the insertions using both the central value of the SM amplitude for $B \to (\rho, \omega)\gamma$ and taking into account the 1σ error.

The allowed areas in the parameter space indicate regions where the insertion can produce a supersymmetric contribution which is within the experimental 1σ bounds on BR$(B \to (\rho, \omega)\gamma)$. These figures show that using the data imposes quite stringent restrictions on the parameter space, the most impact coming from the low error on the $R_{\text{exp}}[(\rho, \omega)\gamma/K^*\gamma]$ measurement.

We can also consider the effect of a double mass insertion, for the cases where $(\delta^d_{13})_{LL} = (\delta^d_{13})_{RR}$ or $(\delta^d_{13})_{LR} = (\delta^d_{13})_{RL}$. This sort of scenario is motivated by a number of different SUSY models, such as the left-right supersymmetric

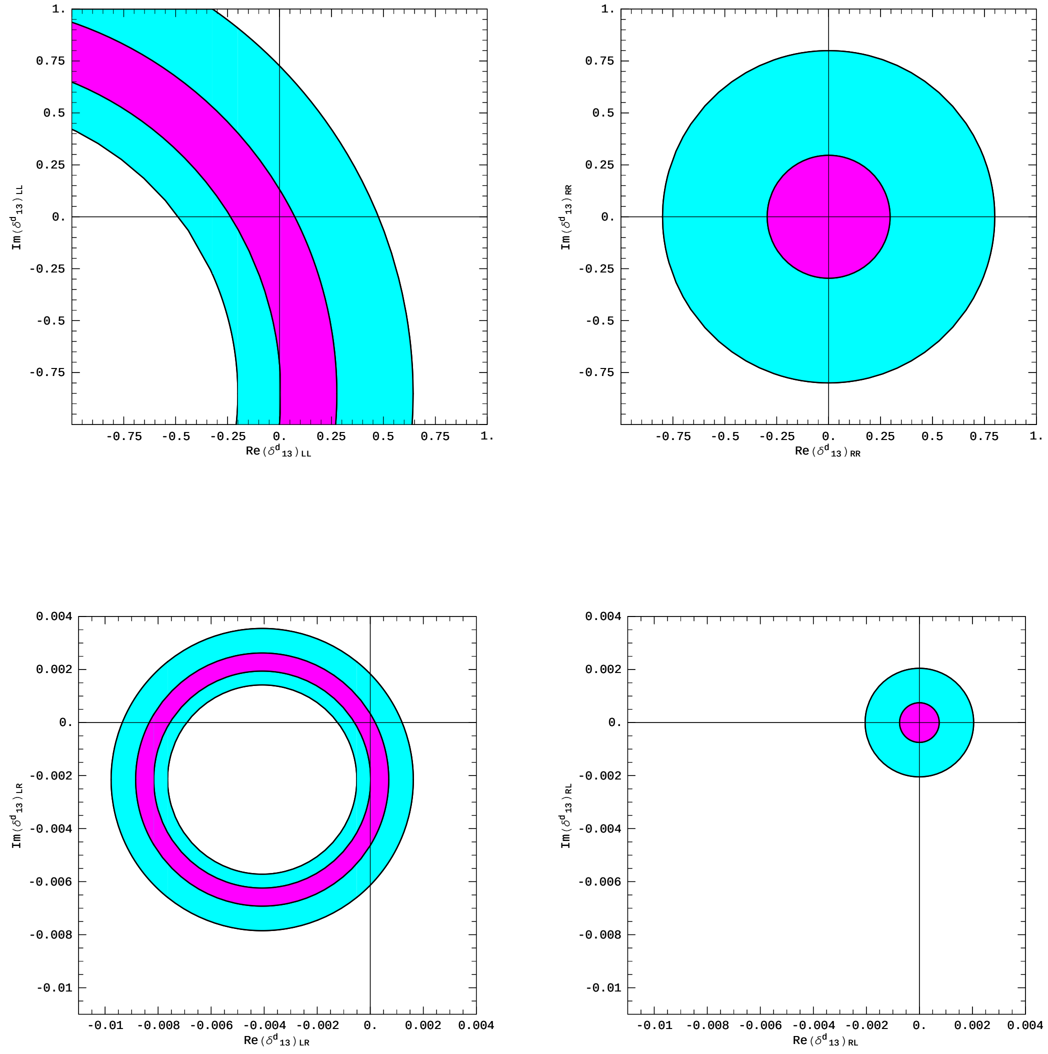

Figure 5.9: Allowed regions in $Re(\delta^d_{13})_{ij} - Im(\delta^d_{13})_{ij}$ parameter space for $ij =$ LL, RR, LR, RL. We use $m_{\tilde{q}} = m_{\tilde{g}} = 500$ GeV, and constraints from Belle measurement of BR$(B \to (\rho,\omega)\gamma)$ and additionally $R\left[(\rho,\omega)\gamma/K^*\gamma\right]$. The overlay in magenta indicates allowed regions using central value of SM amplitude.

model or minimal supergravity (mSUGRA) which demands $\delta_{LL} = \delta_{RR} = 0$ and $\delta_{LR} = \delta_{RL}$. The results for both cases are shown in figure 5.10.

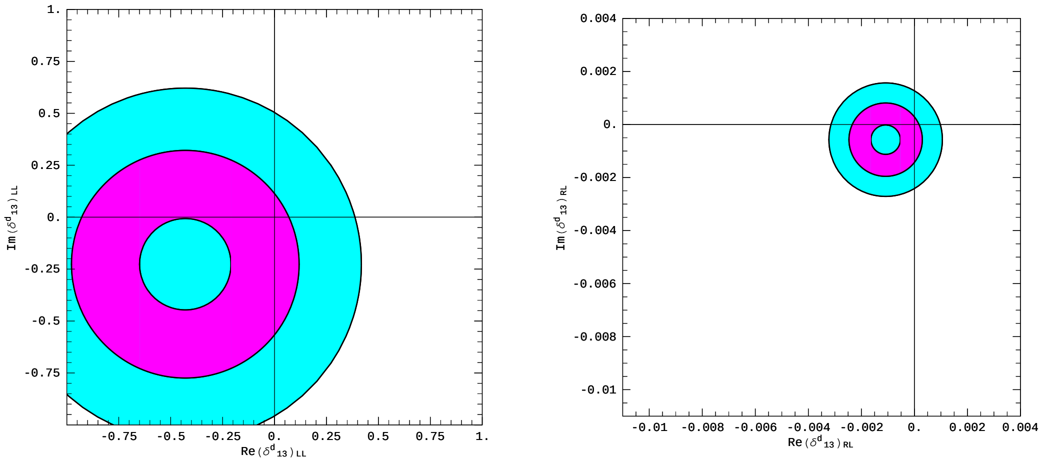

Figure 5.10: Allowed regions in $Re(\delta^d_{13})_{ij} - Im(\delta^d_{13})_{ij}$ parameter space for double mass insertions LL = RR and LR = RL. We use $m_{\tilde{q}} = m_{\tilde{g}} = 500$ GeV, and constraints from Belle measurement of BR$(B \to (\rho, \omega)\,\gamma)$ and $R\,[(\rho,\omega)\gamma/K^*\gamma]$.

We see a similar pattern as with the single mass insertion, of a much greater constraint on the helicity-changing insertions than the helicity conserving. The $LL = RR$ case for example, allows ample space for a sizable mass insertion.

5.6 New physics in $b \to s$ transitions

We now perform a similar analysis with the $B \to K^*\gamma$ decays. Although there are strong constraints on new physics contributions to $s \to d$ and $b \to d$ transitions, this is not the case with $b \to s$ transitions. The unitarity fit for example strongly constrains the $s \to d$ and $b \to d$ transitions, but not the $b \to s$ transitions as they do not affect the fit directly (unless they interfere with the amplitude for B_s mixing and reduce the expected value of ΔM_s below its experimental lower bound). In the radiative processes such as $b \to s\gamma$, there can be many new contributions with SUSY particles in the penguin loop. The main contribution is shown diagrammatically in Figure 5.11. The cross on the internal squark line represents a flavour changing

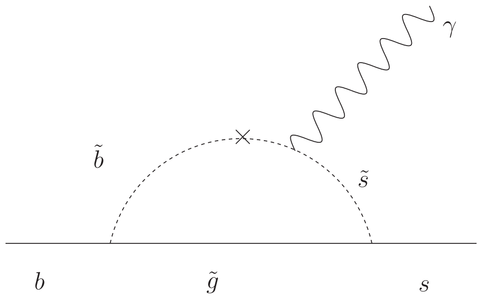

Figure 5.11: Main supersymmetric contribution to $b \to s\gamma$.

mass insertion. The size of this will be determined by the nature of the supersymmetric breaking – our ignorance of this means that the insertion could in principle be as large as any of the other terms.

5.6.1 Constraints on δ^d_{23}

There have been previous studies on constraining new physics in $b \to s\gamma$ decays such as [117], which concentrates on using the bounds from the inclusive process $B \to X_s\gamma$. These studies have shown that there is still ample room in the parameter space for SUSY contributions to various different observables. The constraints that can be determined from the branching ratio and CP asymmetry in $B \to X_s\gamma$ mainly affect the helicity-changing contributions i.e. the SUSY insertions $(\delta^d_{23})_{LR}$ and $(\delta^d_{23})_{RL}$. We can therefore use the measurement of our exclusive decay $B \to K^*\gamma$, and see if additional constraints (specifically in the LL and RR sectors) can be determined.

The graphs in Figure 5.12 show the constraints on the $Re(\delta^d_{13})_{ij} - Im(\delta^d_{13})_{ij}$ plane once the bounds from the $B \to K^*\gamma$ branching ratio have been applied.

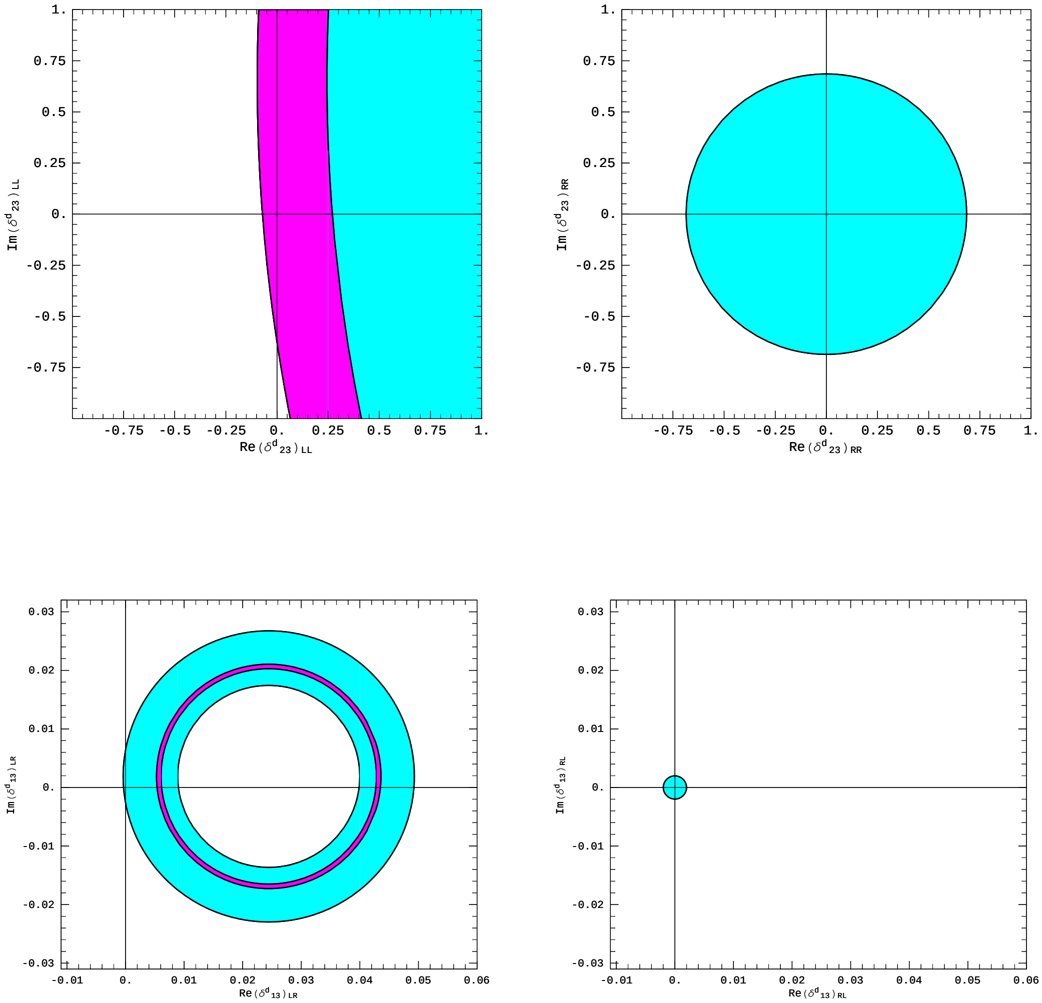

Figure 5.12: Allowed regions in $Re(\delta^d_{23})_{ij} - Im(\delta^d_{23})_{ij}$ parameter space for double mass insertions LL = RR and LR = RL. We use $m_{\tilde{q}} = m_{\tilde{g}} = 500$ GeV, and constraints from Belle measurement of BR($B \to K^*\gamma$).

These figures show that using the central values for the Standard Model amplitude for the $K^*\gamma$ decay gives extremely tight constraints on the $Re(\delta^d_{23})_{ij}$ – $Im(\delta^d_{23})_{ij}$ parameter space, leaving virtually no room for any significant contribution from a single mass insertion. Also, since there is no available parameter space for the RR and RL single insertions, no reduction of the constraints is obtained by considering the double mass insertions. Including the 1σ theory error on the SM contribution opens up the parameter space a little, as we see in Figure 5.12, specifically with the LL and RR insertions. Overall however, these results do not support the conclusion that there is any new physics in the exclusive $K^*\gamma$ decays.

Chapter 6

Conclusions and outlook

Few can foresee whither their road will lead them, till they come to its end

"The Lord of the Rings", J.R.R.Tolkien

This thesis has examined the non-leptonic decays both within QCD factorisation and beyond it, challenging the assumptions and limitations of the method. Our study was three-fold: we analysed the treatment of the light-cone distribution amplitudes for the light mesons and introduced a new model described by simple physical parameters. We then scrutinised the charmless non-leptonic decays in the context of their incalculable non-factorisable contributions – which we consider the main limitation of the QCD factorisation method. Finally, we analysed the new results on the exclusive $B \to V\gamma$ within QCDF and generic supersymmetric models.

Our main new result is the development of a new model for the symmetric part of the leading-twist light-cone distribution amplitude of light mesons. This was done with particular reference to the pion, although the results are applicable to all light mesons. The models depend on three parameters, two which control the fall-off behaviour of the Gegenbauer moments a_n in n, and a third Δ, which parameterises the maximum possible impact of the higher-order moments on a factorised physical amplitude. This is given by the first inverse moment of the DA. The model is defined at a low energy scale ($\mu = 1.2$GeV for the π) and can be easily evolved up to higher scales by solving the evolution equation numerically. In contrast to the conformal expansion, which in computation becomes numerically unstable at high orders, our model DAs are very well behaved numerically and can be easily implemented in computer codes. We discussed how the evolution equation can be solved at the leading order, but this could in principle also be solved to next-to-leading order.

We have introduced a similar model for the antisymmetric part of the distribution amplitude, relevant for the K, and the K^* mesons; these models are normalised to a_1, the first Gegenbauer moment. For the π DA, where experimental data exists, we have formulated constraints on the model parameters, likely to be valid for other meson DAs as well. The constraints on the allowed values of Δ are tighter for the models ϕ^- with an alternating sign fall-off of the Gegenbauer moments than for those with a equal sign behaviour ϕ^+.

We feel that these models are better suited for estimating hadronic uncertainties of processes calculated within factorisation than using the standard truncated conformal expansion. This is true in particular for processes that involve convolutions with singular kernels $\sim 1/u$, as the corresponding integral, Δ, is the basic parameter of the model.

Our models also should prove particularly useful for describing DAs of mesons other than the π which are also symmetric by virtue of G-parity, but for which no experimental or other reliable theoretical information is available — in particular the ρ, ω and ϕ. For these particles we argue that existing theoretical indications from local QCD sum rules [41, 99, 100] point to the DAs being narrower than the π, which implies $\Delta < 1.2$ at the scale 1.2GeV. These results also imply that a_2 is positive, hence constraining $\Delta \geq 1$. For the parameter a, which controls the fall-off the a_n with n, we have found that the perturbative contributions to QCD sum rules indicate it to be 3 [69, 70], but that smaller values of a are not excluded unless one can rigorously prove that all leading-twist DAs must behave as $\sim u(1-u)$ near the endpoints $u = 0, 1$ at all scales. Any further input, either from experiment or lattice would be welcome to help constrain the model, however, even without the constraints being taken literally our models provide a convenient way to test the impact of non-asymptotic DAs on physical amplitudes without resorting to the conformal expansion.

We illustrated the impact of our models on the calculation of the $B \to \pi\pi$ branching ratios and CP asymmetries and found that the branching ratios are more sensitive to the precise values of the model parameters than the CP-asymmetries. The observed discrepancy between experimental data and the predictions of QCD factorisation cannot however be explained by non-standard DAs, which indicates the presence of non-negligible non-factorisable contributions — a conclusion that agrees with the findings of other authors, e.g. [50, 140].

In order to quantitatively justify this premise, we analysed in detail the non-factorisable Λ_{QCD}/m_b corrections to $B \to \pi\pi$ decay amplitudes. We showed how the experimental information can be used to extract valuable information on the size and nature of these non-factorisable corrections. We aimed to move beyond the model-dependent treatment presented in [1], where non-factorisable contributions are identified from convolution integrals which have endpoint divergences. The chirally enhanced power corrections which originate from hard-spectator scattering diagrams and annihilation topologies, are each parameterised by an arbitrary complex number, the modulus of which is estimated from regularising the end-point divergences. We replaced these terms with generic non-factorisable corrections via a decomposition of the $B \to \pi\pi$ decays into isospin amplitudes $A_{1/2}$ and $A_{3/2}$. Three scenarios were constructed using differing levels of non-factorisable corrections on top of the factorisable terms found via QCDF.

Our analysis included the effect of a non-standard DA, to simulate greater impact from higher-order moments, as parameterised by the physical parameter Δ. We found that the maximum contribution allowed within the physical range of Δ was required to give the best-fit to the data. Variation of the $B \to \pi$ transition form factor also required an extremal (minimum) allowed value, as found from the χ^2 fitting across the full data set. Our combined analysis of all of the most up-to-date experimental data available on the $B \to \pi\pi$ system (as of September 2005), showed clearly that sizable non-factorisable effects are required to bring all of the $B \to \pi\pi$ results into agreement. Even for extremal values of our input parameters, the best-fit scenarios do not give a reasonable 2σ agreement to the experimental data until at least 30% contributions are included. For the Belle data and combined HFAG results, a minimum level of 40% is needed to produce the same level of agreement.

Our third scenario showed how the long-distance enhanced charming penguin diagrams can contribute constructively to the decay amplitudes. The size of the enhancement must be tightly constrained in order to keep within the error bounds of the data (particularly for CP asymmetries) and as taking $|R| > 1.5$ will make the charm penguin the dominant non-factorisable effect. The branching ratios and $\pi^+\pi^-$ CP asymmetry can be independently brought into excellent agreement, however we discussed how the phases of the charm correction are at odds for these two scenarios. The best-fit for the scenario with 20% NF correction in addition to the charming penguin gives a considerable improvement above the scenario with only the 20% correction. However, further NF corrections are still required to bring the theory into the experimental 2σ error bound. Hence, we can conclude that a sizable NF correction is still required even in this scenario.

It will be interesting to watch how any future experimental results on $B \to \pi\pi$ develop, particularly those on the branching ratios for $B \to \pi^+\pi^-$ and $B \to \pi^0\pi^0$. The current situation makes it difficult to make conclusive statements, as measurements from BaBar and Belle currently disagree by approximately 2σ for both the $\pi^+\pi^-$ and $\pi^0\pi^0$ channels. A notable rise in the central value for the $\pi^+\pi^-$ channel (as was the case for BaBar and the figures released in summer 2004 and 2005) would act favourably for a lower requirement of non-factorisable corrections. The converse however, could leave us looking at approaching 50% non-factorisable corrections in order to obtain a good 2σ agreement with the HFAG data.

The results of our analysis leave us with many more questions than when we started. When the experimental situation is resolved and the accuracy improves the question remains of the source of the disagreement with the $B \to \pi\pi$ data; whether this can be explained by significant non-factorisable effects within the Standard Model, or if it points to new physics beyond it. This also presents the more pertinent question of the validity of the factorisation scheme itself, if indeed such high levels of power-suppressed corrections are required to satisfy the data. The next step in this puzzle will be to analyse $B \to \pi K$ decays, by fitting a set of generic non factorisable contributions to the experimental data [104].

Finally, we took a step sideways and analysed the recently released data on $B \to (\rho, \omega)\gamma$ decays. We examined the Standard Model predictions within QCD factorisation using the technique first presented in [4] using updated non perturbative input, e.g. form factors [58], and testing the effect of our non standard DA introduced in Chapter 3. We found predictions for $B \to \rho\gamma$ in agreement with that presented in [4]

$$\mathrm{BR}(B^0 \to \rho^0\gamma) = (0.72 \pm 0.22) \times 10^{-6} \qquad \mathrm{BR}(B^\pm \to \rho^\pm\gamma) = (1.52 \pm 0.45) \times 10^{-6}$$

and estimated the combined branching ratio as

$$\mathrm{BR}(B \to (\rho, \omega)\gamma) = (1.60 \pm 0.48) \times 10^{-6}$$

which is within the error bounds of the new Belle measurement. We found that the variation of the branching ratio with the non standard DA was minimal, and that there was less than a 3% effect across the full physical range of Δ. We found the same results for an analogous analysis of $B \to K^*\gamma$ where we estimated a central value for the branching ratio of

$$\mathrm{BR}(B \to K^*\gamma) = (5.49 \pm 1.64) \times 10^{-5}$$

This differs from the central value presented in [4] predominantly due to the drop in the value of the $B \to K^*$ form factor. We then discussed how these two branching ratios can be combined into a ratio $R[(\rho,\omega)\gamma/K^*\gamma]$ which can be used to extract the value of the CKM ratio $|V_{td}/V_{ts}|$. We obtained a value of

$$R[(\rho,\omega)\gamma/K^*\gamma] = 0.030 \pm 0.008$$

in excellent agreement with the measured result. This led to an extracted value of $|V_{td}/V_{ts}| = 0.195 \pm 0.051$. This shows how well the ratio can reduce the theoretical uncertainty.

Since previously only an upper bound for the $B \to (\rho,\, \omega)\gamma$ has been available, this was an opportune moment to examine how much room for new physics remains in the $b \to d\gamma$ decays. We examined these decays and $B \to K^*\gamma$ in the context of a generic minimal supersymmetric model, using the dominant gluino contributions as derived using the mass insertion approximation. The contributions from charged Higgs, neutralino and chargino contributions are sub-leading and can be safely neglected in an indicative analysis of this type.

We found constraints on the parameter space for the mass insertion δ^d_{13} which is relevant for the $b \to d$ transitions. We showed how the allowed regions are very stringently constrained, primarily due to the constraint from $R[(\rho,\omega)\gamma/K^*\gamma]$. Taking into account the 1σ theory error opens up more of the parameter space, but still leaving only the LL and RR insertions as realistic possibilities. We examined the parameter space for the δ^d_{23} insertion using the bounds from the $B \to K^*\gamma$ decay. We used the central value of the SM amplitude and found virtually no parameter space available for a significant mass insertion. This is to be expected, considering the good agreement of theory with the measurement for the inclusive decay $B \to X_s\gamma$, which implies that all of the short-distance physics in the $b \to s\gamma$ transition is under good control.

As we rapidly approach the new era of particle physics heralded by the LHC, precision measurements in the flavour sector will become an essential component of testing the Standard Model expectations, and to uncover potential sources of new physics. We need therefore complete control over the long distance physics to ensure that the theory errors do not remain significantly larger than the experimental errors as the measurements continue to improve. I believe that this work presents an unbiased examination of methods to tackle and understand the uncertainties and limitations of the QCD factorisation formalism and points to a direction in which further study could go.

The Road goes ever on and on,
Down from the door where it began.
Now far ahead the Road has gone
And I must follow if I can.

Pursuing it with eager feet,
Until it meets some larger way,
Where many paths and errands meet.
And whither then? I cannot say.

J.R.R. Tolkien

Appendix A

Wilson coefficients for $\mathcal{H}_{\text{eff}}^{\Delta B=1}$

A.1 6×6 operator basis

We give the explicit formulae for the Wilson coefficients in the naive dimensional regularization scheme. We consider the 6×6 matrix which is made up of the operators $Q_1 \ldots Q_6$. Recalling that we can expand the Wilson coefficients in powers of α_s, we have

$$C_i(\mu) = C_i^{(0)}(\mu) + \frac{\alpha_s(\mu)}{4\pi} C_i^{(1)}(\mu) + \ldots \tag{A.1}$$

The evolution of the effective Wilson coefficients is governed by the anomalous dimension matrix (ADM). The expansion of the ADM including only gluonic corrections (no electroweak penguins) is, to order α_s,

$$\hat{\gamma} = \frac{\alpha_s}{4\pi} \hat{\gamma}_s^{(0)} + \left(\frac{\alpha_s}{4\pi}\right)^2 \hat{\gamma}_s^{(1)} \tag{A.2}$$

The leading order matrix in this expansion is given (using the operators in Section 1.2.3)

$$\gamma^{(0)} = \begin{pmatrix} -2 & 6 & 0 & 0 & 0 & 0 \\ 6 & -2 & -\frac{2}{9} & \frac{2}{3} & -\frac{2}{9} & \frac{2}{3} \\ 0 & 0 & -\frac{22}{9} & \frac{22}{3} & -\frac{4}{9} & \frac{4}{3} \\ 0 & 0 & 6-\frac{2f}{9} & -2+\frac{2f}{3} & -\frac{2f}{9} & \frac{2f}{3} \\ 0 & 0 & 0 & 0 & 2 & -6 \\ 0 & 0 & -\frac{2f}{9} & \frac{2f}{3} & -\frac{2f}{9} & -16+\frac{2f}{3} \end{pmatrix} \tag{A.3}$$

The number of quark colours has been set to $N_c = 3$, and the number of active flavours is denoted by f. At next-to-leading order we have the following matrix governing the mixing of current-current and QCD-penguin operators among each other:

$$\gamma^{(1)} = \begin{pmatrix} -\frac{21}{2}-\frac{2f}{9} & \frac{7}{2}+\frac{2f}{3} & \frac{79}{9} & -\frac{7}{3} & -\frac{65}{9} & -\frac{7}{3} \\ \frac{7}{2}+\frac{2f}{3} & -\frac{21}{2}-\frac{2f}{9} & -\frac{202}{243} & \frac{1354}{81} & -\frac{1192}{243} & \frac{904}{81} \\ 0 & 0 & -\frac{5911}{486}+\frac{71f}{9} & \frac{5983}{162}+\frac{f}{3} & -\frac{2384}{243}-\frac{71f}{9} & \frac{1808}{81}-\frac{f}{3} \\ 0 & 0 & \frac{379}{18}+\frac{56f}{243} & -\frac{91}{6}+\frac{808f}{81} & -\frac{130}{9}-\frac{502f}{243} & -\frac{14}{3}+\frac{646f}{81} \\ 0 & 0 & -\frac{61f}{9} & -\frac{11f}{3} & \frac{71}{3}+\frac{61f}{9} & -99+\frac{11f}{3} \\ 0 & 0 & -\frac{682f}{243} & \frac{106f}{81} & -\frac{225}{2}+\frac{1676f}{243} & -\frac{1343}{6}+\frac{1348f}{81} \end{pmatrix} \tag{A.4}$$

At $\mu_0 = M_W$ the matching conditions can be split into the leading order and

NLO corrections, $C_i^{(0)}(M_W)$ and $C_i^{(1)}(M_W)$ respectively. These are given by

$$C_i^{(0)}(M_W) = \begin{cases} 1 & \text{for } i = 2 \\ 0 & \text{otherwise} \end{cases} \tag{A.5}$$

and

$$C_i^{(1)}(M_W) = \begin{cases} \frac{11}{2} & \text{for } i = 1 \\ -\frac{11}{6} & \text{for } i = 2 \\ -\frac{1}{6}\widetilde{E_0}(x_t) & \text{for } i = 3,5 \\ \frac{1}{2}\widetilde{E_0}(x_t) & \text{for } i = 4,6 \end{cases} \tag{A.6}$$

with $\widetilde{E_0}(x)$ being the Inami-Lim function

$$\begin{aligned} \widetilde{E_0}(x) &= E_0(x) - \frac{2}{3} \\ E_0(x) &= \left(-\frac{2}{3}\ln(x) + \frac{x(18-11x-x^2)}{12(1-x)^3} + \frac{x^2(15-16x+4x^2)}{6(1-x)^4}\ln(x) \right) \end{aligned} \tag{A.7}$$

and

$$x_t = \frac{m_t^2}{M_W^2} \tag{A.8}$$

A.2 10×10 operator basis, including electroweak penguins

The expansion of the ADM including gluonic and photonic corrections is

$$\hat{\gamma} = \frac{\alpha_s}{4\pi}\hat{\gamma}_s^{(0)} + \frac{\alpha_s}{4\pi}\hat{\gamma}_e^{(0)} + \left(\frac{\alpha_s}{4\pi}\right)^2 \hat{\gamma}_s^{(1)} + \frac{\alpha_s}{4\pi}\frac{\alpha_e}{4\pi}\hat{\gamma}_{se}^{(1)} \tag{A.9}$$

where we include the leading QED contributions from $\hat{\gamma}_e^{(0)}$. but do not include the two-loop QCD-QED anomalous dimension matrix $\hat{\gamma}_{se}^{(1)}$. The other matrices are given below, again in the NDR scheme.

$$\hat{\gamma}_{\mathrm{s}}^{(0)} = \begin{pmatrix} -2 & 6 & 0 & 0 & 0 & 0 & 0 & 0 & 0 & 0 \\ 6 & -2 & \frac{-2}{9} & \frac{2}{3} & \frac{-2}{9} & \frac{2}{3} & 0 & 0 & 0 & 0 \\ 0 & 0 & \frac{-22}{9} & \frac{22}{3} & \frac{-4}{9} & \frac{4}{3} & 0 & 0 & 0 & 0 \\ 0 & 0 & 6-\frac{2f}{9} & -2+\frac{2f}{3} & \frac{-2\,f}{9} & \frac{2f}{3} & 0 & 0 & 0 & 0 \\ 0 & 0 & 0 & 0 & 2 & -6 & 0 & 0 & 0 & 0 \\ 0 & 0 & \frac{-2f}{9} & \frac{2f}{3} & \frac{-2f}{9} & -16+\frac{2f}{3} & 0 & 0 & 0 & 0 \\ 0 & 0 & 0 & 0 & 0 & 0 & 2 & -6 & 0 & 0 \\ 0 & 0 & \frac{-2(u-d/2)}{9} & \frac{2(u-d/2)}{3} & \frac{-2(u-d/2)}{9} & \frac{2(u-d/2)}{3} & 0 & -16 & 0 & 0 \\ 0 & 0 & \frac{2}{9} & -\frac{2}{3} & \frac{2}{9} & -\frac{2}{3} & 0 & 0 & -2 & 6 \\ 0 & 0 & \frac{-2(u-d/2)}{9} & \frac{2(u-d/2)}{3} & \frac{-2(u-d/2)}{9} & \frac{2(u-d/2)}{3} & 0 & 0 & 6 & -2 \end{pmatrix}$$

$$\hat{\gamma}_{\mathrm{e}}^{(0)} = \begin{pmatrix} -\frac{8}{3} & 0 & 0 & 0 & 0 & 0 & \frac{16\,N}{27} & 0 & \frac{16\,N}{27} & 0 \\ 0 & -\frac{8}{3} & 0 & 0 & 0 & 0 & \frac{16}{27} & 0 & \frac{16}{27} & 0 \\ 0 & 0 & 0 & 0 & 0 & 0 & -\frac{16}{27}+\frac{16\,N\,(u-d/2)}{27} & 0 & -\frac{88}{27}+\frac{16\,N\,(u-d/2)}{27} & 0 \\ 0 & 0 & 0 & 0 & 0 & 0 & \frac{-16\,N}{27}+\frac{16\,(u-d/2)}{27} & 0 & \frac{-16\,N}{27}+\frac{16\,(u-d/2)}{27} & -\frac{8}{3} \\ 0 & 0 & 0 & 0 & 0 & 0 & \frac{8}{3}+\frac{16\,N\,(u-d/2)}{27} & 0 & \frac{16\,N\,(u-d/2)}{27} & 0 \\ 0 & 0 & 0 & 0 & 0 & 0 & \frac{16\,(u-d/2)}{27} & \frac{8}{3} & \frac{16\,(u-d/2)}{27} & 0 \\ 0 & 0 & 0 & 0 & \frac{4}{3} & 0 & \frac{4}{3}+\frac{16\,N\,(u+d/4)}{27} & 0 & \frac{16\,N\,(u+d/4)}{27} & 0 \\ 0 & 0 & 0 & 0 & 0 & \frac{4}{3} & \frac{16\,(u+d/4)}{27} & \frac{4}{3} & \frac{16\,(u+d/4)}{27} & 0 \\ 0 & 0 & -\frac{4}{3} & 0 & 0 & 0 & \frac{8}{27}+\frac{16\,N\,(u+d/4)}{27} & 0 & -\frac{28}{27}+\frac{16\,N\,(u+d/4)}{27} & 0 \\ 0 & 0 & 0 & -\frac{4}{3} & 0 & 0 & \frac{8\,N}{27}+\frac{16\,(u+d/4)}{27} & 0 & \frac{8\,N}{27}+\frac{16\,(u+d/4)}{27} & -\frac{4}{3} \end{pmatrix}$$

$$\hat{\gamma}_{\mathrm{s}}^{(1)} = \begin{pmatrix} -\frac{209}{18} & \frac{41}{6} & \frac{79}{9} & -\frac{7}{3} & -\frac{65}{9} & -\frac{7}{3} & 0 & 0 & 0 & 0 \\ \frac{41}{6} & -\frac{209}{18} & -\frac{202}{243} & \frac{1354}{81} & -\frac{1192}{243} & \frac{904}{81} & 0 & 0 & 0 & 0 \\ 0 & 0 & -\frac{13259}{486} & \frac{6253}{162} & -\frac{11959}{243} & -\frac{1673}{81} & 0 & 0 & 0 & 0 \\ 0 & 0 & \frac{10793}{486} & -\frac{5623}{162} & -\frac{6020}{243} & -\frac{2852}{81} & 0 & 0 & 0 & 0 \\ 0 & 0 & -\frac{305}{9} & \frac{-55}{3} & \frac{518}{9} & -\frac{242}{3} & 0 & 0 & 0 & 0 \\ 0 & 0 & -\frac{3410}{243} & \frac{530}{81} & -\frac{37915}{486} & -\frac{22781}{162} & 0 & 0 & 0 & 0 \\ 0 & 0 & -\frac{61}{18} & -\frac{11}{6} & \frac{83}{18} & -\frac{11}{6} & \frac{103}{9} & -\frac{187}{3} & 0 & 0 \\ 0 & 0 & -\frac{682}{729} & \frac{53}{81} & \frac{352}{243} & \frac{368}{81} & -\frac{185}{2} & -\frac{3349}{18} & 0 & 0 \\ 0 & 0 & \frac{2375}{486} & -\frac{2735}{162} & \frac{467}{486} & -\frac{1835}{162} & 0 & 0 & -\frac{209}{18} & \frac{41}{6} \\ 0 & 0 & -\frac{2186}{243} & \frac{602}{81} & \frac{1504}{243} & \frac{512}{81} & 0 & 0 & \frac{41}{6} & -\frac{209}{18} \end{pmatrix}$$

N is the number of colours, f, the number of active flavours and u and d denote the number of up- and down-type flavours respectively $(u + d = f)$. We have also specified $f = 5$ for presentation of $\gamma_s^{(1)}$.

The additional initial conditions for the Wilson coefficients of order α_e are:

$$C_i^e(M_W) = \frac{\alpha_e}{4\pi} * \begin{cases} 0 & \text{for } i = 1, 4-6, 8, 10 \\ -\frac{35}{18} & \text{for } i = 2 \\ \frac{2}{3}\frac{1}{s_w^2}\left(2B_0(x_t) + C_0(x_t)\right) & \text{for } i = 3 \\ \frac{2}{3}\left(4C_0(x_t) + \widetilde{D}_0(x_t)\right) & \text{for } i = 7 \\ \frac{2}{3}\left(4C_0(x_t) + \widetilde{D}_0(x_t) + \frac{1}{s_w^2}\left(10B_0(x_t) - 4C_0(x_t)\right)\right) & \text{for } i = 9 \end{cases} \tag{A.10}$$

with

$$
\begin{aligned}
B_0(x_t) &= \frac{x_t}{4(x_t-1)} + \frac{x_t}{4(x_t-1)^2}\ln x_t \\
C_0(x_t) &= \frac{x_t(x_t-6)}{8(x_t-1)} + \frac{x_t(2+3x_t)}{8(x_t-1)^2}\ln x_t \\
\widetilde{D}_0(x_t) &= -\frac{4}{9}lnx_t(\frac{-19x_t^3+25x_t^2}{36(x_t=1)^3} + \frac{x_t^2(5x_t^2-2x_t-6)}{18(x_t-1)^4}\ln x_t - \frac{4}{9}
\end{aligned}
\tag{A.11}
$$

Appendix B

Additional formulae from QCD factorisation

B.1 Decay amplitudes for $B \to \pi\pi$

In terms of the QCD factorisation coefficients defined in Section (2.3.1), the $B \to \pi\pi$ decay amplitudes are written as follows:

$$\begin{aligned}
-\sqrt{2}\mathcal{A}(B^- \to \pi^-\pi^0) &= \left[\lambda_u^{(d)} a_1 + \tfrac{3}{2}\lambda_p^{(d)}(-a_7 + a_9 + a_{10}^p + r_\chi^\pi a_8^p)\right] A_{\pi\pi} \\
-\mathcal{A}(\bar{B}^0 \to \pi^+\pi^-) &= \left[\lambda_u^{(d)} a_1 + \lambda_p^{(d)}(a_4^p + a_{10}^p) + \lambda_p^{(d)} r_\chi^\pi (a_6^p + a_8^p)\right] A_{\pi\pi} \\
-\sqrt{2}\mathcal{A}(\bar{B}^0 \to \pi^0\pi^0) &= \left[\lambda_u^{(d)} a_2 - \lambda_p^{(d)}(a_4^p - \tfrac{1}{2}a_{10}^p) - \lambda_p^{(d)} r_\chi^\pi (a_6^p - \tfrac{1}{2}a_8^p) + \tfrac{3}{2}\lambda_p^{(d)}(a_9 - a_7)\right] A_{\pi\pi}
\end{aligned} \tag{B.1}$$

with $a_i \equiv a_i(\pi\pi)$, $\lambda_p^{(d)} = V_{pb}V_{pd}^*$ for $p = u, c$ and

$$A_{\pi\pi} = i\frac{G_F}{\sqrt{2}}(m_B^2 - m_\pi^2)F_0^{B\to\pi}(m_\pi^2) f_\pi \tag{B.2}$$

The charge conjugate decays are obtained by replacing $\lambda_p \to \lambda_p^*$.

B.2 Annihilation contributions to $B \to V\gamma$

The contributions to the annihilation amplitudes contain two different factors depending if the photon emission if from the light quark in the B-meson, or from one of the constituent quarks of the vector meson. The former give the factor b^V, and the latter d^V, which are expressed as [124]:

$$b^V = \frac{2\pi^2}{F_V}\frac{f_B m_V f_V}{m_B m_b \lambda_B} \qquad d^V(v) = -\frac{4\pi^2}{F_V}\frac{f_B f_V^\perp}{m_B m_b}\int_0^1 \frac{\phi_V^\perp(v)}{v}\,dv$$

The integral over the distribution amplitude in the factor d^V will give a dependence on Δ (and a_1 where relevant) for all mesons. We include these components in the decay amplitudes via

$$a_7^u \longrightarrow a_7^u + a_{ann}^u$$
$$a_7^c \longrightarrow a_7^c + a_{ann}^c$$

where

$$\begin{aligned} a_{ann}^u(\rho^0\gamma) &= Q_d\left[-a_2 b^\rho + a_4 b^\rho + 2a_6 d^\rho(v)\right] \\ a_{ann}^c(\rho^0\gamma) &= Q_d\left[a_4 b^\rho + 2a_6 d^\rho(v)\right] \end{aligned}$$

$$\begin{aligned} a_{ann}^u(\rho^-\gamma) &= Q_u\left[a_1 b^\rho + a_4 b^\rho + (Q_s/Q_u + 1)\, a_6 d^\rho(v)\right] \\ a_{ann}^c(\rho^-\gamma) &= Q_u\left[a_4 b^\rho + (Q_s/Q_u + 1)\, a_6 d^\rho(v)\right] \end{aligned}$$

$$
\begin{aligned}
a^u_{ann}(\bar{K}^{*0}\gamma) &= Q_d\left[a_4 b^{K^*} + a_6(d^{K^*}(v) + d^{K^*}(\bar{v}))\right] \\
a^c_{ann}(\bar{K}^{*0}\gamma) &= Q_d\left[a_4 b^{K^*} + a_6(d^{K^*}(v) + d^{K^*}(\bar{v}))\right]
\end{aligned}
$$

$$
\begin{aligned}
a^u_{ann}(\bar{K}^{*-}\gamma) &= Q_u\left[a_1 b^{K^*} + a_4 b^{K^*} + Q_s/Q_u\, a_6 d^{K^*}(v) + a_6 d^{K^*}(\bar{v})\right] \\
a^c_{ann}(\bar{K}^{*-}\gamma) &= Q_u\left[a_4 b^{K^*} + Q_s/Q_u\, a_6 d^{K^*}(v) + a_6 d^{K^*}(\bar{v})\right]
\end{aligned}
$$

The a_i are combinations of Wilson coefficients:

$$
\begin{aligned}
a_{1,2} &= C_{1,2} + \frac{1}{N_c} C_{1,2} \\
a_4 &= C_4 + \frac{1}{N_c} C_3 \\
a_6 &= C_6 + \frac{1}{N_c} C_5
\end{aligned}
$$

Appendix C

Analytic evolution of light-cone distribution amplitudes

The pion distribution amplitude is by nature a non-perturbative quantity, but has evolution governed by perturbative QCD. The evolution is described by the ER-BL equation given in (3.22); we can recast this as

$$\phi_\pi(u,\mu^2) = \int_0^1 dv\, U(u,v,\mu^2,\mu_0^2)\,\phi_\pi(v,\mu_0^2), \tag{C.1}$$

where the operator $U(u,v,\mu,\mu_0^2)$ represents the solution to an evolution equation equivalent to (3.22) and describes evolution from the scale μ_0^2 to some scale μ^2. This presents a general solution to NLO [87] of

$$\begin{aligned} U(u,v,\mu^2,\mu_0^2) \;=\; & \sum_{n=0}^{\infty} E_n(\mu^2,\mu_0^2)\Bigg[C_n^{3/2}(2u-1) + \frac{\alpha_s(\mu^2)}{4\pi}\sum_{k=n+2}^{\infty} d_{kn}(\mu^2,\mu_0^2)C_k^{3/2}(2u-1) \\ & + \mathcal{O}(\alpha_s^3)\Bigg]\frac{u(1-u)}{N_n}C_n^{3/2}(2v-1). \end{aligned} \tag{C.2}$$

At leading order, the mixing of the moments of the distribution ampiltude are triangular, so that the LO kernal is diagonal with respect to the Gegenbauer polynomials. This implies that only the diagonal terms of the (triangular) anomalous dimension matrix $\gamma_{nn}^{(0)} \equiv \gamma_n^{(0)}$ will appear and are completely encoded in the function $E_n^{LO}(\mu^2, \mu_0^2)$

$$E_n^{LO}(\mu^2, \mu_0^2) = \exp\left[-\int_{\alpha_s(\mu_0^2)}^{\alpha_s(\mu^2)} d\alpha_s \frac{\gamma_n(\alpha_s)}{2\beta(\alpha_s)}\right] = \left[\frac{\alpha_s(\mu^2)}{\alpha_s(\mu_0^2)}\right]^{\gamma_n^{(0)}/2b_0}, \qquad \text{(C.3)}$$

with

$$\gamma_n^{(0)} = 2C_F\left[-3 - \frac{2}{(n+1)(n+2)} + 4\sum_{i=1}^{n+1}\frac{1}{i}\right] \qquad \text{(C.4)}$$

The anomalous dimensions are identical to those known from deep inelastic scattering [87, 141].

At next-to-leading order, the conformal operators mix under renormalisation, so that both the diagonal and non-diagonal terms will contribute to the evolution. The equivalent function to (C.3), E_n^{NLO}, is written

$$E_n^{NLO}(\mu^2, \mu_0^2) = \left[\frac{\alpha_s(\mu^2)}{\alpha_s(\mu_0^2)}\right]^{\gamma_n^{(0)}/2b0} \left[\frac{1 + \frac{b_1}{4\pi b_0}\alpha_s(\mu^2)}{1 + \frac{b_1}{4\pi b_0}\alpha_s(\mu_0^2)}\right]^{w(n)}, \qquad \text{(C.5)}$$

with

$$w(n) \equiv \frac{\gamma_n^{(1)} b_0 - \gamma_n^{(0)} b_1}{2b_0 b_1}. \qquad \text{(C.6)}$$

The off-diagonal contributions to $U(u, v, \mu^2, \mu_0^2)$ denoted d_{nk} in the full solution (C.2) given by

$$d_{kn}(\mu^2, \mu_0^2) = 2\frac{N_n}{N_k} S_{kn}(\mu^2, \mu_0^2)\, c_{kn}, \qquad \text{(C.7)}$$

where

$$
\begin{aligned}
c_{kn} &= (2n+3)\left\{\frac{-\gamma_n^{(0)} - 2b_0 + 8C_F A_{kn}}{2(k-n)(k+n+3)} + \frac{2C_F[A_{kn} - \psi(k+2) + \psi(1)]}{(n+1)(n+2)}\right\} \\
S_{kn}(\mu^2, \mu_0^2) &= \frac{\gamma_k^{(0)} - \gamma_n^{(0)}}{\gamma_k^{(0)} - \gamma_n^{(0)} - 2b_0}\left\{1 - \left[\frac{\alpha_s(\mu^2)}{\alpha_s(\mu_0^2)}\right]^{-1+(\gamma_k^{(0)} - \gamma_n^{(0)})/2b_0}\right\}, \\
A_{kn} &= \psi\left(\frac{k+n+4}{2}\right) - \psi\left(\frac{k-n}{2}\right) + 2\psi(k-n) - \psi(k+2) - \psi(1)
\end{aligned}
\tag{C.8}
$$

and with the function $\psi(z)$ defined as $\psi(z) \equiv \frac{d\ln\Gamma(z)}{dz}$. The NLO anomalous dimensions are given [141, 142] as

$$
\begin{aligned}
\gamma_n^{(1)} \;=\; & -(C_F^2 - \tfrac{1}{2}C_F C_A)\left\{16 S_1(n)\frac{2n+1}{n^2(n+1)^2} + 16\left[2S_1(n) - \frac{1}{n(n+1)}\right][S_2(n) - S_2'(\tfrac{1}{2}n)]\right. \\
& \left. + 64\tilde{S}(n) + 24 S_2(n) - 3 - 8S_3'(\tfrac{1}{2}n) - 8\frac{3n^3 + n^2 - 1}{n^3(n+1)^3} - 16(-1)^n\frac{2n^2+2n+1}{n^3(n+1)^3}\right\} \\
& -C_F C_A\left\{S_1(n)\left[\tfrac{536}{9} + 8\frac{2n+1}{n^2(n+1)^2}\right] - 16 S_1(n) S_2(n) + S_2(n)\left[-\tfrac{52}{3} + \frac{8}{n(n+1)}\right]\right. \\
& \left. -\tfrac{43}{6} - 4\frac{151n^4 + 263n^3 + 97n^2 + 3n + 9}{9n^3(n+1)^3}\right\} - \frac{C_F n_f}{2}\left\{-\tfrac{160}{9}S_1(n) + \tfrac{32}{3}S_2(n) + \tfrac{4}{3}\right. \\
& \left. + 16\frac{11n^2 + 5n - 3}{9n^2(n+1)^2}\right\}
\end{aligned}
\tag{C.9}
$$

where the n-dependent functions are

$$
\begin{aligned}
S_i(n) &= \sum_{j=1}^{n}\frac{1}{j^i} \\
S_i'(\tfrac{1}{2}n) &= \frac{1+(-1)^n}{2}S_i(\tfrac{1}{2}n) + \frac{1-(-1)^n}{2}S_i(\tfrac{n-1}{2}) \\
\tilde{S}(n) &= \sum_{j=1}^{n}\frac{(-1)^j}{j^2}S_1(j)
\end{aligned}
\tag{C.10}
$$

and $C_F = \frac{4}{3}$, $C_A = 3$.

The distribution amplitude to NLO will then be of the form

$$\begin{aligned}\phi_\pi(u,\mu^2) &= 6u(1-u)\sum_{n=0}^{\infty}\Bigg\{a_n(\mu_0^2)E_n^{NLO}(\mu^2,\mu_0^2)C_n^{3/2}(2u-1) \\ &\quad + \frac{\alpha_s(\mu^2)}{4\pi}\sum_{k=n+2}^{\infty}a_n(\mu_0^2)E_n^{NLO}(\mu^2,\mu_0^2)d_{kn}(\mu^2,\mu_0^2)C_k^{3/2}(2u-1)\Bigg\}\end{aligned} \tag{C.11}$$

The Gegenbauer moments a_n contain all of the important non-perturbative information. They can be independently evolved from their input values at some scale μ_0^2 to any scale μ^2 using the (NLO) evolution functions discussed above. Generalising to include the dependence on all higher-order Gegegnbauer moments we can write the following as an alternative to equation (C.11), using the shorthand $a_n(\mu_0^2) \equiv a_n^0$:

$$\phi_\pi(u,\mu^2) = 6u(1-u)\sum_{n=0}^{\infty}a_n(\mu^2)C_n^{3/2}(2u-1) \tag{C.12}$$

where

$$a_n(\mu^2) \equiv a_n^0\, E_n^{NLO}(\mu^2,\mu_0^2) + \frac{\alpha_s(\mu^2)}{4\pi}\sum_{k=0}^{n-2}d_{nk}(\mu^2,\mu_0^2)E_k(\mu^2,\mu_0^2)a_k^0 \tag{C.13}$$

for example:

$$\begin{aligned}a_2(\mu^2) &= a_2^0E_2 + \frac{\alpha_s}{4\pi}d_{20}\\ a_4(\mu^2) &= a_4^0E_4 + \frac{\alpha_s}{4\pi}(d_{40} + d_{42}E_2a_2^0)\\ a_6(\mu^2) &= a_6^0E_6 + \frac{\alpha_s}{4\pi}(d_{60} + d_{62}E_2a_2^0 + d_{64}E_4a_4^0)\end{aligned}$$

When the evolution from $\mu_0^2 \to \mu^2$ crosses any heavy flavour thresholds these expressions will be modified. Taking μ_0^2 at a low scale $\sim 1\text{GeV}^2$ where the number of active flavours n_f is three, the above expressions apply for all $\mu^2 \leq m_c^2$. Above this value there are two distinct regions: (i) with $n_f = 4$ when $m_c^2 < \mu^2 \leq m_b^2$ and (ii) with $n_f = 5$ for $\mu^2 > m_b^2$. These can be summarised in a similar expression to (C.13)

$$a_n^{NLO}(\mu^2) = a_n^0 E_n^{(n_f)}(\mu^2, \mu_0^2) + \frac{\alpha_s(\mu^2)}{4\pi} \sum_{k=0}^{n-2} d_{nk}^{(n_f)}(\mu^2, \mu_0^2) E_k^{(n_f)}(\mu^2, \mu_0^2) a_k^0 \tag{C.14}$$

where the evolution function $E_n^{(n_f)}$ takes on a different form in each region above the charm and beauty thresholds.

Region (i)

$$\begin{aligned} E_n^{(n_f)}(\mu^2, \mu_0^2)|_{R1} &= E_n^{(4)}(\mu^2, m_c^2) E_n^{(3)}(m_c^2, \mu_0^2) \\ d_{nk}^{(n_f)}(\mu^2, \mu_0^2) &= d_{nk}^{(4)}(\mu^2, m_c^2) E_n^{(n_f)}(\mu^2, \mu_0^2)|_{R1} + d_{nk}^{(3)}(m_c^2, \mu_0^2) E_n^{(4)}(\mu^2, m_c^2) \end{aligned} \tag{C.15}$$

Region (ii)

$$\begin{aligned} E_n^{(n_f)}(\mu^2, \mu_0^2)|_{R2} &= E_n^{(5)}(\mu^2, m_b^2) E_n^{(4)}(m_b^2, m_c^2) E_n^{(3)}(m_c^2, \mu_0^2) \\ d_{nk}^{(n_f)}(\mu^2, \mu_0^2) &= \left\{ d_{nk}^{(5)}(\mu^2, m_b^2) + d_{nk}^{(4)}(m_b^2, \mu_0^2) \right\} E_n^{(n_f)}(\mu^2, \mu_0^2)|_{R2} \\ &\quad + d_{nk}^{(3)}(m_c^2, \mu_0^2)\, E_n^{(5)}(\mu^2, m_b^2)\, E_n^{(4)}(m_b^2, m_c^2) \end{aligned} \tag{C.16}$$

Appendix D

Summary of input parameters

Masses			
m_c	$m_{b,pole}$	$m_{t,pole}$	M_W
1.3GeV	4.8GeV	174.3GeV	80.4GeV
m_π	m_ρ	m_ω	m_{K^*}
140MeV	770MeV	782MeV	894MeV

CKM Parameters and couplings			
$\bar{\eta}$	$\bar{\rho}$	V_{cb}	V_{cd}
0.347	0.196	0.0415	-0.2258
γ	β	α	$\alpha_s(M_Z)$
$60.3^\circ \pm 6.8^\circ$	23.4°	1/137	0.1187

Decay constants [58]			
f_B	f_π	f_{K^*}	$f_{K^*}^\perp$
200 ± 30MeV	133MeV	217MeV	170MeV
f_ρ	$f_\rho^\perp$	f_ω	$f_\omega^\perp$
205MeV	160MeV	195MeV	145MeV

Form factors [46, 58]			
F_π	F_{K^*}	F_ρ	F_ω
0.258 ± 0.031	0.333 ± 0.028	0.267 ± 0.021	0.242 ± 0.022

B-meson parameters			
m_B	λ_B	τ_{B^+}	τ_{B^0}
5.28GeV	350 ± 150MeV	1.65ps	1.53ps

Bibliography

[1] M. Beneke, G. Buchalla, M. Neubert, and C. T. Sachrajda, "QCD factorization for $B \to \pi\pi$ decays: Strong phases and CP violation in the heavy quark limit," Phys. Rev. Lett. **83** (1999) 1914–1917, hep-ph/9905312.

[2] M. Beneke, G. Buchalla, M. Neubert, and C. T. Sachrajda, "QCD factorization in $B \to \pi K$, $\pi\pi$ decays and extraction of Wolfenstein parameters," Nucl. Phys. **B606** (2001) 245–321, hep-ph/0104110.

[3] M. Beneke and M. Neubert, "QCD factorization for $B \to PP$ and $B \to PV$ decays," Nucl. Phys. **B675** (2003) 333–415, hep-ph/0308039.

[4] S. W. Bosch and G. Buchalla, "The radiative decays $B \to V\gamma$ at next-to-leading order in QCD," Nucl. Phys. **B621** (2002) 459–478, hep-ph/0106081.

[5] P. Ball and A. N. Talbot, "Models for light-cone meson distribution amplitudes," JHEP **06** (2005) 063, hep-ph/0502115.

[6] M. Gell-Mann, "A Schematic model of baryons and mesons," Phys. Lett. **8** (1964) 214–215.

[7] M. Y. Han and Y. Nambu, "Three-triplet model with double SU(3) symmetry," Phys. Rev. **139** (1965) B1006–B1010.

[8] H. D. Politzer, "Reliable perturbative results for strong interactions?," Phys. Rev. Lett. **30** (1973) 1346–1349.

[9] H. Fritzsch and M. Gell-Mann, "Current algebra: Quarks and what else?," hep-ph/0208010.

[10] H. Fritzsch, M. Gell-Mann, and H. Leutwyler, "Advantages of the color octet gluon picture," Phys. Lett. **B47** (1973) 365–368.

[11] **Particle Data Group** Collaboration, S. Eidelman *et. al.*, "Review of particle physics," Phys. Lett. **B592** (2004) 1.

[12] S. L. Glashow, "Partial symmetries of weak interactions," Nucl. Phys. **22** (1961) 579–588.

[13] S. Weinberg, "A model of leptons," Phys. Rev. Lett. **19** (1967) 1264–1266.

[14] A. Salam, *Elementary particle theory: Relativistic Groups and Analyticity*, vol. 8th Nobel Symposium. Stockholm, 1968. edited by Svartholm, Almqvist and Wiksell.

[15] **ALEPH** Collaboration, R. Barate *et. al.*, "Search for the standard model Higgs boson at LEP," Phys. Lett. **B565** (2003) 61–75, hep-ex/0306033.

[16] R. N. Mohapatra *et. al.*, "Theory of neutrinos," hep-ph/0412099.

[17] B. Kayser, "Neutrino physics," ECONF **C040802** (2004) L004, hep-ph/0506165.

[18] N. Cabibbo, "Unitary symmetry and leptonic decays," Phys. Rev. Lett. **10** (1963) 531–532.

[19] M. Kobayashi and T. Maskawa, "CP violation in the renormalizable theory of weak interaction," Prog. Theor. Phys. **49** (1973) 652–657.

[20] L. Wolfenstein, "Parametrization of the Kobayashi-Maskawa Matrix," Phys. Rev. Lett. **51** (1983) 1945.

[21] **CKMfitter Group** Collaboration, J. Charles *et. al.*, "CP violation and the CKM matrix: Assessing the impact of the asymmetric B factories," Eur. Phys. J. **C41** (2005) 1–131, hep-ph/0406184.

[22] K. G. Wilson, "Nonlagrangian models of current algebra," Phys. Rev. **179** (1969) 1499–1512.

[23] W. Zimmermann, "Normal products and the short distance expansion in the perturbation theory of renormalizable interactions," Ann. Phys. **77** (1973) 570–601.

[24] E. Witten, "Anomalous cross-section for photon - photon scattering in gauge theories," Nucl. Phys. **B120** (1977) 189–202.

[25] N. H. Christ, B. Hasslacher, and A. H. Mueller, "Light cone behavior of perturbation theory," Phys. Rev. **D6** (1972) 3543.

[26] G. 't Hooft and M. J. G. Veltman, "Regularization and renormalization of gauge fields," Nucl. Phys. **B44** (1972) 189–213.

[27] G. Buchalla, "Heavy quark theory," hep-ph/0202092.

[28] M. A. Shifman, A. I. Vainshtein, and V. I. Zakharov, "QCD and resonance physics: sum rules," Nucl. Phys. **B147** (1979) 385–447.

[29] V. M. Braun and I. E. Filyanov, "QCD sum rules in exclusive kinematics and pion wave function," Z. Phys. **C44** (1989) 157.

[30] V. L. Chernyak and I. R. Zhitnitsky, "B meson exclusive decays into baryons," Nucl. Phys. **B345** (1990) 137–172.

[31] **CP-PACS** Collaboration, A. Ali Khan *et. al.*, "B meson decay constant from two-flavor lattice QCD with non-relativistic heavy quarks," Phys. Rev. **D64** (2001) 054504, hep-lat/0103020.

[32] **JLQCD** Collaboration, S. Aoki *et. al.*, "B0 anti-B0 mixing in unquenched lattice QCD," Phys. Rev. Lett. **91** (2003) 212001, hep-ph/0307039.

[33] M. Okamoto *et. al.*, "Semileptonic D → pi / K and B → pi / D decays in 2+1 flavor lattice QCD," Nucl. Phys. Proc. Suppl. **140** (2005) 461–463, hep-lat/0409116.

[34] J. Shigemitsu *et. al.*, "Semileptonic B decays with N(f) = 2+1 dynamical quarks," hep-lat/0408019.

[35] R. Gupta, "Introduction to lattice QCD," hep-lat/9807028.

[36] J. R. Ellis, M. K. Gaillard, and D. V. Nanopoulos, "On the weak decays of high mass hadrons," Nucl. Phys. **B100** (1975) 313.

[37] M. J. Dugan and B. Grinstein, "QCD basis for factorization in decays of heavy mesons," Phys. Lett. **B255** (1991) 583–588.

[38] J. D. Bjorken, "Topics in B physics," Nucl. Phys. Proc. Suppl. **11** (1989) 325–341.

[39] D. Fakirov and B. Stech, "F and D decays," Nucl. Phys. **B133** (1978) 315–326.

[40] M. Beneke, G. Buchalla, M. Neubert, and C. T. Sachrajda, "QCD factorization for exclusive, non-leptonic B meson decays: General arguments and the case of heavy-light final states," Nucl. Phys. **B591** (2000) 313–418, hep-ph/0006124.

[41] V. L. Chernyak and A. R. Zhitnitsky, "Asymptotic behavior of exclusive processes in QCD," Phys. Rept. **112** (1984) 173.

[42] M. Peskin and D. Schroeder, *An Introduction to Quantum Field Theory*. Westview Press, 1995.

[43] G. P. Korchemsky, D. Pirjol, and T.-M. Yan, "Radiative leptonic decays of B mesons in QCD," Phys. Rev. **D61** (2000) 114510, hep-ph/9911427.

[44] A. G. Grozin and M. Neubert, "Asymptotics of heavy-meson form factors," Phys. Rev. **D55** (1997) 272–290, hep-ph/9607366.

[45] Y.-Y. Keum, H.-n. Li, and A. I. Sanda, "Fat penguins and imaginary penguins in perturbative QCD," Phys. Lett. **B504** (2001) 6–14, hep-ph/0004004.

[46] P. Ball and R. Zwicky, "New results on $B \to \pi, K, \eta$ decay formfactors from light-cone sum rules," Phys. Rev. **D71** (2005) 014015, hep-ph/0406232.

[47] R. Ruckl, "Exclusive decays of charm and beauty," hep-ph/9810338.

[48] C. W. Bauer, D. Pirjol, and I. W. Stewart, "A proof of factorization for $B \to D\pi$," Phys. Rev. Lett. **87** (2001) 201806, hep-ph/0107002.

[49] M. Gronau and D. London, "Isospin analysis of CP asymmetries in B decays," Phys. Rev. Lett. **65** (1990) 3381–3384.

[50] T. Feldmann and T. Hurth, "Non-factorizable contributions to $B \to \pi\pi$ decays," JHEP **11** (2004) 037, hep-ph/0408188.

[51] E. E. Salpeter and H. A. Bethe, "A Relativistic equation for bound state problems," Phys. Rev. **84** (1951) 1232–1242.

[52] M. Gell-Mann and F. Low, "Bound states in quantum field theory," Phys. Rev. **84** (1951) 350–354.

[53] V. L. Chernyak and A. R. Zhitnitsky, "Asymptotic behavior of hadron form-factors in quark model. (in russian)," JETP Lett. **25** (1977) 510.

[54] V. L. Chernyak and A. R. Zhitnitsky, "Asymptotics of hadronic form-factors in the quantum chromodynamics. (in russian)," Sov. J. Nucl. Phys. **31** (1980) 544–552.

[55] A. V. Efremov and A. V. Radyushkin, "Factorization and asymptotical behavior of pion form-factor in QCD," Phys. Lett. **B94** (1980) 245–250.

[56] G. P. Lepage and S. J. Brodsky, "Exclusive processes in quantum chromodynamics: evolution equations for hadronic wave functions and the form-factors of mesons," Phys. Lett. **B87** (1979) 359–365.

[57] G. P. Lepage and S. J. Brodsky, "Exclusive processes in perturbative quantum chromodynamics," Phys. Rev. **D22** (1980) 2157.

[58] P. Ball and R. Zwicky, "$B_{(d,s)} \to \rho, \omega, K^*, \phi$ decay form factors from light-cone sum rules revisited," Phys. Rev. **D71** (2005) 014029, hep-ph/0412079.

[59] P. Colangelo and A. Khodjamirian, "QCD sum rules: A modern perspective," hep-ph/0010175.

[60] A. Khodjamirian, "QCD sum rules for heavy flavour physics," AIP Conf. Proc. **602** (2001) 194–205, hep-ph/0108205.

[61] V. M. Belyaev, A. Khodjamirian, and R. Ruckl, "QCD calculation of the B → pi, K form-factors," Z. Phys. **C60** (1993) 349–356, hep-ph/9305348.

[62] P. Ball and V. M. Braun, "Use and misuse of QCD sum rules in heavy-to-light transitions: The decay $B \to \rho\, e\, \nu$ reexamined," Phys. Rev. **D55** (1997) 5561–5576, hep-ph/9701238.

[63] P. Ball, "$B \to \pi$ and $B \to K$ transitions from QCD sum rules on the light-cone," JHEP **09** (1998) 005, hep-ph/9802394.

[64] P. Ball and V. M. Braun, "Exclusive semileptonic and rare B meson decays in QCD," Phys. Rev. **D58** (1998) 094016, hep-ph/9805422.

[65] A. Khodjamirian, R. Ruckl, S. Weinzierl, C. W. Winhart, and O. I. Yakovlev, "Predictions on $B \to \pi \bar{l} \nu_l$, $D \to \pi \bar{l} \nu_l$ and $D \to K \bar{l} \nu_l$ from QCD light-cone sum rules," Phys. Rev. **D62** (2000) 114002, hep-ph/0001297.

[66] P. Ball and R. Zwicky, "Improved analysis of $B \to \pi\, e\, \nu$ from QCD sum rules on the light-cone," JHEP **10** (2001) 019, hep-ph/0110115.

[67] M. Beneke and T. Feldmann, "Symmetry-breaking corrections to heavy-to-light B meson form factors at large recoil," Nucl. Phys. **B592** (2001) 3–34, hep-ph/0008255.

[68] C. W. Bauer, D. Pirjol, and I. W. Stewart, "Factorization and endpoint singularities in heavy-to-light decays," Phys. Rev. **D67** (2003) 071502, hep-ph/0211069.

[69] P. Ball, V. M. Braun, Y. Koike, and K. Tanaka, "Higher twist distribution amplitudes of vector mesons in QCD: Formalism and twist three distributions," Nucl. Phys. **B529** (1998) 323–382, hep-ph/9802299.

[70] P. Ball and V. M. Braun, "Higher twist distribution amplitudes of vector mesons in QCD: Twist-4 distributions and meson mass corrections," Nucl. Phys. **B543** (1999) 201–238, hep-ph/9810475.

[71] V. M. Braun and I. E. Filyanov, “Conformal invariance and pion wave functions of nonleading twist,” Z. Phys. **C48** (1990) 239–248.

[72] P. Ball, “Theoretical update of pseudoscalar meson distribution amplitudes of higher twist: The nonsinglet case,” JHEP **01** (1999) 010, hep-ph/9812375.

[73] D. J. Gross and F. Wilczek, “Asymptotically free gauge theories. 2,” Phys. Rev. **D9** (1974) 980–993.

[74] V. M. Braun, G. P. Korchemsky, and D. Muller, “The uses of conformal symmetry in QCD,” Prog. Part. Nucl. Phys. **51** (2003) 311–398, hep-ph/0306057.

[75] V. M. Braun, S. E. Derkachov, G. P. Korchemsky, and A. N. Manashov, “Baryon distribution amplitudes in QCD,” Nucl. Phys. **B553** (1999) 355–426, hep-ph/9902375.

[76] F. M. Dittes and A. V. Radyushkin, “Two loop contribution to the evolution of the pion wave function,” Phys. Lett. **B134** (1984) 359–362.

[77] S. V. Mikhailov and A. V. Radyushkin, “Evolution kernels in QCD: two loop calculation in Feynman gauge,” Nucl. Phys. **B254** (1985) 89.

[78] **CLEO** Collaboration, J. Gronberg *et. al.*, “Measurements of the meson photon transition form factors of light pseudoscalar mesons at large momentum transfer,” Phys. Rev. **D57** (1998) 33–54, hep-ex/9707031.

[79] I. V. Musatov and A. V. Radyushkin, “Transverse momentum and Sudakov effects in exclusive QCD processes: $\gamma^*\gamma\pi^0$ form factor,” Phys. Rev. **D56** (1997) 2713–2735, hep-ph/9702443.

[80] S. J. Brodsky, C.-R. Ji, A. Pang, and D. G. Robertson, “Optimal renormalization scale and scheme for exclusive processes,” Phys. Rev. **D57** (1998) 245–252, hep-ph/9705221.

[81] G. Martinelli and C. T. Sachrajda, “A Lattice calculation of the second moment of the pion’s distribution amplitude,” Phys. Lett. **B190** (1987) 151.

[82] T. A. DeGrand and R. D. Loft, “Lattice pseudoscalar meson wave function properties,” Phys. Rev. **D38** (1988) 954.

[83] D. Daniel, R. Gupta, and D. G. Richards, “A Calculation of the pion’s quark distribution amplitude in lattice QCD with dynamical fermions,” Phys. Rev. **D43** (1991) 3715–3724.

[84] **UKQCD** Collaboration, L. Del Debbio, M. Di Pierro, A. Dougall, and C. T. Sachrajda, "The second moment of the pion's distribution amplitude," Nucl. Phys. Proc. Suppl. **83** (2000) 235–237, hep-lat/9909147.

[85] L. Del Debbio, M. Di Pierro, and A. Dougall, "The second moment of the pion light cone wave function," Nucl. Phys. Proc. Suppl. **119** (2003) 416–418, hep-lat/0211037.

[86] A. P. Bakulev, S. V. Mikhailov, and N. G. Stefanis, "QCD-based pion distribution amplitudes confronting experimental data," Phys. Lett. **B508** (2001) 279–289, hep-ph/0103119.

[87] A. P. Bakulev, K. Passek-Kumericki, W. Schroers, and N. G. Stefanis, "Pion form factor in QCD: From nonlocal condensates to NLO analytic perturbation theory," Phys. Rev. **D70** (2004) 033014, hep-ph/0405062.

[88] S. V. Mikhailov and A. V. Radyushkin, "The Pion wave function and QCD sum rules with nonlocal condensates," Phys. Rev. **D45** (1992) 1754–1759.

[89] S. V. Mikhailov and A. V. Radyushkin, "Quark condensate nonlocality and pion wave function in QCD: general formalism," Sov. J. Nucl. Phys. **49** (1989) 494.

[90] S. V. Mikhailov and A. V. Radyushkin, "Nonlocal condensates and QCD sum rules for pion wave function," JETP Lett. **43** (1986) 712.

[91] **BABAR** Collaboration, e. Harrison, P. F. and e. Quinn, Helen R., "The BaBar physics book: Physics at an asymmetric B factory,". Papers from Workshop on Physics at an Asymmetric B Factory (BaBar Collaboration Meeting), Rome, Italy, 11-14 Nov 1996, Princeton, NJ, 17-20 Mar 1997, Orsay, France, 16-19 Jun 1997 and Pasadena, CA, 22-24 Sep 1997.

[92] A. Khodjamirian, "Form factors of $\gamma^*\rho \to \pi$ and $\gamma^*\gamma \to \pi^0$ transitions and light-cone sum rules," Eur. Phys. J. **C6** (1999) 477–484, hep-ph/9712451.

[93] A. Schmedding and O. I. Yakovlev, "Perturbative effects in the form factor $\gamma\gamma^* \to \pi^0$ and extraction of the pion wave function from CLEO data," Phys. Rev. **D62** (2000) 116002, hep-ph/9905392.

[94] A. P. Bakulev, S. V. Mikhailov, and N. G. Stefanis, "Unbiased analysis of CLEO data at NLO and pion distribution amplitude," Phys. Rev. **D67** (2003) 074012, hep-ph/0212250.

[95] A. P. Bakulev, S. V. Mikhailov, and N. G. Stefanis, "CLEO and E791 data: A smoking gun for the pion distribution amplitude?," Phys. Lett. **B578** (2004) 91–98, hep-ph/0303039.

[96] A. D. Martin, R. G. Roberts, and W. J. Stirling, "Structure function analysis and psi, jet, W, Z production: pinning down the gluon," Phys. Rev. **D37** (1988) 1161.

[97] A. D. Martin, R. G. Roberts, and W. J. Stirling, "Improved parton distributions and W, Z production at p anti-p colliders," Mod. Phys. Lett. **A4** (1989) 1135.

[98] P. N. Harriman, A. D. Martin, W. J. Stirling, and R. G. Roberts, "Parton distributions extracted from data on deep inelastic lepton scattering, prompt photon production and the Drell- Yan process," Phys. Rev. **D42** (1990) 798–810.

[99] P. Ball and M. Boglione, "SU(3) breaking in K and K* distribution amplitudes," Phys. Rev. **D68** (2003) 094006, hep-ph/0307337.

[100] P. Ball and V. M. Braun, "The ρ Meson Light-Cone Distribution Amplitudes of Leading Twist Revisited," Phys. Rev. **D54** (1996) 2182–2193, hep-ph/9602323.

[101] **BaBar** Collaboration, B. Aubert *et. al.*, "Improved measurements of CP-violating asymmetry amplitudes in $B^0 \to \pi^+\pi^-$ decays," hep-ex/0501071.

[102] **Belle** Collaboration, K. Abe *et. al.*, "CP-violating asymmetries in $B^0 \to \pi^+\pi^-$ decays with 275 million B anti-B pairs," hep-ex/0502035.

[103] **UTfit** Collaboration, M. Bona *et. al.*, "The 2004 UTfit collaboration report on the status of the unitarity triangle in the standard model," hep-ph/0501199.

[104] P. Ball, G. W. Jones, and A. N. Talbot. In preparation.

[105] **Belle** Collaboration, Y. Chao *et. al.*, "Improved measurements of branching fractions for $B \to K\pi, \pi\pi$ and $K\bar{K}$ decays," Phys. Rev. **D69** (2004) 111102, hep-ex/0311061.

[106] **BABAR** Collaboration, B. Aubert *et. al.*, "Improved measurements of branching fractions for $B^0 \to \pi^+\pi^-$, $K^+\pi^-$, and search for K^+K^- at BaBar," hep-ex/0508046.

[107] **BABAR** Collaboration, B. Aubert *et. al.*, "Branching fractions and CP asymmetries in $B^0 \to \pi^0\pi^0$, $B^+ \to \pi^+\pi^0$ and $B^+ \to K^+\pi^0$ decays and isospin analysis of the $B \to \pi\pi$ system," Phys. Rev. Lett. **94** (2005) 181802, hep-ex/0412037.

[108] **Belle** Collaboration, K. Abe *et. al.*, “Observation of $B^0 \to \pi^0\pi^0$,” Phys. Rev. Lett. **94** (2005) 181803, hep-ex/0408101.

[109] A. Khodjamirian, T. Mannel, M. Melcher, and B. Melic, “Annihilation effects in $B \to \pi\pi$ from QCD light-cone sum rules,” hep-ph/0509049.

[110] W. N. Cottingham, I. B. Whittingham, and F. F. Wilson, “Factorization fits to charmless strangeless B decays,” Phys. Rev. **D71** (2005) 077301, hep-ph/0501040.

[111] M. Ciuchini, E. Franco, G. Martinelli, and L. Silvestrini, “Charming penguins in B decays,” Nucl. Phys. **B501** (1997) 271–296, hep-ph/9703353.

[112] M. Ciuchini, R. Contino, E. Franco, G. Martinelli, and L. Silvestrini, “Charming-penguin enhanced B decays,” Nucl. Phys. **B512** (1998) 3–18, hep-ph/9708222.

[113] A. J. Buras and L. Silvestrini, “Non-leptonic two-body B decays beyond factorization,” Nucl. Phys. **B569** (2000) 3–52, hep-ph/9812392.

[114] M. Ciuchini, E. Franco, G. Martinelli, M. Pierini, and L. Silvestrini, “Charming penguins strike back,” Phys. Lett. **B515** (2001) 33–41, hep-ph/0104126.

[115] **BELLE** Collaboration, P. Krizan, “FCNC decays of B mesons,” Int. J. Mod. Phys. **A20** (2005) 652–657.

[116] M. Neubert, “Radiative B decays: Standard candles of flavor physics,” hep-ph/0212360.

[117] M. Ciuchini, E. Franco, A. Masiero, and L. Silvestrini, “$b \to s$ transitions: A new frontier for indirect SUSY searches,” Phys. Rev. **D67** (2003) 075016, hep-ph/0212397.

[118] F. Borzumati, C. Greub, T. Hurth, and D. Wyler, “Gluino contribution to radiative B decays: Organization of QCD corrections and leading order results,” Phys. Rev. **D62** (2000) 075005, hep-ph/9911245.

[119] S. Bertolini, F. Borzumati, and A. Masiero, “Supersymmetric enhancement of noncharmed B decays,” Nucl. Phys. **B294** (1987) 321.

[120] A. L. Kagan and M. Neubert, “Direct CP violation in $B \to X_s\gamma$ decays as a signature of new physics,” Phys. Rev. **D58** (1998) 094012, hep-ph/9803368.

[121] T. Besmer, C. Greub, and T. Hurth, "Bounds on flavor violating parameters in supersymmetry," Nucl. Phys. **B609** (2001) 359–386, hep-ph/0105292.

[122] K. Abe, "Observation of $b \to d\gamma$ and determination of $|V(td)/V(ts)|$," hep-ex/0506079.

[123] L. J. Hall, V. A. Kostelecky, and S. Raby, "New flavor violations in supergravity models," Nucl. Phys. **B267** (1986) 415.

[124] S. W. Bosch, "Exclusive radiative decays of B mesons in QCD factorization. ((U))," hep-ph/0208203.

[125] A. L. Kagan and M. Neubert, "Isospin breaking in $B \to K^*$ gamma decays," Phys. Lett. **B539** (2002) 227–234, hep-ph/0110078.

[126] M. Beneke, T. Feldmann, and D. Seidel, "Exclusive radiative and electroweak $b \to d$ and $b \to s$ penguin decays at NLO," Eur. Phys. J. **C41** (2005) 173–188, hep-ph/0412400.

[127] A. Ali, E. Lunghi, and A. Y. Parkhomenko, "Implication of the $B \to (\rho, \omega)\gamma$ branching ratios for the CKM phenomenology," Phys. Lett. **B595** (2004) 323–338, hep-ph/0405075.

[128] S. W. Bosch and G. Buchalla, "Constraining the unitarity triangle with $B \to V\gamma$," JHEP **01** (2005) 035, hep-ph/0408231.

[129] P. Ball and R. Zwicky. In preparation.

[130] **BABAR** Collaboration, B. Aubert *et. al.*, "Measurement of branching fractions, and CP and isospin asymmetries, for $B \to K^*\gamma$," Phys. Rev. **D70** (2004) 112006, hep-ex/0407003.

[131] **BELLE Colaboration** Collaboration, M. Nakao *et. al.*, "Measurement of the $B \to K^*\gamma$ branching fractions and asymmetries," Phys. Rev. **D69** (2004) 112001, hep-ex/0402042.

[132] B. M. et al. UTfit collaboration Summer 2005 results, http://utfit.roma1.infn.it/.

[133] M. Drees, "An introduction to supersymmetry," hep-ph/9611409.

[134] S. P. Martin, "A supersymmetry primer," hep-ph/9709356.

[135] M. Green, J. Schwarz, and E. Witten, *Superstring theory.* Cambridge University Press, 1987.

[136] D. J. H. Chung *et. al.*, “The soft supersymmetry-breaking Lagrangian: Theory and applications,” Phys. Rept. **407** (2005) 1–203, hep-ph/0312378.

[137] I. Bigi and A. Sanda, *CP Violation*. Cambridge University Press, 2000.

[138] F. Gabbiani, E. Gabrielli, A. Masiero, and L. Silvestrini, “A complete analysis of FCNC and CP constraints in general SUSY extensions of the standard model,” Nucl. Phys. **B477** (1996) 321–352, hep-ph/9604387.

[139] D. Becirevic *et. al.*, “$B_d - \bar{B}_d$ mixing and the $B_d \to J\psi K_S$ asymmetry in general SUSY models,” Nucl. Phys. **B634** (2002) 105–119, hep-ph/0112303.

[140] A. J. Buras, R. Fleischer, S. Recksiegel, and F. Schwab, “Anatomy of prominent B and K decays and signatures of CP- violating new physics in the electroweak penguin sector,” Nucl. Phys. **B697** (2004) 133–206, hep-ph/0402112.

[141] A. Gonzalez-Arroyo, C. Lopez, and F. J. Yndurain, “Second order contributions to the structure functions in deep inelastic scattering. i. theoretical calculations,” Nucl. Phys. **B153** (1979) 161–186.

[142] E. G. Floratos, D. A. Ross, and C. T. Sachrajda, “Higher order effects in asymptotically free gauge theories: the anomalous dimensions of Wilson operators,” Nucl. Phys. **B129** (1977) 66–88.